TECHNISCHE UNIVERSITÄT MÜNCHEN

Lehrstuhl für Technische Chemie II

Transformation of triglycerides and fatty acids into biofuels with sulfur-free catalysts

Baoxiang Peng

Vollständiger Abdruck der von der Fakultät für Chemie der Technischen Universität München zur Erlangung des akademischen Grades eines

Doktors der Naturwissenschaften (Dr. rer. nat.)

genehmigten Dissertation.

Vorsitzender: Univ.-Prof. Dr. Dr. h.c. B. Rieger

Prüfer der Dissertation:

1. Univ.-Prof. Dr. J. A. Lercher
2. Univ.-Prof. Dr. Th. Brück

Die Dissertation wurde am 02.01.2012 bei der Technischen Universität München eingereicht und durch die Fakultät für Chemie am 08.03.2012 angenommen.

"Imagination is more important than knowledge"

Albert Einstein (1879 – 1955)

Acknowledgements

After finishing my dissertation, I would like to thank all the people who have contributed to this thesis in innumerable ways during the past three years.

First and foremost, I want to express my sincere gratitude to my advisor Johannes (Prof. Dr. J. A. Lercher). Thank you for offering me a working position to be part of your international and prestigious group, and for your warm encouragement and thoughtful guidance in the daily research as well as during paper or thesis writing. The joy and enthusiasm you have for scientific research are always motivational for me. I also appreciate the chances you gave me to attend lots of winter or summer school and international scientific conferences.

I am very grateful to my supervisor Andy (Prof. Dr. A. Jentys) for your support, especially in the first two years. I learned many things from the valuable discussions with you.

I am also very grateful to Chen (Dr. C. Zhao) for being my supervisor in the last one year. I enjoyed the time working together with you, and I must say that our cooperation were very productive and successful, especially in paper working.

Then I want to thank all the students who worked on their diploma thesis or master practical training under my supervision. Xiaoguo Yuan, Yuan Yao, and Yao Wu, many thanks for being with me and you helped me a lot during that time.

I would like to thank Xaver Hecht for always being there whenever I need help to solve technical problems, and for the BET and hydrogen chemisorption measurements. I am also very grateful to Martin Neukamm for the help of AAS measurement; Andreas Marx for solving computer problems; Hui Shi and Sonja Wyrzgol for their help in TEM measurements; Sarah Maier, Linus Schulz and Stefan Schallmoser for the help in TPD

Abstract

The transformation of microalgae oil into hydrocarbons as well as the mechanism of hydrodeoxygenation and aqueous phase reforming of glycerol has been systematically investigated. C-C bond cleavage for C_3 alcohols with terminal hydroxyl groups occurs via either decarbonylation of aldehydes or decarboxylation of acids. Microalgae oil can be quantitatively converted into diesel range alkanes over Ni/ZrO_2 via hydrogenolysis-hydrogenation-decarbonylation route. The hydrogenation of fatty acid to aldehyde (rate determining step) is synergistically promoted by the ZrO_2 support. Microalgae oil can also be hydrodeoxygenated to alkanes with bifunctional Ni/zeolite catalysts. The integrated hydrogenolysis, hydrogenation and decarbonylation are catalyzed by metallic Ni sites, while the acid function catalyzes the dehydration, cracking and isomerization.

Die Umsetzung von Mikroalgenöl zu Kohlenwasserstoffen sowie der Mechanismus der Hydrodeoxygenierung und die Reformierung von Glycerin in wässriger Phase wurden systematisch untersucht. Bei C_3-Alkoholen mit terminalen Hydroxylgruppen findet die Spaltung von C-C Bindungen durch entweder Decarbonylierung von Aldehyden oder Decarboxylierung von Carbonsäuren statt. Mikroalgenöl kann quantitativ zu Alkanen im Diesel-Bereich über Ni/ZrO_2 durch eine Hydrogenolyse-Hydrierungs-Decarbonylierungs Route umgesetzt werden. Die Hydrierung von Fettsäuren zu Aldehyden (geschwindigkeitsbestimmender Schritt) synergistisch durch den ZrO_2-Träger begünstigt wird. Mikroalgenöl kann auch zu Alkanen an bifunktionellen Ni/Zeolith Katalysatoren hydrodeoxygeniert werden. Die Hydrogenolyse, Hydrierung und Decarbonylierung werden durch der metallischen Funktion katalysiert, während die Säurefunktion die Dehydrierung, Isomerisierung und Cracken katalysiert.

Table of contents

Chapter 6

Chapter 7

Chapter 1

Introduction

1.1. General background

Nowadays, social and economical demands as well as environmental concerns necessitate the development of alternative and sustainable renewable energy supply. As the reserve of petroleum is diminishing and the energy demand to meet the growth of economy and population is persistently increasing, the price of fossil-based fuels will continually rise. On the other hand, the combustion of fossil fuels results in severely environmental problems, e.g., global warming caused by the emission of greenhouse gas CO_2 and acid rain related with NO_x and SO_x emissions.[1] In addition, more rigid government regulations and full or partial tax exemption are established to promote the utilization of sustainable fuels. For example, the EU has set a target that 10% of the total transportation fuels will be biofuels by 2020.[2] These three aspects require us to search for alternative energy resources.

Figure 1-1 shows the outlook of world energy consumption to 2050 by Shell.[3] It is forecasted that the global energy consumption will double in size by 2050. Coal, gas and oil will still be the main and stable energy sources, but the energy derived from biomass will increase dramatically in this half century. It also has been said that plant biomass is the only sustainable source for fuels and chemical in the near future. And prior to the discovery of cheap fossil fuels, the energy demands of society was totally met by plant biomass. Biomass possesses many advantages in comparison with fossil fuels, e.g., abundant, carbon-neutral in life cycle, and sulfur-free.

Currently, three types of processes can be employed for the production of liquid fuels from biomass (see Figure 1-2).[4] The first process involves gasification to produce syn-gas, followed by Fischer-Tropsch synthesis or methanol synthesis to produce alkanes or methanol, respectively. The second employs pyrolysis and thermochemical liquefaction for bio-oils production, which are subsequently further refined to produce alkanes. The third relies on hydrolysis of lignocellulose for sugar monomer production, and it is further converted into ethanol and/or aromatic hydrocarbons through fermentation and/or dehydration.

Biomass can be simply classified into cellulose, hemicellulose, lignin, starch, protein and oil. As feedstock, vegetable oils have the problems of limited quantities and they are

more expensive than lignocellulosic biomass. However, biodiesel produced from transesterification of vegetable oils dominates 80% of the current biofuel market in Europe due to high energy densities and efficient conversion of triglycerides.[5] In this context, triglycerides and fatty acids were selected for detailed study as representative biomass in this thesis.
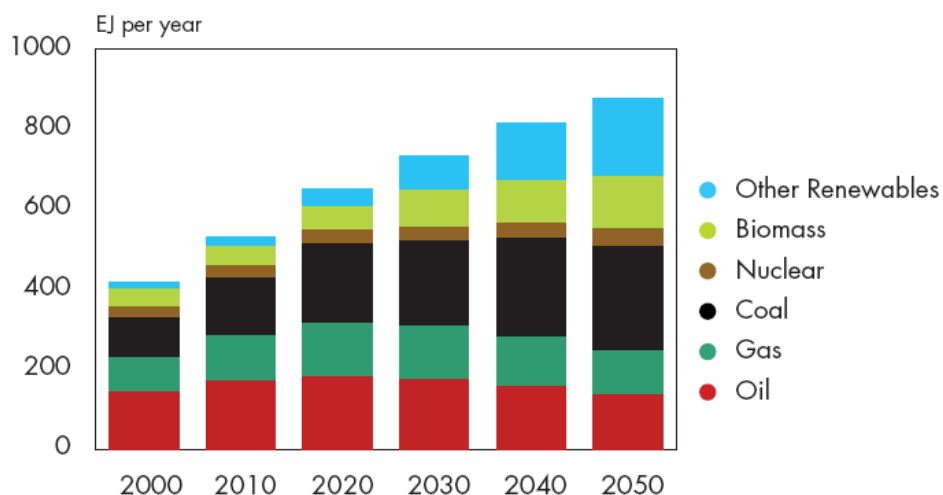
Figure 1-1. The world energy consumption outlook to 2050 by Shell [3]
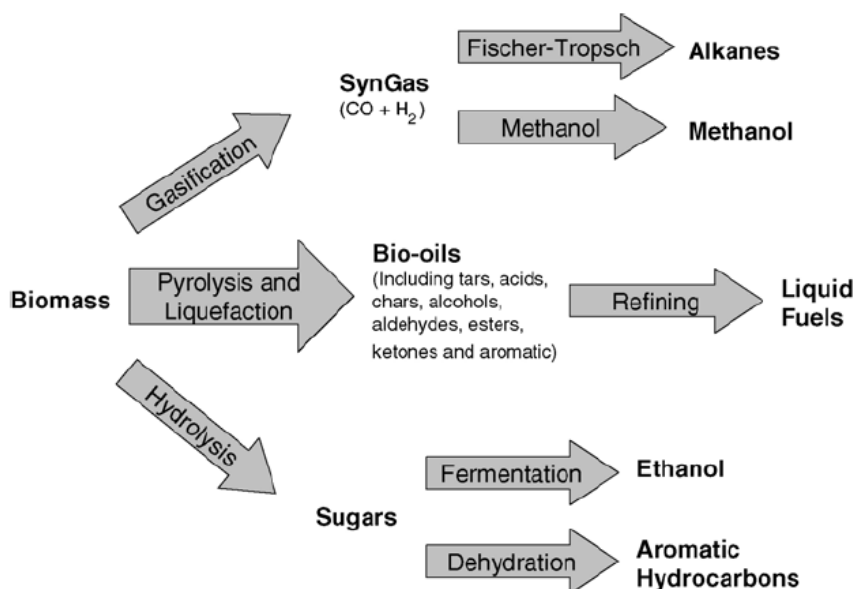
Figure 1-2. Strategies for production of liquid fuels from biomass [4]

1.2. Triglyceride feedstocks

1.2.1. Vegetable oils

Triglycerides (vegetable oils or animal fats) are hydrophobic substances that are formed by one molecule of glycerol and three molecules of fatty acids. There are many types of vegetable oils have been considered as potential raw feedstocks for biofuel production mainly according to geography and climate. Rapeseed oils are used for biodiesel production in Europe, corn and soybean oils are favored in the USA, while the abundant palm and coconut oils are employed in tropical countries. Furthermore, other types of vegetable oils, e.g., cottonseed, canola, peanut, and sunflower oils have also been studied.[1] The fatty acid compositions of typical vegetable oils are shown in Table 1-1.[6] Most the vegetable oils are highly unsaturated and the main compositions are C_{18} fatty acids, except palm oil having saturated palmitic acid as main component.

Table 1-1. Fatty acid composition of typical vegetable oils[6]

	Fatty acid composition (wt%)				
	Myristic	Palmitic	Stearic	Oleic	Linoleic
Oils	14:0 [a]	16:0	18:0	18:1	18:2
Rapeseed	0.1	5.1	2.1	57.9	24.7
Corn	-	7-13	2.5-3	30.5-43	39-52
Soybean	-	2.3-11	2.4-6	22-30.8	49-53
Palm	0.6-2.4	32-46.3	4-6.3	37-53	6-12
Cottonseed	0.8-1.5	22-24	2.6-5	19	50-52.5
Canola	-	4-5	1-2	55-63	20-31
Peanut	0.5	6-12.5	2.5-6	37-61	13-41
Sunflower	-	3.5-6.5	1.3-5.6	14-43	44-68.7

[a] The nomenclature shows the number of carbon atoms and the number of C=C double bonds: for example, the present sample contained 14 C atoms and no double bonds.

However, the production of biofuels from the above mentioned vegetable oils has the problem of competing with arable land culture and edible food supply. Thus, some alternative non-edible raw feedstocks that can be cultured in non-arable land with relatively fast growth rate have been searched, such crops including mahua, jatropha, and Chinese tallow tree.[7, 8] In addition, waste cooking oils with high free fatty acid content also can be treated as an alternative source.

1.2.2. Microalgae

Microalgae, a large and diverse group of unicellular photo and heterotrophic organisms, are considered to be another promising source of triglycerides without directly competing with edible food/oil production.[9,10] The growth rates of microalgae are extremely rapid that they usually double their biomass within 24 h, and the triglyceride contents of microalgae are quite high that even can exceed 80% by weight of dry biomass.[11] Generally, microalgae have triglyceride production rates 10-200 times faster than terrestrial oil crops such as soybean and rapeseed.[9] Microalgae can be cultivated in large scale by raceway ponds and tubular photobioreactors. The former method possesses lower production cost, while the latter provides controlled environment to attain specific high value-added products. Microalgae oil is thus selected as alternative triglyceride feedstock for fundamental and applied studies in the present work.

The current limitation for the production of biofuels from microalgae oil is the high cultivation cost, which is 5-10 times higher than the cost of lignocellulosic biomass. The cost for CO_2 is 20-30% of the total cost, and it would decrease by using waste CO_2 from coal power plants. The reduction of cost also strongly depends on the improvements of microalgae biology through genetic and metabolic engineering. In addition, economically feasible biofuels production from microalgae will only be achieved in conjunction with production of bulk chemicals and high value-added food products such as DHA, EPA, omega-3 fatty acids and vitamins.

1.3. Technology for triglyceride conversion

Triglycerides can be directly used in diesel engines, but the direct combustion causes many engine problems due to the high viscosity and low volatility of triglycerides, e.g., carbon deposits, coking on the injector, and oil ring sticking.[12] These problems require triglycerides to be upgraded before using as biofuel. The commercial upgrading process involves transesterification of triglycerides and alcohol into fatty acid alkyl esters (FAAEs) and glycerol which is applied in the first generation biodiesel production. Triglycerides can also be refined by cracking, pyrolysis, hydrotreating and deoxygenation processes to produce hydrocarbons as next generation biofuel.

1.3.1. Transesterification

In Europe, the biodiesel produced from transesterification of triglycerides is increasing exponentially (see Figure 1-3), reaching 9,500,000 tons in 2010.[13] This leads to the overproduction of byproduct glycerol, which is estimated to be 950,000 tons in Europe last year. Transesterification consists three consecutive reversible reactions of triglycerides to diglycerides, followed by diglycerides to monoglycerides, and finally to FAMEs and glycerol. The overall reaction is shown in Eq. 1-1.
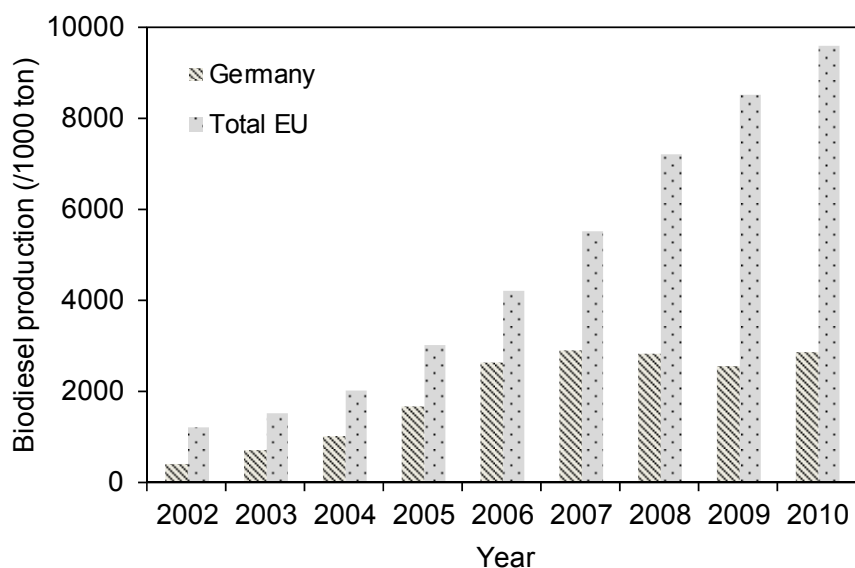
Figure 1-3. Biodiesel production trend in EU 2002-2010

Triglycerides   Methanol   Glycerol   FAMEs (biodiesel)

(1-1)
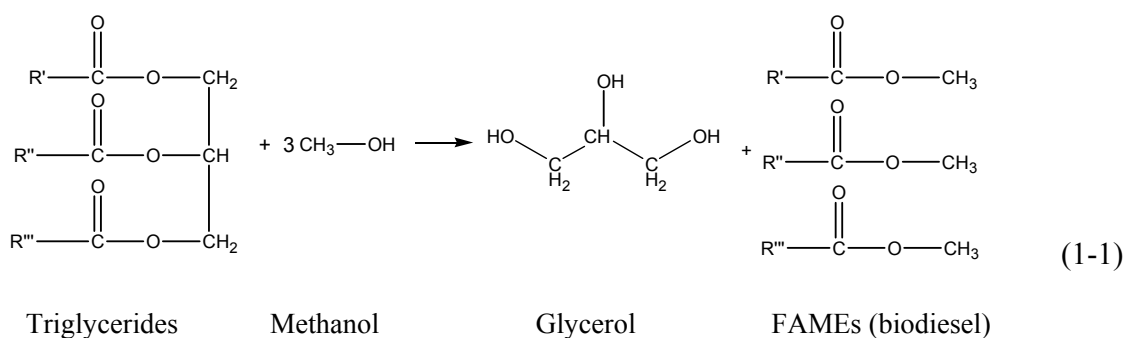
The transesterification reaction can be catalyzed by a homogeneous or a heterogeneous catalyst, or by an enzyme. The homogeneous alkaline catalysts such as sodium or potassium hydroxide and potassium methoxide are commonly used in commercial biodiesel production process.[14] The alkali-catalyzed transesterification leads to complete conversion with 98% ester yields by using a molar ratio of alcohol to triglyceride of 6:1 and reaction temperature close to the alcohol boiling point (65 ^{o}C for methanol). Once the reaction is finished, the products are settled into two phases, i.e., the bottom glycerol-rich phase and the upper ester-rich phase. After phase separation, the excess alcohol in each phase is removed through flash evaporation or by distillation. Finally, the ester is purified to use as biodiesel by washing with warm water to remove residual catalysts and soap followed by dry, while the glycerol is neutralized with acid and is further distilled to high purity.

The homogeneous base catalysts have several advantages like mild reaction conditions, high reaction rates and no mass transfer limitations.[15] However, the use of these catalysts also causes some problems, e.g., catalyst recovery, products separation, and disposal of toxic waste. Moreover, anhydrous alcohols are required to avoid water caused saponification, and only high purity triglycerides, i.e., the free fatty acids (FFAs) content less than 0.5 wt%,[16,17] can be converted with base catalysts due to the possible saponification. On the contrary, an efficient heterogeneous catalyst (especially solid acid) would not face catalyst separation issue, and these catalysts can be recycled and reused. Solid acid catalysts also offer the advantage that they can catalyze transesterification of triglycerides and esterification of FFAs simultaneously, and thus low-grade triglycerides with high content of FFAs can also be converted without any pretreatment. Sulfated

metal oxides (e.g., ZrO_2, TiO_2), mixed metal oxides (e.g., tungstated zirconia, zirconia titania), and supported heteropolyacids have been intensively studied in literatures.[18, 19] Generally, high reaction temperature (120-250 ^oC), high reaction pressure and longer reaction time are required due to the much lower activity of solid acid catalysts in comparison with homogeneous alkaline catalysts.

1.3.2. Cracking

Although most of the current biofuels are produced through transesterification process, these fatty acid alkyl esters have the problems of a relatively high oxygen content and poor flow property at low temperatures, limiting their application as high-grade fuels.[20] Catalytic cracking is an alternative method for upgrading triglycerides to produce fuels, and it has been studied with various zeolite catalysts.[21,22]

HZSM-5, HBeta and USY zeolites have been employed to study the cracking of palm oils in a fix-bed reactor at 350-450 ^oC and atmospheric pressure. These three zeolites lead to 99%, 82% and 53% conversion with gasoline selectivity of 28%, 22% and 7%, respectively.[21] When mesoporous materials such as MCM-41 are applied, the selectivity of gasoline increases to 40% due to the suppressed production of gaseous products.[22]

The main products obtained from zeolite catalyzed cracking are linear and cyclic paraffins, olefins, and oxygenated compounds including aldehydes, ketones and carboxylic acids. Many reactions, e.g. cracking, hydrolysis, isomerization, dehydrogenation, aromatization (Diels-Alder reaction) and coking occur during this process. Scheme 1-1 shows a proposed reaction mechanism for soybean oil conversion.[23] Usually these reactions proceed through either a free radical or carbonium ion mechanism.

The utilization of cracking method to upgrade triglycerides has several drawbacks. The large amount of oxygenated compounds in the products would obstacle the application as fuels due to the challenges both in storage and in internal combustion engine. Another issue is that the products contain many aromatic compounds, and their use is strictly regulated in Europe. Most importantly, zeolite cracking is a non-selective process that produces a wide range of compounds and undesired coking formation.
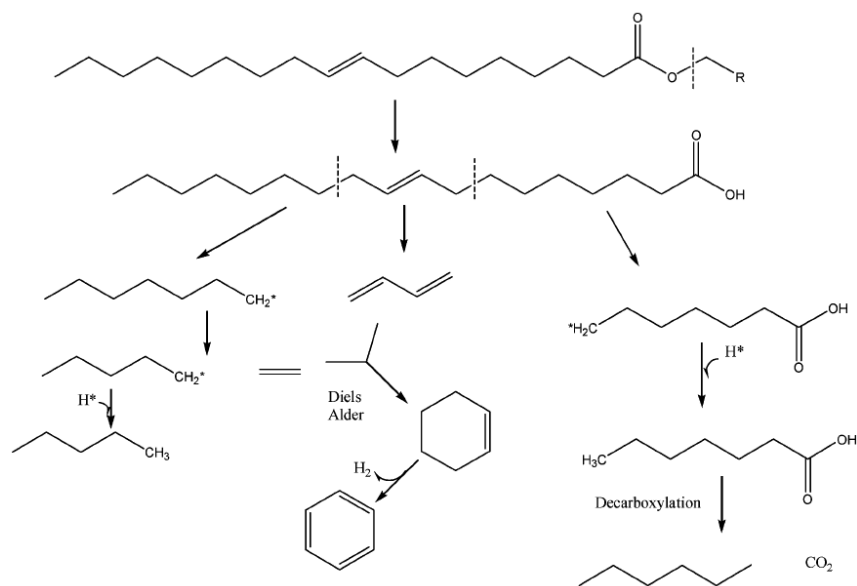
Scheme 1-1. Mechanism for triglycerides cracking[23]

1.3.3. Hydrotreating

Triglycerides can also be hydrotreated with conventional hydrotreating catalyst (e.g., sulfided NiMo and CoMo) by petroleum refinery infrastructure to produce straight chain alkanes ranging from C_{12} to C_{18} at 350-450 ^{o}C in presence of 40-150 bar H_2.[24, 25] It has been commercialized by Neste Oil and UOP. Compared with catalytic cracking, hydrotreating process is much more selective in producing diesel range hydrocarbons. For example, hydroprocessing of pure sunflower oil with sulfided NiMo/Al$_2$O$_3$ at 350 ^{o}C leads to full conversion with 71% yield of straight chain C_{15}-C_{18} alkanes (based on carbon basis).[24]

The conversion of triglycerides via hydrotreating process involves, i) hydrogenation of double bonds in the alkyl chain of fatty acids, ii) hydrogenolysis of saturated triglycerides leading to fatty acids, iii) hydrodeoxygenation, or decarbonylation, or decarboxylation of fatty acids to alkanes (see Scheme 1-2). The carbon backbone of triglycerides is converted into propane as a valuable byproduct. The oxygen in the triglycerides is removed either through decarboxylation/decarbonylation to CO_2/CO or via hydrodeoxygenation to H_2O.

However, these sulfided catalysts contaminate products via sulfur leaching, and deactivate due to its removal from the surface by a reverse Mars van Krevelen mechanism.[26] The trace amount of produced water would accelerate the leaching process and severely affect the lifetime of these sulfided catalysts. Furthermore, the formed carbon oxides cause issues with the separation from the recycle gas. It would be attractive to develop stable and active non-sulfided catalysts to replace conventional hydrotreating catalysts.
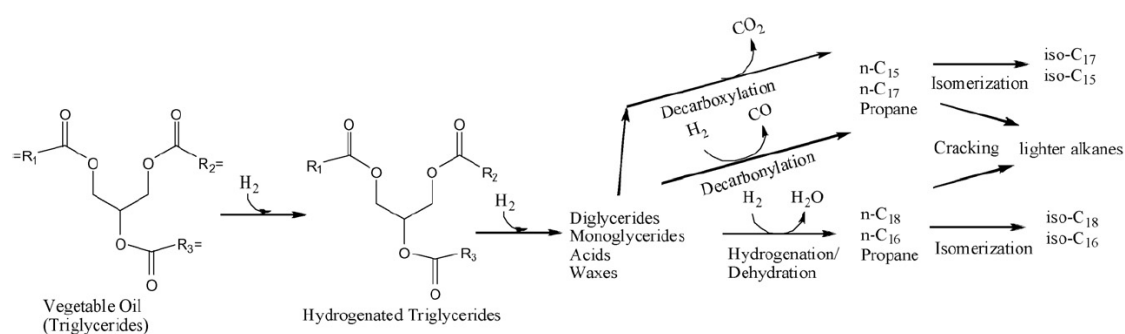
Scheme 1-2. Reaction pathways for conversion of triglycerides to alkanes[24]

1.3.4. Deoxygenation

Catalytic deoxygenation is another alternative technique that can be applied for fatty acids and triglycerides upgrading.[27-30] Noble metal supported catalysts (e.g., commercial Pd/C and Pt/C) are usually employed. Compared with hydrotreating process, catalytic deoxygenation possesses several advantages, including higher selectivity to the target linear hydrocarbons and less additional hydrogen cost because of no or few hydrogen requirement. Stearic acid can be completely converted into linear C_{17} alkanes with 95% selectivity over 5 wt% Pd/C in semi-batch mode at 300 $^{\circ}$C under 17 bar of 5% H_2 in argon. Catalyst screening shows that the deoxygenation rates decrease in the sequence of Pd > Pt > Ni > Rh > Ir > Ru > Os.[27]

The proposed plausible reaction route for the conversion of fatty acids to linear alkanes is shown below (see Eq.1-2 to Eq. 1-4). Decarboxylation, decarbonylation and hydrodeoxygenation are the main reaction routes. As the hydrogen consumption for the

deoxygenation of fatty acids follows the increasing orders of decarboxylation < decarbonylation < hydrodeoxygenation, in principle, the decarbonylation or decarboxylation route is more applicable than the hydrodeoxygenation pathway. In the vapor phase, methanation and water gas shift are the main reactions. Thermodynamic data are provided for the conversion of palmitic acid to C_{15} and C_{16} alkanes together with gas phase reactions at 260 °C.

These noble metal catalysts showed high activities and selectivities for fatty acids conversion; however, they exhibited much lower activities and selectivities to the target alkanes when converting triglycerides. The performance was only somewhat improved by a Pt-Re/ZSM-5 catalyst.[31] Moreover, the high price of noble metal also limits the application in large-scale industrial production.

Liquid phase		ΔG_{533} (kJ/mol)	ΔH_{533} (kJ/mol)	
Hydrodeoxygenation:	$R\text{-}COOH + 3\ H_2 \longrightarrow R\text{-}CH_3 + 2\ H_2O$	-88.0	-112.6	(1-2)
Decarbonylation:	$R\text{-}COOH + H_2 \longrightarrow R\text{-}H + CO + H_2O$	-59.5	49.7	(1-3)
Decarboxylation:	$R\text{-}COOH \longrightarrow R\text{-}H + CO_2$	-78.6	10.1	(1-4)
Gas phase				
Methanation:	$CO + 3\ H_2 \longrightarrow CH_4 + H_2O$	-88.4	-215.3	(1-5)
Methanation:	$CO_2 + 4\ H_2 \longrightarrow CH_4 + 2\ H_2O$	-69.2	-175.7	(1-6)
Water gas shift:	$CO + H_2O \longrightarrow CO_2 + H_2$	-19.1	-39.6	(1-7)

1.4. Glycerol utilization

Glycerol is a very attractive feedstock due to its relatively low cost and wide availability as a byproduct of biodiesel production. It is considered to be, therefore, one

of the top 12 building block chemicals of a biorefinery process.[32] Glycerol can be either converted to high value-added oxygenated chemicals such as propanediols via hydrodeoxygenation, or can be used to produce hydrogen through aqueous phase reforming or gas phase reforming process. The aqueous phase deoxygenation of glycerol to propanediols requires selectively cleaving one of the C-O bonds, but preserving the C-C bonds. It occurs catalytically on dual functional catalysts via consecutive dehydration and hydrogenation in the presence of H_2 at moderate temperatures (180-270 ^{o}C) and relatively high pressures (20-150 bar).[33,34] On the other hand, the parallel route of aqueous phase reforming (APR) also occurs at identical conditions used for hydrodeoxygenation of alcohols, by contrast, it requires cleaving C-C bonds but preserving C-O bonds.[4]

The influence of metal (Pt, Pd, Ru, Rh, Ir, and Ni supported on silica) on APR has been comparatively investigated for ethylene glycol conversion at reaction temperature of 225 ^{o}C and 22 bar reaction pressure.[35] The reaction rates of ethylene glycol reforming decrease in the sequence of Pt $\approx$ Ni > Ru > Rh $\approx$ Pd > Ir. Furthermore, Rh, Ru and Ni based catalysts show low selectivity for hydrogen production, while Pt and Pd exhibit relatively high selectivity to hydrogen. The influence of support (TiO_2, Al_2O_3, C, SiO_2, SiO_2-Al_2O_3, ZrO_2, CeO_2, and ZnO supported Pt) also has been explored for the APR of ethylene glycol under identical reaction conditions. It is observed that the turnover frequencies for the hydrogen production follow the order as TiO_2 > Al_2O_3 $\approx$ C > SiO_2-Al_2O_3 $\approx$ ZrO_2 > CeO_2 $\approx$ ZnO $\approx$ SiO_2. Pt supported on Al_2O_3, and to a less extent ZrO_2 exhibit high selectivity to hydrogen production. Whereas, Pt supported on C, TiO_2, and SiO_2-Al_2O_3 show poor selectivity to hydrogen due to severe side reactions leading to gaseous alkanes and liquid phase compounds.
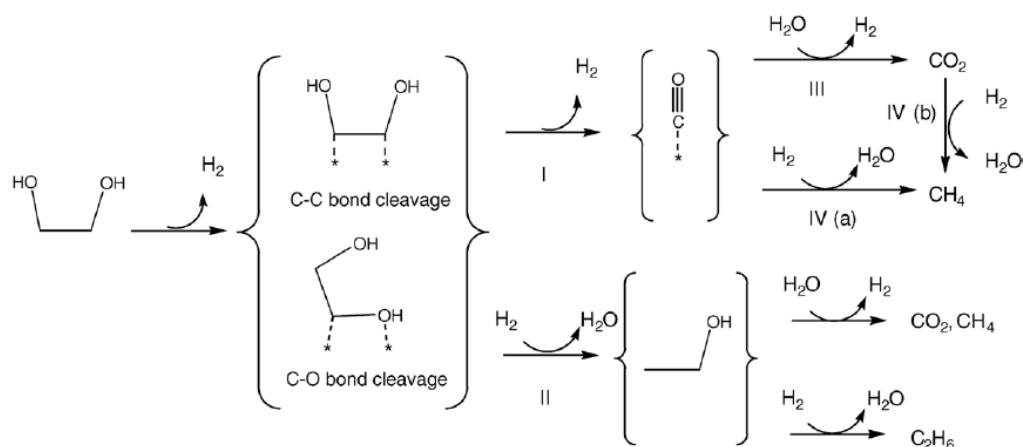
Scheme 1-3. Proposed reaction pathways for the conversion of ethylene glycol[36]
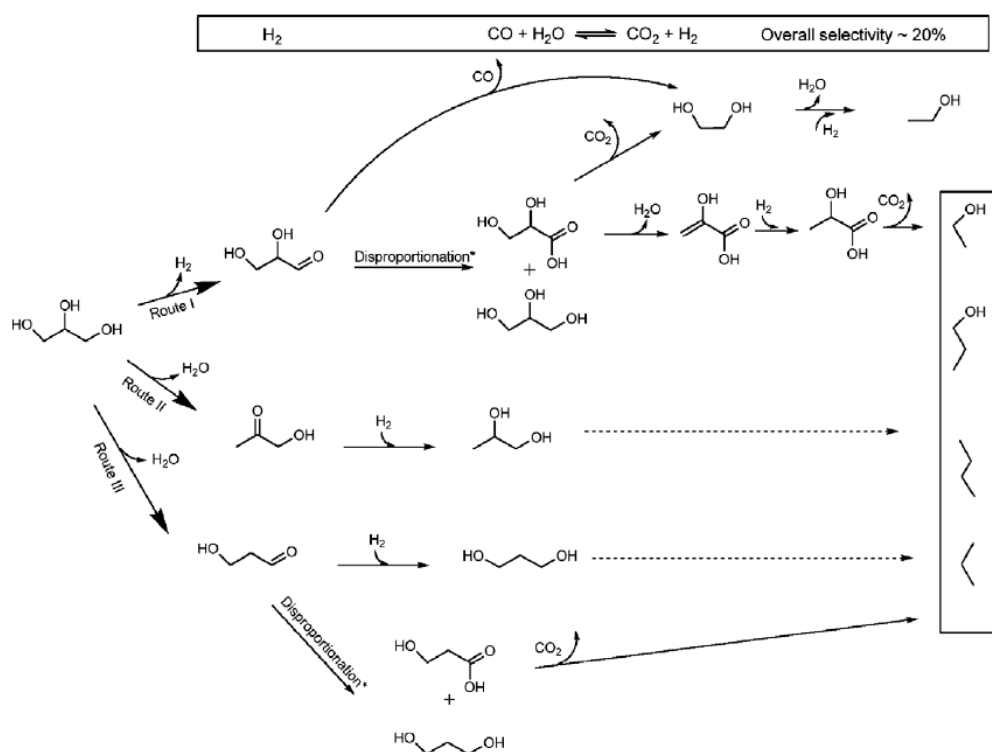
Scheme 1-4. Reaction pathways for an aqueous phase glycerol reforming, dotted arrows indicate a series of reaction in analogy to those depicted in route I (*either via Tishchenko or Cannizzaro type reactions)[37]

The competing pathways of aqueous phase reforming have been studied by Dumesic (see Scheme 1-3).[36] The pathway for C-O bond cleavage was suggested to occur either

through dehydrogenation to form surface adsorbed species followed by direct cleavage catalyzed by metallic sites or via dehydration reactions catalyzed by acid sites associated with catalyst support. The mechanism for C-C bond cleavage was also speculated to be cleaved by the metal catalyzed direct hydrogenolysis to form surface adsorbed CO species, which was in turn removed from the surface by water gas shift reaction to form CO_2 and H_2.

However, we showed the first evidence in a recent paper that direct hydrogenolytic cleavage of C-C bonds does not occur. Detailed analysis of the reaction network shows that ''reforming'' and hydrodeoxygenation require the presence of a bifunctional catalyst, i.e., the presence of an acid–base and a metal function. The initial reaction steps are identified to be dehydrogenation and dehydration. The dehydrogenation of hydroxyl groups at primary carbon atoms is followed by decarbonylation and subsequent water gas shift or by disproportionation to the carboxylic acid (and the alcohol) followed by decarboxylation (see Scheme 1-4).[37]

1.5. Scope of this thesis

In this doctoral thesis, selective transformation of triglycerides (microalgae oil) and fatty acids (palmitic acid and stearic acid) into diesel range alkanes by heterogeneous transition metal catalysts is the major purpose. The overall strategy for triglycerides conversion is shown in Scheme 1-5. Liquid hydrocarbons are produced through triglycerides hydrotreating process with sulfur-free supported metal catalysts, and hydrogen is provided from aqueous phase reforming of glycerol which is the byproduct derived from the transesterification of triglycerides to biodiesel.

In the first part, the kinetics in the catalytic conversion of C_3 alcohol molecules with different position of the hydroxyl group and number of hydroxyl groups (mono-alcohols, i.e., 1-propanol and 2-propanol; diols, i.e., 1,2-propanediol and 1,3-propanediol; and triol, i.e., glycerol) were systematically studied over Pt/Al_2O_3 in order to elucidate the reaction pathways and fundamental chemistry that lead to the C-C and C-O bond cleavage in the aqueous phase alcohol transformation. In addition, the different activity performances of

2-propanol in the gas phase and in the aqueous phase over Pt/Al_2O_3 have also been compared to elucidate specific effects of the aqueous environment.

Prior to the conversion of triglycerides, the deoxygenation of fatty acid (i.e., C_{16} palmitic acid) to C_{15} *n*-pentadecane was systematically investigated with a variety of sulfur-free supported metal catalysts in the presence or absence of H_2. The kinetics in the catalytic conversion of palmitic acid and the reaction intermediates, i.e., 1-hexadecanol and palmityl palmitate, were also investigated over Ni/ZrO_2 in order to elucidate the reaction pathways. The influences of metal (Pt, Pd, and Ni), support (C, ZrO_2, Al_2O_3, SiO_2, HBeta, and HZSM-5), and carrier gas (H_2, N_2, and H_2-N_2 mixture) have also been comparatively explored.

After detailed study of fatty acids conversion, crude microalgae oil (triglycerides) were also quantitatively and efficiently converted into diesel range alkanes in both batch and continuous flow reactors either with Ni/ZrO_2 via hydrogenolysis-hydrogenation-decarbonylation route or with Ni/HBeta through hydrogenolysis-hydrodeoxygenation route. Meanwhile, the detailed transformation reaction pathways and fundamental chemistry were explored by studying the kinetics of reactant and intermediates conversion.
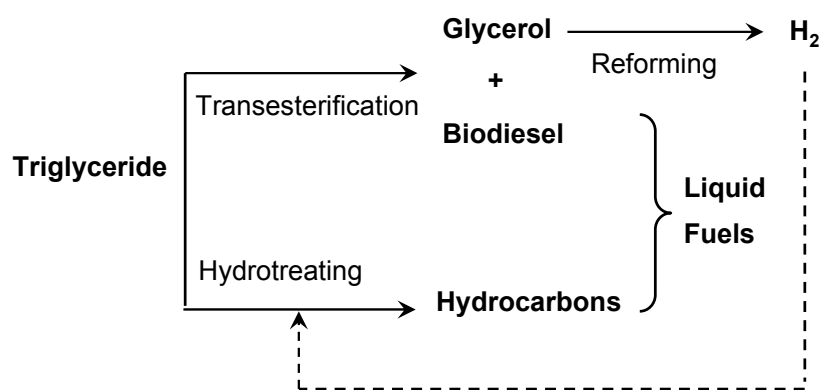
Scheme 1-5. Strategy for converting triglycerides into biofuels

1.6. References

1. J. Van Gerpen, Fuel Process. Technol. 86 (2005) 1097.

2. Commission of the European Communities, An EU strategy for biofuels, 2006. Available from http://ec.europa.eu/agriculture/biomass/biofuel/com2006_34_en.pdf.

3. Shell energy scenarios to 2050, 2008. Available from http://www-static.shell.com/static/public/downloads/brochures/corporate_pkg/scenarios/shell_energy_scenarios_2050.pdf.

4. G. W. Huber, J. A. Dumesic, Catal. Today 111 (2006) 119.

5. K. Bendz, EU-25 oilseeds and products biofuels situation in the European Union 2005.

6. G. Knothe, Fuel Process. Technol. 86 (2005) 1059.

7. S. V. Ghadge, H. Raheman, Bioresour. Technol. 97 (2006) 379.

8. P. K. Sahoo, L. M. Das, Fuel 88 (2009) 994.

9. Y. Chisti, Biotech. Adv. 25 (2007) 294.

10. R. H. Wijffels, M. J. Barbosa, Science, 329 (2010) 796.

11. P. Spolaore, C. Joannis-Cassan, E. Duran, A. Isambert, J. Biosci. Bioeng. 101 (2006) 87.

12. F. Ma, M. A. Hanna, Bioresour. Technol. 70 (1999) 1.

13. European Biodiesel Board, http://www.ebb-eu.org/stats.php.

14. J. V. Gerpen, G. Knothe, In the biodiesel handbook, AOCS Press: Champaign, IL, 2005.

15. I. K. Mbaraka, B. H. Shanks, J. Am. Oil Chem. Soc. 83 (2006) 79.

16. E. Lotero, J. G. Goodwin, D. A. Bruce, K. Suwannakarn, L. Liu, D. E. Lopez, Catalysis 19 (2006) 41.

17. E. Lotero, Y. Liu Y, D. E. Lopez, K. Suwannakarn K, D. A. Bruce, J. G. Goodwin, Ind. Eng. Chem. Res. 44 (2005) 5353.

18. J. A. Melero, J. Iglesias, G. Morales, Green Chem. 11 (2009) 1285.

19. B. X. Peng, Q. Shu, J. F. Wang, G. R. Wang, D. Z. Wang, M. H. Han, Process. Saf. Environ. Prot. 86 (2008) 441.

20. P. Šimácek, D. Kubicka, G. Šebor, M. Pospíšil, Fuel 88 (2009) 456.

21. A. Corma, G. W. Huber, L. Sauvanaud, P. O'Connor, J. Catal. 247 (2007) 307.

22. F. A. Twaiq, N. A. M. Zabidi, A. R. Mohamed, S. Bhatia, Fuel Process.Technol. 84 (2003) 105.

23. A.W. Schwab, G.J. Dystra, E. Selke, S.C. Sorenson, E.H. Pryde, J. Am. Oil Chem. Soc. 65 (1988) 1781.

24. G. W. Huber, P. O'Connor, A. Corma, Appl. Catal. A: Gen. 329 (2007) 120

25. P. Simácek, D. Kubicka, G. Sebor, M. Pospíšil, Fuel 88 (2009) 456.

26. E. Laurent, B. Delmon, J. Catal. 146 (1994) 281.

27. M. Snåre, I. Kubičková, P. Mäki-Arvela, K. Eränen, D. Y. Murzin, Ind. Eng. Chem. Res. 45 (2006) 5708.

28. M. Snåre, I. Kubičková, P. Mäki-Arvela, D. Chichova, K. Eränen, D. Yu. Murzin, Fuel 87 (2008) 933.

29. J. G. Immer, M. J. Kelly, H. H. Lamb, Appl. Catal. A: Gen. 375 (2010) 134.

30. W. F. Maier, W. Roth, I. Thies, P. Ragué Schleyer, Chem. Ber. 115 (1982) 808.

31. K. Murata, Y. Liu, M. Inaba, I. Takahara, Energy Fuels 24 (2010) 2404.

32. T. Werpy, G. Petersen, Top value added chemicals from biomass, US DOE Report, 2004.

33. T. Miyazawa, S. Koso, K. Kunimori, K. Tomishige, Appl. Catal. A 329 (2007) 30.

34. D.G. Lahr, B.H. Shanks, J. Catal. 232 (2005) 386.

35. R.R. Davda, J.W. Shabaker, G.W. Huber, R.D. Cortright, J.A. Dumesic, Appl. Catal. B 43 (2003) 13.

36. J.W. Shabaker, G.W. Huber, J.A. Dumesic, J. Catal. 222 (2004) 180.

37. A. Wawrzetz, B. Peng, A. Hrabar, A. Jentys, A. A. Lemonidou, J. A. Lercher, J. Catal. 269 (2010) 411.

Chapter 2

Comparison of kinetics and reaction pathways for hydrodeoxygenation of C$_3$ alcohols on Pt/Al$_2$O$_3$

The catalytic hydrodeoxygenation of C$_3$ alcohols (1- and 2-propanol, 1,2- and 1,3-propanediol, and glycerol) on Pt/Al$_2$O$_3$ has been mechanistically explored in the aqueous phase. Dehydrogenation on Pt and dehydration on alumina are the main elementary reaction pathways. In water, carbon-carbon bond cleavage for alcohols with terminal hydroxyl groups occurs via decarbonylation of aldehydes (generated by dehydrogenation of alcohols) and decarboxylation of acids, the latter being formed by disproportionation from aldehydes. The presence of water as solvent suppresses the dehydration for mono-alcohols mainly via blocking of Lewis acid sites by water. Dehydration is still the dominating primary reaction for 1,3-propanediol and glycerol, as the higher number of hydroxyl groups weakens the C-O bond strength. The overall reactivity of C$_3$ alcohols decreases in the order of 1,3-propanediol ≈ glycerol > 1,2-propanediol ≈ 1-propanol.

2.1. Introduction

Selective conversion of biomass resources such as polysaccharides [1,2], lignin [3,4], bio-ethanol, and glycerol [5-11] requires highly efficient catalysts. Within this biomass feedstock, glycerol is a very attractive option due to its relatively low cost and wide availability as a by-product of bio-diesel production. It is considered to be, therefore, one of the top 12 building block chemicals of a biorefinery process [12].

Glycerol can be either converted to high value-added oxygenated chemicals such as propanediols via hydrodeoxygenation, or can be used to produce hydrogen through aqueous phase reforming process. The aqueous phase deoxygenation of glycerol to propanediols requires selectively cleaving one of the C-O bonds, but preserving the C-C bonds. It occurs catalytically on dual functional catalysts via consecutive dehydration and hydrogenation in the presence of H_2 at moderate temperatures (453-543 K) and relatively high pressures (20-150 bar) [13-17]. On the other hand, the parallel route of aqueous phase reforming (APR) also occurs at identical conditions used for hydrodeoxygenation of alcohols [9-11]. The bifunctional catalyst Pt supported on Al_2O_3, which had potential hydrodeoxygenation ability on alcohols and exhibited exceeding 90% hydrogen selectivity from APR of alcohols [18,19], was selected in this work.

The competing pathways of aqueous phase hydrodeoxygenation and reforming have been extensively explored by Dumesic [9-11], Davis [20,21], Tomishige [14,22], and ourselves [23]. The key feature in determining the selectivity is the way and the extent of C-C and C-O bond cleavage. The pathway for C-O bond cleavage was suggested to occur either through dehydrogenation to form surface adsorbed species followed by direct cleavage catalyzed by metallic sites or via dehydration reactions catalyzed by acid sites associated with catalyst support [9]. The mechanism for C-C bond cleavage in aqueous phase reforming of alcohols producing smaller alkanes, CO_2, and H_2 has not been unequivocally explained. While, the C-C bonds in alcohols were speculated to be cleaved by the metal catalyzed direct hydrogenolysis [9,18], we showed first evidence in a recent paper that direct hydrogenolytic cleavage of C-C bonds does not occur [23].

In the present paper, the kinetics in the catalytic conversion of C₃ alcohol molecules with different position of the hydroxyl group and number of hydroxyl groups (mono-

alcohols, i.e., 1-propanol and 2-propanol; diols, i.e., 1,2-propanediol and 1,3-propanediol; and triol, i.e., glycerol) were systematically studied over Pt/Al$_2$O$_3$ in order to elucidate the reaction pathways and fundamental chemistry that lead to the C-C and C-O bond cleavage in the aqueous phase alcohol transformation. In addition, the different activity performances of 2-propanol in the gas phase and in the aqueous phase over Pt/Al$_2$O$_3$ have also been compared to elucidate specific effects of the aqueous environment.

2.2. Experimental section

2.2.1. Catalysts preparation

The 3 wt.% Pt/Al$_2$O$_3$ catalyst was prepared by the incipient wetness impregnation method, with platinum(II)-ammonium nitrate ([Pt(NH$_3$)$_4$](NO$_3$)$_2$, Strem chemicals) as precursor and γ-Al$_2$O$_3$ (Aeroxide Alu C-Degussa, specific surface area: 105 m^2/g) as carrier. After impregnating the carrier with the aqueous solution of Pt precursor at ambient temperature, the catalyst was dried in air at 393 K for 12 hours and calcined in synthetic air for 2 hours at 673 K. Prior to the reaction and characterization, the catalyst was reduced in H$_2$ at 573 K for 2 hours.

2.2.2. Catalyst characterization

Atomic absorption spectroscopy (AAS) was used for analyzing the metal loading. The nitrogen adsorption-desorption was adopted for measuring BET surface area and pore size distribution. The fraction of accessible Pt atoms was detected by hydrogen chemisorption. The temperature programmed desorption (TPD) of ammonia and carbon dioxide were used for acid and basic sites measuring. The characterization methods have been described in detail in a previous publication [23].

2.2.3. Catalyzed reactions

Gas phase reaction

The dehydrogenation/dehydration of 2-propanol was performed in a continuous fixed bed flow reactor at atmospheric pressure and temperature ranging from 393 to 523 K. The quartz tubular reactor (4 mm diameter) was packed with 20 mg catalyst diluted in 100 mg SiC. After the catalyst activation in H_2 at 573 K for 2 hours, the reaction was performed by introducing a H_2 flow saturated with 2-propanol at 286.2 K (the 2-propanol partial pressure was 25 mbar) into the reactor. The effluent products were analyzed by a gas chromatography equipped with FID detector and Supelco-Wax column.

Aqueous phase reaction

Experiments with 1-propanol, 2-propanol, 1,2-propanediol, 1,3-propanediol, and glycerol were conducted in a 300 ml batch autoclave (Parr Instrument). The reactants and the catalyst loaded in a closed glass vial were charged into the reactor, and then the reactor was purged with N_2, which was also used as internal standard for vapor phase products analysis. When the required temperature and pressure were reached, the reaction was started after breaking the glass vial by stirring. The vapor phase was analyzed online by a gas chromatograph with TCD detector and two capillary columns (MS-5A and HP-Plot Q). Liquid samples were manually collected during the run and analyzed in a gas chromatography equipped with an FID detector and a CP-Wax 57CB column. Typical reactions were conducted under the following conditions: 473 K, 40 bar total pressure of H_2, 100 g of 10 wt.% reactant aqueous solution, 0.3 g 3 wt.% Pt/Al_2O_3, and 600 rpm stirring speed. All results were calculated and reported based on carbon basis.

2.2.4. Equilibrium and CO_2 solubility calculation

The reaction equilibrium compositions were calculated using the HSC software. Under reaction temperature and pressure, CO_2 would be produced and partially dissolved in water. This part of CO_2 cannot be detected by gas chromatograph, but needs to be considered for an accurate analysis. The solubility of CO_2 in water was, therefore,

calculated according to the published literature [24]. At 473 K and a relatively low CO$_2$ partial pressure, the solubility of CO$_2$ in water approximately equals to $10^{-2}*p_{CO2}$ (mol/kg water, p_{CO2} in unit of bar).

2.3. Results and discussion

2.3.1. Catalysts characterization

The physicochemical properties of the 3 wt.% Pt/Al$_2$O$_3$ are summarized in Table 2-1. The BET specific surface area was 88 m^2/g, while the dispersion of Pt was 90%. The acid and base site concentrations of 3 wt.% Pt/Al$_2$O$_3$ were 0.160 and 0.015 mmol/g, respectively. It should be noted that the acid-base properties only represent the starting catalyst, as the alumina support transforms during the reaction under hydrothermal environment into aluminum hydroxide (Böhmite).

Table 2-1: Physicochemical properties of Pt/Al$_2$O$_3$ catalyst

Catalyst	Pt loading (wt.%)	Surface area (m^2/g)	Dispersion (H/Pt)	Acidity (mmolNH$_3$/g)	Basicity (mmolCO$_2$/g)
Pt/Al$_2$O$_3$	2.93	88	0.90	0.16	0.015

2.3.2. Conversion of 2-propanol on Pt/Al$_2$O$_3$ in the gas phase

In order to compare the catalytic conversion of an alcohol at the gas-solid interface with the conversion at the aqueous-solid interface, we firstly explored the reactions of 2-propanol on Pt/Al$_2$O$_3$ in the gas phase. It is known that the catalyst acidity is related to its ability to dehydrate 2-propanol to propene, while its dehydrogenation to acetone is catalyzed by a catalytic function that is able to abstract a proton by a strong basic site and the hydride anion by a Lewis acid site or a metal function [25, 26]. The results of 2-propanol conversion over 3 wt.% Pt/Al$_2$O$_3$ at 1 bar in the gas phase are shown in Fig.2-1.
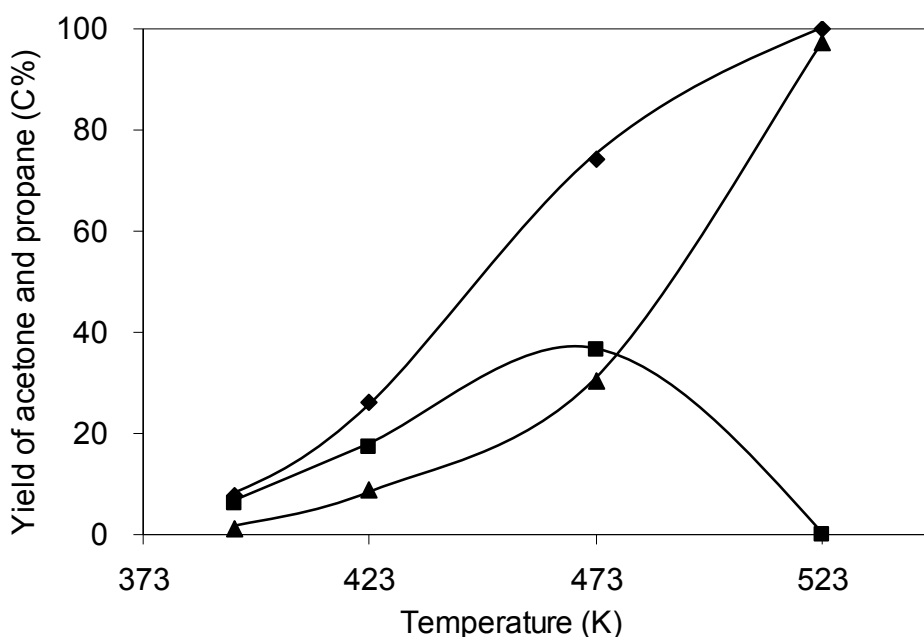
Figure 2-1. Conversion of 2-propanol (◆) and yield of acetone (■) and propane (▲) as a function of temperature on 3 wt. % Pt/Al$_2$O$_3$ in gas phase reaction. (Reaction conditions: 3 wt.% Pt/Al$_2$O$_3$ 20 mg, 2-propanol partial pressure 25 mbar, H$_2$ flow 40 ml/min)

It shows that the dehydrogenation and dehydration competed over the whole conversion range. Dehydrogenation of 2-propanol to acetone over 3 wt.% Pt/Al$_2$O$_3$ was the dominating reaction at relatively low temperatures (below 473 K), while propane formed via consecutive dehydration and hydrogenation became the major product at higher temperatures. In addition, pure Al$_2$O$_3$ selectively dehydrated of 2-propanol to propene at identical conditions. Therefore, it can be concluded that dehydration was catalyzed by the Lewis acid sites of Al$_2$O$_3$ (reaction rate at 473 K: 69.0 mmol$^.$s^{-1}·mol$_{acid site}^{-1}$) and Pt was responsible for the dehydrogenation (reaction rate at 473 K: 96.0 mmol$^.$s^{-1}·mol$_{Pt\text{-}surf.atom}^{-1}$). The apparent activation energies for dehydration and dehydrogenation of 2-propanol over 3 wt.% Pt/Al$_2$O$_3$ were 71 and 44 kJ/mol, respectively.

2.3.3. Conversion of 2-propanol on Pt/Al₂O₃ in the aqueous phase

The dehydrogenation to acetone was the dominating primary reaction of the conversion of 2-propanol on Pt/Al₂O₃ at 473 K in the aqueous phase (see Fig. 2-2). The initial rate of dehydrogenation (48.0 mmol·s⁻¹·mol$_{Pt-surf.atom}$⁻¹) was reduced to 50% of the rate found in the gas phase (96.0 mmol·s⁻¹·mol$_{Pt-surf.atom}$⁻¹). As the hydrogen concentration (0.023 mol/L, calculated from the solubility of hydrogen in water [27]) in aqueous phase reaction is comparable with that in the gas phase reaction (0.026 mol/L), the activity coefficient of hydrogen is close to one. We speculate that the slower dehydrogenation rate in aqueous phase is, therefore, mainly related to the competitive adsorption of water and 2-propanol on Pt active sites. Only a small fraction was converted to propane, presumably via the slow dehydration of the alcohol on the Al₂O₃ support (initial rate: 0.4 mmol·s⁻¹·mol$_{acid\ site}$⁻¹) and the following hydrogenation on Pt.

Figure 2-2. Yield of acetone (■) and propane (▲) on conversion of 2-propanol over 3 wt.% Pt/Al₂O₃ as a function of time in aqueous solution. (Experimental conditions: T=473 K, total pressure 40 bar H₂, 2-propanol concentration 10 wt.%)

It is important to note that the dehydration rate of 2-propanol in the aqueous phase was two orders of magnitude slower than that in the gas phase (see Table 2-2). This could be attributed either to the decrease in Lewis acidity caused by the transformation of γ-Al_2O_3 to aluminum hydroxide (Böhmite) [28, 29], or to the fact that water essentially blocks the Lewis acid sites active in dehydrating 2-propanol in the gas phase. As it has been established that the transformation of γ-Al_2O_3 in water is a relatively slow process [29], and the decrease of 2-propanol dehydration rate is substantial even at initial time when alumina is still not measurably converted, we conclude the drastic activity change of Pt/Al_2O_3 in aqueous solution is mainly caused by the competitive adsorption of water on Lewis acid sites.

Table 2-2: Comparison of reaction rates for conversion of C_3 alcohols in aqueous phase at 473 K

Reactants	Reaction pathways, products and reaction rates		
	Dehydrogenation $(mmol \cdot s^{-1} \cdot mol_{Pt\text{-}surf.atom}^{-1})$	Dehydration $(mmol \cdot s^{-1} \cdot mol_{acid\ site}^{-1})$	Decarbonylation /decarboxylation $(mmol \cdot s^{-1} \cdot mol_{Pt\text{-}surf.atom}^{-1})$
2-propanol [a]	96.0* acetone	69.0 propane	- -
2-propanol	48.0* acetone	0.4 propane	- -
1-propanol	- -	0.3 propane	1.1* ethane, CO_2
1,2-propanediol	8.5* hydroxyacetone	0.2 1-propanol, 2-propanol	1.0 ethanol, methane, CO_2
1,3-propanediol	- -	11.5* 1-propanol	1.0 ethane, ethane, CO_2
glycerol	- -	4.6* hydroxyacetone, 1,2-propanediol	1.4 ethylene glycol, ethanol, methanol, CO_2

[a] Reaction performed under gas phase

* Primary reaction pathway and main products

Experiments with pure γ-Al_2O_3 showed a significantly lower conversion, which confirmed again that Pt is essential for 2-propanol dehydrogenation. It is noted that the potential products of C-C or C-O bond cleavage from 2-propanol were not observed, suggesting that Pt/Al_2O_3 is not able to cleave these bonds in 2-propanol under the reaction conditions. It shows unequivocally that hydrogenolysis reactions do not occur.

2.3.4. Aqueous phase conversion of 1-propanol

The products of 1-propanol conversion versus reaction time over 3 wt.% Pt/Al_2O_3 are plotted in Fig. 2-3. In contrast to 2-propanol conversion, the reaction of 1-propanol mainly led to CO_2 and ethane (initial rate: 1.1 mmol$\cdot$s$^{-1}\cdot$mol$_{Pt\text{-surf. atom}}^{-1}$). The ratio of ethane to CO_2 was approximately 2.0 based on carbon basis. The presence of H_2 (cannot be detected in H_2 atmosphere) is inferred from the reaction stoichiometry. Similar to the reaction of 2-propanol, only small amounts of propane (not shown at here) were formed from the C_3 alcohol dehydration-hydrogenation on Al_2O_3. The dehydration rate of 1-propanol (0.3 mmol$\cdot$s$^{-1}\cdot$mol$_{acid\ site}^{-1}$) was slightly lower than the rate of 2-propanol (0.4 mmol$\cdot$s$^{-1}\cdot$mol$_{acid\ site}^{-1}$) (see Table 2-2), which is in agreement with the literature [30] that the secondary hydroxyl group exhibits higher dehydration activity than the primary hydroxyl group.

Propanal was only observed in traces (concentration < 0.02 %), which suggests rapid decarbonylation to ethane and CO or disproportionation of the formed propanal to propanol and propionic acid followed by decarboxylation to ethane and CO_2. Propanal and propionic acid were clearly detected as reaction intermediates in relatively large amounts for 1-propanol conversion in the absence of hydrogen [23]. The direct pathway of hydrogenolysis of 1-propanol can be excluded, as the C-C bond strengths in 1-propanol and 2-propanol are quite similar (see Table 2-3, i.e., 357 kJ/mol for 1-propanol and 368 kJ/mol for 2-propanol). This indicates that the formation of hydrogen, ethane, and CO_2 follows a reaction pathway characterized by dehydrogenation, decarbonylation (-CO) or disproportionation (Tishchenko or Cannizzaro type reactions), and decarboxylation (-CO_2).
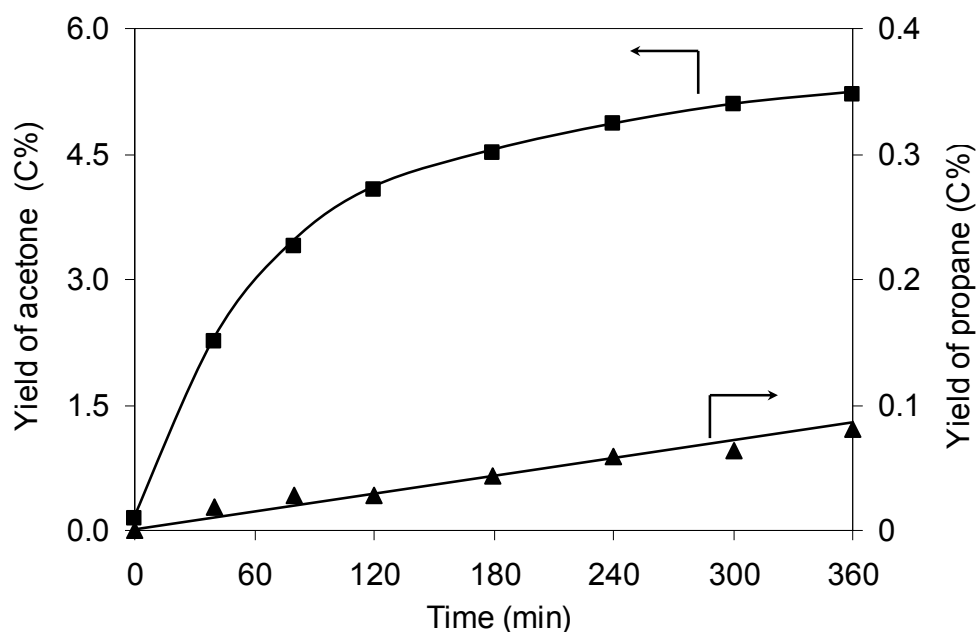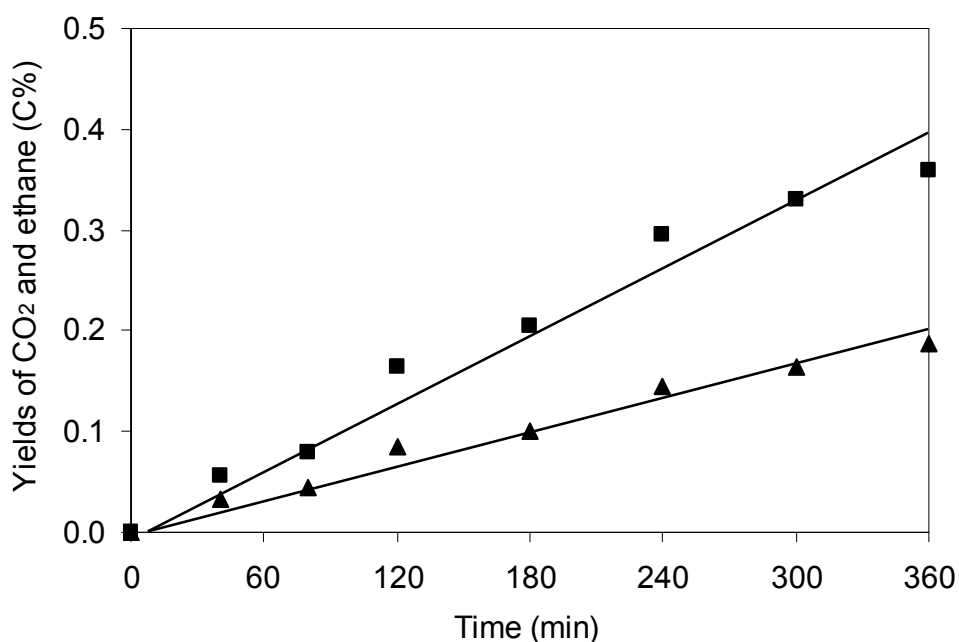
Figure 2-3. Yield of ethane (■), carbon dioxide (▲) on conversion of 1-propanol over 3 wt.% Pt/Al_2O_3 as a function of time in aqueous solution. (Experimental conditions: T=473 K, total pressure 40 bar, 1-propanol concentration 10 wt.%)

Table 2-3: C-C and C-O bond energies in C₃ alcohols [31]

Compounds	1-Propanol	2-Propanol	1,2-Propanediol	Glycerol	Glycerol
Structure	$C_2H_5CH_2$—OH	OH | CH_3-CH-CH_3	OH OH | | CH_3-CH-CH_2	OH OH OH | | | CH_2-CH-CH_2	OH OH OH | | | CH_2-CH-CH_2
C-O bond energy (kJ/mol)	392.0	397.9	-	335.6	333.0
Structure	C_2H_5—CH_2OH	OH | CH_3—CH-CH_3	OH OH | | CH_3-CH—CH_2	OH OH OH | | | CH_2-CH—CH_2	
C-C bond energy (kJ/mol)	356.9	367.8	358.9	347.0	

At present, it is not possible to differentiate between these two latter mechanisms (Tishchenko or Cannizzaro) for the disproportionation of aldehyde into an acid and an alcohol. The Tishchenko reaction is catalyzed by acid catalysts, and an ester (propylpropionate) is formed in the first step, which is subsequently rapidly hydrolyzed at the current reaction conditions. On the other hand, the occurrence of Cannizzaro reaction requires basic sites of the catalysts, and it can be strongly enhanced by transition metals [32]. Both disproportionation pathways are possible with Pt/Al_2O_3, as the Böhmite compound contains both acid and base sites.

In the potential route of propanal decarbonylation to ethane and CO, the produced CO is converted further to CO_2 and hydrogen through the water gas shift reaction. It has been observed that the concentration of CO in the products was slightly higher (0.015 C%) than the expected equilibrium value (0.007 C%, calculated from the observed CO_2 concentration). Therefore, it can be concluded that the parallel reaction of decarbonylation also contributes to 1-propanol conversion. However, quantitative differentiation between the reaction pathways of disproportionation followed by decarboxylation of the acid and decarbonylation followed by water gas shift is not attempted here.

2.3.5. Aqueous phase conversion of 1,2- and 1,3-propanediols

The reactions of 1,2-propanediol having a primary and a secondary hydroxyl group, and 1,3-propanediol with two primary hydroxyl groups were studied at identical reaction conditions (see Figs. 2-4 and 2-5). Hydroxyacetone, ethanol, and CO_2 were the main products of 1,2-propanediol conversion, and small amounts of 1-propanol, 2-propanol, and methane were also formed. The yield of hydroxyacetone formed through dehydrogenation of 1,2-propanediol (initial rate: 8.5 $mmol^.s^{-1.}mol_{Pt-surf.\ atom}^{-1}$) rapidly reached a constant value, which is determined by the high hydrogen pressure limiting further conversion.
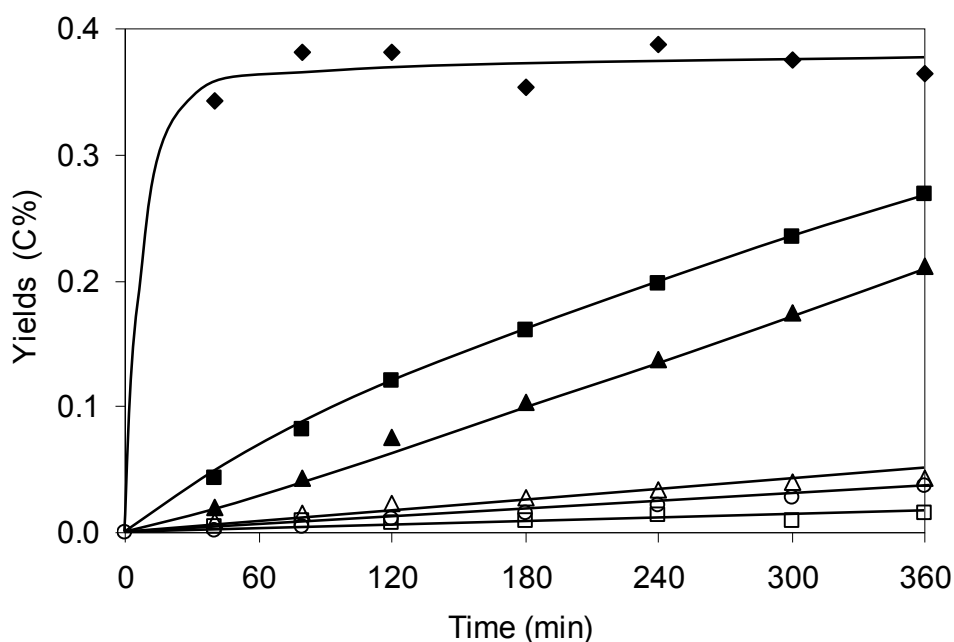
Figure 2-4. Yield of hydroxyacetone (◆), ethanol (■), carbon dioxide (▲), methane (○), 1-propanol (△), and 2-propanol (□) on conversion of 1,2-propanediol over 3 wt.% Pt/Al₂O₃ as a function of time in aqueous solution. (Experimental conditions: T=473 K, total pressure 40 bar, 1,2-propanediol concentration 10 wt.%)

Because the direct hydrogenolysis of C-C bonds of propanol does not occur under the present reaction conditions (see above), and the C-C bond strengths of 1,2-propanediol (359 kJ/mol) is quite close to that of propanol (357 kJ/mol) (see Table 2-3), ethanol and CO_2 are concluded to be formed via decarbonylation or decarboxylation (initial rate: 1.0 $mmol^{-1} \cdot mol_{Pt\text{-surf. atom}}^{-1}$). For the reaction pathway, 1,2-propanediol is dehydrogenated to 2-hydroxypropionaldehyde (not detected due to its high reactivity), which is either instantly decarbonylated to ethanol and CO followed by water gas shift reaction, or rapidly converted to 1,2-propanediol and 2-hydroxypropanoic acid via Tishchenko/Cannizzaro type disproportionation followed by decarboxylation of the acid, leading to ethanol and CO_2.

The formation rate of ethanol decreased slightly, while the formation rate of CO_2 increased moderately with the reaction time, leading to a ratio of ethanol to CO_2 that is lower than the 2.0 on carbon basis expected for ideal stoichiometry. This indicates that

ethanol underwent further reaction to methane and CO_2 via analogous reaction pathways as described above. If the converted ethanol was also taken into account, the initial ratio of ethanol to CO_2 (calculated by (ethanol+2×methane)/(CO_2-methane) according to stoichiometry) was very close to 2.0 on carbon basis, clarifying that ethanol is involved to some extent in decarboxylation or decarbonylation reactions. 1-Propanol and 2-propanol were produced through sequential dehydration-hydrogenation of 1,2-propanediol over Al_2O_3 (initial rate: 0.2 $mmol^.s^{-1.}mol_{acid\ site}^{-1}$), and the produced amount of 1-propanol was higher than that of 2-propanol, which is attributed to the higher dehydration activity of secondary hydroxyl group than that of the primary hydroxyl group.

The results of the conversion of 1,3-propanediol at 473 K and 40 bar hydrogen are compiled in Fig. 2-5. 1-Propanol was the main product at initial conversion. Ethane, ethanol, CO_2, and trace amounts of propane, propanal, propionic acid, methane, and methanol were also observed.
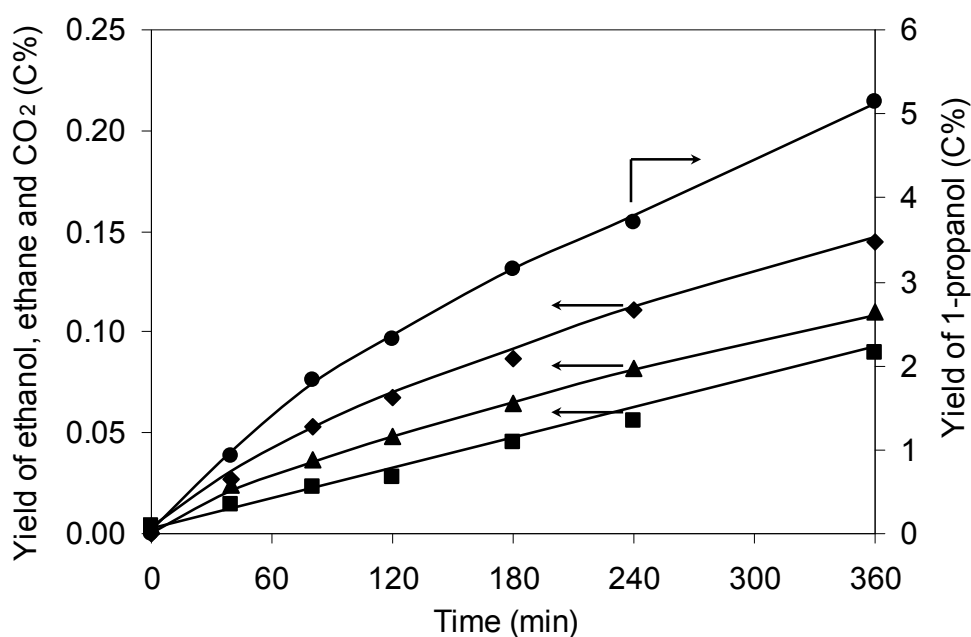
Figure 2-5. Products distribution for 1,3-propanediol conversion over 3 wt.% Pt/Al_2O_3 in aqueous solution in the presence of H_2; 1-propanol (●), ethanol (◆), carbon dioxide (▲), ethane (■) (Experimental conditions: T=473 K, total pressure 40 bar, 1,3-propanediol concentration 10 wt.%)

1-Propanol is highly selectively produced through the dehydration of 1,3-propanediol (initial rate: 11.5 mmol$\cdot$s$^{-1}\cdot$mol$_{acid\ site}^{-1}$) and the subsequent hydrogenation, which then further undergoes the same reaction sequences of dehydrogenation, followed by either decarbonylation with a subsequent water gas shift reaction or disproportionation with a subsequent decarboxylation, leading to CO$_2$ and ethane. The observation of trace amounts of propanal and propionic acid provides strong evidence for this proposed decarbonylation and decarboxylation reaction pathway. CO$_2$ also can be produced directly from the starting reactant 1,3-propanediol via the parallel reaction pathway of dehydrogenation, decarbonylation and decarboxylation (initial rate: 1.0 mmol$\cdot$s$^{-1}\cdot$mol$_{Pt\text{-}surf.\ atom}^{-1}$). The ratio of C$_2$ compounds (ethanol and ethane) to CO$_2$ is approximately 2.0 based on carbon basis, suggesting that CO$_2$ is produced through both reaction pathways. Propane is concluded to be formed via the dehydration of 1-propanol. We speculate at present that methane is formed by the dehydrogenation, decarboxylation/decarbonylation of 1,3-propanediol.

2.3.6. Aqueous phase conversion of glycerol

The results of glycerol conversion in the aqueous phase at 473 K in the presence of H$_2$ (40 bar) are compiled in Fig. 2-6. Hydroxyacetone, 1,2-propanediol, ethylene glycol, ethanol, and CO$_2$ were the main products, and 1-propanol, 2-propanol, and methanol were formed in small concentrations.

1,2-Propanediol was selectively produced from glycerol (75% selectivity). It can be seen from Fig.2-6 that the increase of 1,2-propanediol nearly equals the decrease of hydroxyacetone in selectivity as a function of time, suggesting that 1,2-propanediol is produced from the hydrogenation of hydroxyacetone. A control experiment with hydroxyacetone as reactant shows 98.5 % selectivity to 1,2-propanediol under identical conditions, which confirms the proposed reaction route. Therefore, the dehydration to hydroxyacetone is the dominating primary reaction step for glycerol conversion (initial rate: 4.6 mmol$\cdot$s$^{-1}\cdot$mol$_{acid\ site}^{-1}$).
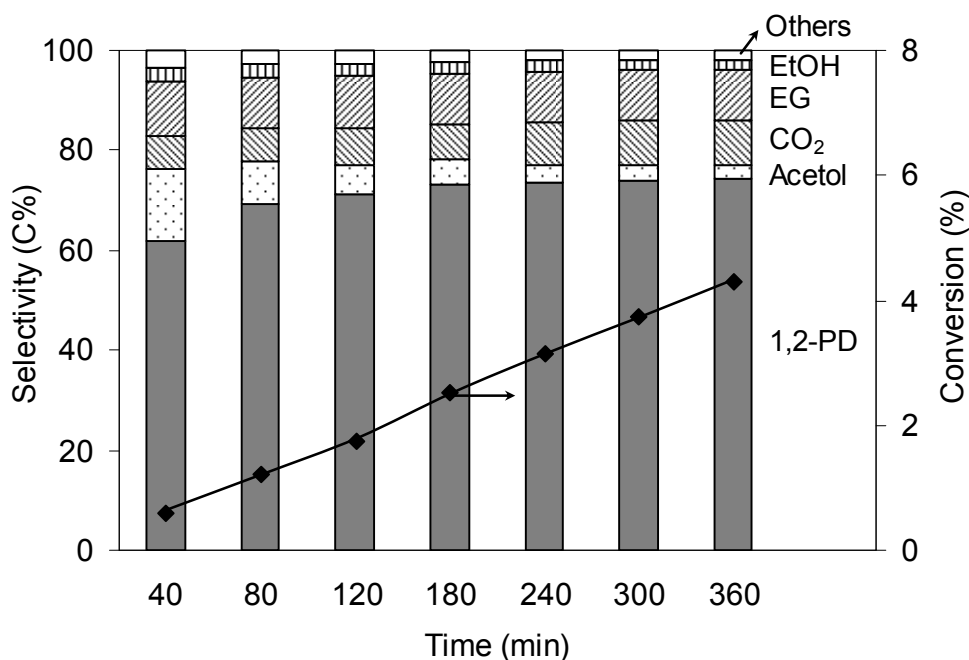
Figure 2-6. Glycerol conversion over 3 wt.% Pt/Al_2O_3 in the aqueous solution in the presence of H_2. 1,2-PD, 1,2-propanediol; Acetol, hydroxyacetone; EG, ethylene glycol; EtOH, ethanol; Others = 1-propanol + 2-propanol + methanol. (Experimental conditions: T=473 K, total pressure 40 bar, glycerol concentration 10 wt.%)

It is important to emphasize that all the other products appear to be formed along the same pathways as for other alcohols. Glyceraldehyde generated by dehydrogenation of glycerol is rapidly converted to ethylene glycol and CO_2, either through sequential decarbonylation and water gas shift reaction or via Tishchenko/Cannizzaro type disproportionation reactions over acid-base sites of Pt/Al_2O_3 followed by subsequent decarboxylation of glyceric acid. These intermediates were not detected, because their concentrations were very low due to their high reactivity and the equilibrium limitations caused by the high hydrogen pressure. Ethylene glycol can be further converted, either it is dehydrated to acetaldehyde, which in turn is hydrogenated to ethanol, or it is decomposed to CO_2 via dehydrogenation, disproportionation, and decarboxylation reactions (or decarbonylation reaction). The slight difference (5%) of C-C bond strengths in glycerol and propanols allows us to exclude direct hydrogenolysis for C-C bond

cleavage pathway (see Table 2-3). 1-Propanol and 2-propanol were formed by subsequent conversion of propanediols along the pathways discussed above.

It is still not clear, if the acid sites active in the dehydration in water are of Brønsted or Lewis acid character. The strong absorption of water onto Lewis acid sites allows the conversion of Lewis acid sites to surface hydroxyl groups via rehydroxylation (or rehydration). This two-step rehydroxylation transformation involves nondissociative adsorption of H$_2$O on the Lewis acid sites followed by the subsequent dissociative chemisorption of H$_2$O and modification of the alumina surface [33,34]. Although the transformation of bulk γ-Al$_2$O$_3$ to hydroxide is slow, the surface rehydroxylation is fairly rapid and thorough and so the concentration of exposed Lewis acid sites is limited. We speculate at present that weak Brønsted acid sites resulting e.g., from some isolated surface hydroxyl groups and identified by the shift of v_{OH} on CO infrared adsorption [35], act as active sites for dehydration.

2.3.7. Summary of reaction pathways and reaction rates for aqueous phase conversion of C$_3$ alcohols over Pt/Al$_2$O$_3$

Summarizing the aqueous phase reactions with C$_3$ alcohols over Pt/Al$_2$O$_3$, dehydrogenation of alcohols to ketones on Pt is the main route for conversion of 2-propanol and 1,2-propanediol, and dehydration on alumina is the main route for conversion of 1,3-propanediol and glycerol. It has been demonstrated that the direct hydrogenolysis of C-C and C-O bonds of the alcohols does not take place over Pt/Al$_2$O$_3$ under the used reaction conditions. In comparison, the C-O bonds of C$_3$ alcohols are cleaved by dehydration reaction in the present work, while the C-C bonds of C$_3$ alcohols with terminal hydroxyl groups are cleaved by sequential dehydrogenation to aldehyde, followed by either disproportionation (Tishchenko or Cannizzaro type reactions) with a subsequent decarboxylation reaction, or decarbonylation with a subsequent water gas shift reaction (see Fig. 2-7).
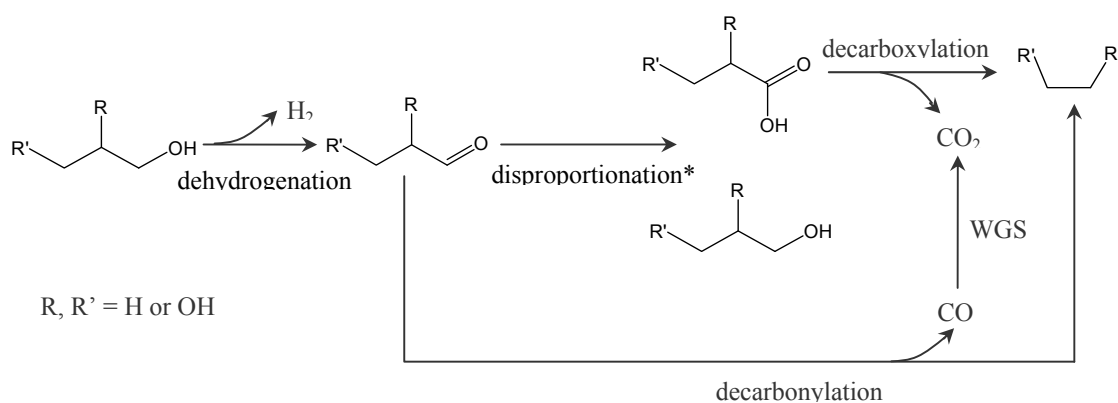
Figure 2-7. Proposed main reaction pathways for C-C bond cleavage in aqueous phase conversion of glycerol derived alcohols over Pt/Al_2O_3 (* either via Tishchenko or Cannizzaro type reactions)

The reaction rates of individual steps for C_3 alcohols conversion in aqueous phase are compiled in Table 2-2. For 2-propanol and 1,2-propanediol conversion, dehydrogenation is the major step (initial rates: 48.0 and 8.5 $mmol \cdot s^{-1} \cdot mol_{Pt\text{-surf. atom}}^{-1}$, respectively), while dehydration is the minor reaction for mono-alcohols conversion with slow dehydration rates (i.e., 0.4 and 0.3 $mmol \cdot s^{-1} \cdot mol_{acid\ site}^{-1}$ for 2-propanol and 1-propanol, respectively), which is mainly attributed to the blocking of Lewis acid sites by water.

Dehydration, however, is the dominating primary reaction for both 1,3-propanediol (initial rate: 11.5 $mmol \cdot s^{-1} \cdot mol_{acid\ site}^{-1}$) and glycerol (initial rate: 4.6 $mmol \cdot s^{-1} \cdot mol_{acid\ site}^{-1}$), with the dehydration rates being 10-40 times faster than that of mono-alcohols. We attribute this to the distinctly weaker C-O bond strengths with the increase of hydroxyl group number in alcohol molecule, e.g., 398 kJ/mol for 2-propanol and 333 kJ/mol for glycerol (see Table 2-3), which supposedly should lower the activation energies for 1,3-propanediol and glycerol dehydration compared with mono-alcohols. The C-C bond cleavage through decarbonylation and decarboxylation occurs at the C_3 alcohols with terminal hydroxyl groups and produces smaller alkanes and CO_2, attaining the comparable rates of ca. 1.0 $mmol \cdot s^{-1} \cdot mol_{Pt\text{-surf. atom}}^{-1}$. The overall reactivity decrease in the sequence of 1,3-propanediol (2.3×10^{-6} $mol \cdot s^{-1} \cdot g_{catalyst}^{-1}$) ≈ glycerol ($1.2 \times 10^{-6}$ $mol \cdot s^{-1} \cdot g_{catalyst}^{-1}$) > 1,2-propanediol ($5.1 \times 10^{-7}$ $mol \cdot s^{-1} \cdot g_{catalyst}^{-1}$) ≈ 1-propanol ($2.2 \times 10^{-7}$ $mol \cdot s^{-1} \cdot g_{catalyst}^{-1}$).

2.4. Conclusions

The catalytic conversion of 2-propanol at the gas-solid and aqueous-solid interfaces with Pt/Al$_2$O$_3$ shows that the rate of 2-propanol dehydration in the aqueous phase was two orders of magnitude slower than that in the gas phase. Because the catalytic dehydration in the gas phase is generally accepted to be initiated by OH$^-$ abstraction from the alcohol, we conclude that this step is drastically retarded when the reaction is conducted in water. As γ-Al$_2$O$_3$ slowly transforms into aluminum hydroxide (Böhmite) under hydrothermal conditions, the weaker Lewis acidity due to rehydroxylation is possibly responsible for the rate decrease to some extent. However, the substantial decrease of 2-propanol dehydration rate even at initial conversion, when alumina is still not measurably converted, suggests that blocking of Lewis acid sites by the abundant water is the main reason leading to the drastic decrease of dehydration rate.

The C-O bonds of C$_3$ alcohols are cleaved by dehydration, while the C-C bonds of C$_3$ alcohols with terminal hydroxyl groups are cleaved by sequential dehydrogenation to aldehyde, followed by either disproportionation (Tishchenko or Cannizzaro type reactions) with a subsequent decarboxylation reaction, or decarbonylation with a subsequent water gas shift reaction. The presence of terminal hydroxyl group of alcohols is proved to be critical for C-C bond cleavage in this reaction sequence, as it allows forming the essential aldehyde intermediate, which opens the reaction pathway to decarbonylation and decarboxylation. The overall reaction rates decrease in the sequence of 1,3-propanediol ≈ glycerol > 1,2-propanediol ≈ 1-propanol, which depends on the number of hydroxyl groups in the molecule, as well as the number of primary hydroxyl groups. The higher concentration of the hydroxyl groups in one molecule weakens the C-O bond strengths, leading to higher dehydration rates.

2.5. Acknowledgements

.

2.6. References

1. G. W. Huber, J. N. Chheda, C. J. Barrett, J. A. Dumesic, Science 308 (2005) 1446.

2. J. P. Lange, R. Price, P. M. Ayoub, J. Louis, L. Petrus, L. Clarke, H. Gosselink, Angew. Chem. Int. Ed. 49 (2010) 4479.

3. C. Zhao, Y. Kou, A. A. Lemonidou, X. Li, J. A. Lercher, Angew. Chem. Int. Ed. 48 (2009) 3987.

4. C. Zhao, J. He, A. A. Lemonidou, X. Li, J. A. Lercher, J. Catal. 280 (2011) 8.

5. G. W. Huber, S, Iborra, A. Corma, Chem. Rev. 106 (2006) 4044.

6. S. Czernik , R. French, C. Feik, E. Chornet, Ind. Eng. Chem. Res. 41 (2002) 4209.

7. S. Adhikari, S. Fernando, S.D. Filio, M. Bricka, P.H. Steele, A. Haryanto, Energy Fuels 22 (2008) 1220.

8. G. W. Huber, A. Corma, Angew. Chem. Int. Ed. 46 (2007) 7184.

9. R. D. Cortright, R. R. Davda, J. A. Dumesic, Nature 418 (2002) 964.

10. G. W. Huber, J. W. Shabaker, J. A. Dumesic, Science 300 (2003) 2075.

11. G. W. Huber, J. A. Dumesic, Catal. Today 111 (2006) 119.

12. T. Werpy, G. Petersen, Top Value Added Chemicals from Biomass, US DOE Report, 2004.

13. S. Wang, H. Liu, Catal. Letter. 117 (2007) 62.

14. T. Miyazawa, S. Koso, K. Kunimori, K. Tomishige, Appl. Catal. A 329 (2007) 30.

15. J. Chaminand, L. Djakovitch, P. Gallezot, P. Marion, C. Pinel, C. Rosier, Green Chem. 6 (2004) 359.

16. D.G. Lahr, B.H. Shanks, Ind. Eng. Chem. Res. 42 (2003) 5467.

17. D.G. Lahr, B.H. Shanks, J. Catal. 232 (2005) 386.

18. R. R. Davda, J. W. Shabaker, G. W. Huber, R. D. Cortright, J. A. Dumesic, Appl. Catal. B: Env. 43 (2003) 13.

19. J. W. Shabaker, G.W. Huber, R. R. Davda, R. D. Cortright, J. A. Dumesic, Catal. Lett., 88 (2003) 1.

20. E. P. Maris, R. J. Davis, J. Catal. 249 (2007) 328.

21. E. P. Maris, W. C. Ketchie, M. Murayama, R. J. Davis, J. Catal. 251 (2007) 281.

22. T. Miyazawa, Y. Kusunoki, K. Kunimori, K. Tomishige, J. Catal. 240 (2006) 213.

23. A. Wawrzetz, B. Peng, A. Hrabar, A. Jentys, A. A. Lemonidou, J. A. Lercher, J. Catal. 269 (2010) 411.

24. Z. Duan, R. Sun, Chem. Geol. 193 (2003) 257.

25. A. Gervasini, A. Aroux, J. Catal. 131 (1991) 190.

26. M. A. Aramendia, V. Borau, C. Jimenez, J. M. Marinas, A. Porras, F. J. Urbano, React. Kinet. Catal. Lett. 53 (1994) 397.

27. H. A. Pray, C. E. Schweickert, B. H. Minnich, Ind. Eng. Chem. 44 (1952) 1146.

28. P. Raybaud, M. Digne, R. Iftimie, W. Wellens, P. Euzen, H. Toulhoat, J. Catal. 201 (2001) 236.

29. E. Laurent, B. Delmon, J. Catal. 146 (1994) 281.

30. H. Noller, W. Kladnig, Catal. Rev. Sci. Eng. 13 (1976) 149.

31. Y.R. Luo, in: Comprehensive Handbook of Chemical Bond Energies, CRC Press, Boca Raton, Florida, 2007.

32. J. Cook, P. M. Mailis, J. Chem. Soc., Chem. Commun. 17 (1981) 924.

33. D. Coster, J. J. Fripiat, M. Muscas, A. Auroux, Langmuir 11 (1995) 2615.

34. M. Trueba, S. P. Trasatti, Eur. J. Inorg. Chem. 17 (2005) 3393.

35. W. Daniell, U. Schubert, R. Glöckler, A. Meyer, K. Noweck and H. Knözinger, Appl. Catal. A 196 (2000) 247.

Chapter 3

Catalytic deoxygenation of palmitic acid on the influence of metal site, support, and carrier gas

The mechanism for conversion of palmitic acid to n-pentadecane has been systematically explored with Ni/ZrO$_2$ in the presence of H$_2$. The reaction mainly proceeds with hydrogenation of the carboxylic group of palmitic acid leading to hexadecanal (rate determining step), which is subsequently decarbonylated on the Ni sites to the target n-pentadecane and carbon monoxide. Note that the hydrogenation of fatty acid to aldehyde is synergistically promoted by the ZrO$_2$ support through simultaneously adsorbing the carboxylic group at the oxygen vacancies and dissociating the hydrogen molecules. The deoxygenation rates (unit: mmol·g$_{Cat}^{-1}$·h^{-1}) of palmitic acid follow the orders as r $_{(Ni/HBeta\ or\ Ni/HZSM-5)}$ > r $_{(Ni/ZrO2)}$ > r $_{(Ni/Al2O3\ or\ Ni/SiO2)}$. In the presence of N$_2$, ketonization is the dominating reaction on conversion of palmitic acid catalyzed by ZrO$_2$. Pd/C favors direct decarboxylation route (-CO$_2$), while Pt/C together with Raney Ni lead to the direct decarbonylation pathway (-CO). The individual rates (unit: mmol·h^{-1}·mol$_{metal}^{-1}$) decrease in the sequence of r $_{(Pt\ black)}$ ≈ r $_{(Pd\ black)}$ > r $_{(Raney\ Ni)}$ in N$_2$ carrier gas.

3.1. Introduction

Biodiesel (fatty acid alkyl esters) shows to be a very attractive renewable liquid fuel, but it contains high oxygen content in the ester components. It would be a clear advantage that the diesel range alkanes (without oxygen), as one of the most promising energy carriers, can be produced from animal fat, vegetable or algae oils.[1,2] The long carbon-chain (C_{16}-C_{22}) fatty acids are usually selected as the model compounds for investigating the upgrading process of triglycerides.

Currently, three methods can be efficiently utilized for the deoxygenating of fatty acids to alkanes. The first is relied on the noble metal supported catalysts, e.g., Pd/C and Pt/C, for the decarboxylation and decarbonylation of fatty acids to alkanes with selectivity higher than 98% at 300-330 ^{o}C in the absence of H_2.[3-5] The second is to employ the conventional hydrotreating catalysts, e.g., sulfided NiMo and CoMo, for the deoxygenation of fatty acids to C_{15}-C_{18} alkanes at 300-450 ^{o}C in the presence of H_2.[6-8] However, these sulfided catalysts would contaminate products and cause catalyst deactivation due to sulfur leaching, especially in the presence of trace amount of water.[9-11] The third is to utilize zeolite supported metal catalysts, e.g., Ni/HBeta and Pt-Re/HZSM-5, for the hydrodeoxygenation of fatty acids to alkanes at 250-300 ^{o}C with H_2.[12,13] It has been reported in our and other previous works that for the transformation of triglyceride to alkanes on Ni/HBeta catalysts, it initially proceeds via hydrogenolysis of triglycerides into fatty acids (primary products), followed by deoxygenation of fatty acids into hydrocarbons by the tandem hydrogenation-dehydration-hydrogenation steps.[6,12] Additionally, the involved hydrogenation step on fatty acid with Ni sites is determined to be the rate-determining step.

As the hydrogen consumption for the deoxygenation of fatty acids follows the increasing orders of decarboxylation < decarbonylation < hydrodeoxygenation (see below, thermodynamic data for conversion of palmitic acid (model compound) to C_{15} and C_{16} alkanes together with gas phase reactions at 260 ^{o}C), in principle, the decarbonylation or decarboxylation route is more applicable than the hydrodeoxygenation pathway. In the vapor phase, methanation and water gas shift are the main reactions.

Liquid phase		ΔG_{533} (kJ/mol)	ΔH_{533} (kJ/mol)	
Hydrodeoxygenation:	$R\text{-}COOH + 3\,H_2 \longrightarrow R\text{-}CH_3 + 2\,H_2O$	-88.0	-112.6	(3-1)
Decarbonylation:	$R\text{-}COOH + H_2 \longrightarrow R\text{-}H + CO + H_2O$	-59.5	49.7	(3-2)
Decarboxylation:	$R\text{-}COOH \longrightarrow R\text{-}H + CO_2$	-78.6	10.1	(3-3)
Gas phase				
Methanation:	$CO + 3\,H_2 \longrightarrow CH_4 + H_2O$	-88.4	-215.3	(3-4)
Methanation:	$CO_2 + 4\,H_2 \longrightarrow CH_4 + 2\,H_2O$	-69.2	-175.7	(3-5)
Water gas shift:	$CO + H_2O \longrightarrow CO_2 + H_2$	-19.1	-39.6	(3-6)

In the present work, the deoxygenation of fatty acid, i.e., C_{16} palmitic acid, to C_{15} *n*-pentadecane was systematically investigated with a variety of sulfur-free supported metal catalysts in the presence or absence of H_2. The kinetics in the catalytic conversion of palmitic acid and the reaction intermediates, i.e., 1-hexadecanol and palmityl palmitate, were also investigated over Ni/ZrO_2 in order to elucidate the reaction pathways. The influences of metal (Pt, Pd, and Ni), support (C, ZrO_2, Al_2O_3, SiO_2, HBeta, and HZSM-5), and carrier gas (H_2, N_2, and H_2-N_2 mixture) have also been comparatively explored.

3.2. Experimental

3.2.1. Materials

All chemicals were obtained from commercial suppliers and used as received: palmitic acid (Sigma, ≥99% Reagent Plus), 1-hexadecanol (Aldrich, ≥99%), palmityl palmitate (Sigma, ≥99%), dodecane (Sigma-Aldrich, ≥99% Reagent Plus), eicosane (Aldrich, ≥99% GC assay), *n*-pentadecane (Fluka, ≥99.8% analytical standard), *n*-

hexadecane (Fluka, ≥99.8% analytical standard), palmitone (TCI, >90% GC assay), nickel (II) nitrate hexahydrate (Sigma-Aldrich, ≥98.5%), tetraammineplatinum (II) nitrate (Strem chemicals, 99%), tetraamminepalladium (II) nitrate (Aldrich, 10 wt% aqueous solution).

The supports were also provided from commercial company such as γ-Al_2O_3 (Aeroxide Alu C-Degussa), SiO_2 (Aeroxide Alu C-Degussa), ZrO_2 derived from zirconium hydroxide (MEL Chemicals), HZSM-5 (Süd-Chemie AG, Si/Al=200), and HBeta (Zeolyst, Si/Al=180).

The commercial catalysts including Pt/C (Aldrich, 5 wt%), Pd/C (Aldrich, 5 wt%), Pt black (Aldrich, ≥99.9%), Pd black (Aldrich, ≥99.8%), and Raney®Ni 4200 (Aldrich, slurry in water) were used in the present work.

3.2.2. Catalyst preparation

The Ni supported on γ-Al_2O_3, SiO_2, ZrO_2, HZSM-5, and HBeta catalysts as well as Pt and Pd supported on ZrO_2 catalysts were synthesized by the wetness impregnation method. The ZrO_2 support was prepared by calcination of zirconium hydroxide in static air at 400 ^{o}C for 4 h. For example, the procedure for preparing 5 wt% Ni/ZrO_2 was carried out as follows: Ni(NO$_3$)$_2$·6H$_2$O (2.92 g) was dissolved in water (5 g), and then such solution was slowly dropped onto ZrO_2 (10 g) with continuous stirring. After metal incorporation with support at ambient temperature for 4 h, the catalyst was firstly dried overnight at ambient temperature and then dried at 110 ^{o}C for 12 h. Afterwards, the catalyst was calcined in synthetic air at 400 ^{o}C for 4 h (flow rate: 100 ml/min) and reduced at 500 ^{o}C for 4 h (ramp: 2 ^{o}C/min) in hydrogen (flow rate: 100 ml/min).

3.2.3. Catalyst characterization

Atomic absorption spectroscopy (AAS)

The metal loading was determined by atomic absorption spectroscopy using a UNICAM 939 AA-Spectrometer. Prior to measurement, the sample was dissolved in a

mixture of hydrofluoric acid (48%) and nitro-hydrochloric acid at the boiling point of the mixture (about 110 ^{o}C).

BET specific surface area

The BET specific surface area was determined by nitrogen adsorption-desorption at -196 ^{o}C using the Sorptomatic 1990 Series instrument. The sample was activated in vacuum at 300 ^{o}C for 2 h before measurement.

Temperature programmed desorption (TPD)

Temperature programmed desorption of ammonia or carbon dioxide was performed in a 6 fold parallel reactor system. The catalysts were activated in helium at 500 ^{o}C (ramp: 5 ^{o}C/min) for 1 h. Ammonia or carbon dioxide was adsorbed with a partial pressure of 1 mbar at 100 ^{o}C or 35 ^{o}C, respectively. Subsequently, the samples were purged with 30 ml/min helium for 2 h in order to remove physisorbed molecules. For the temperature programmed desorption experiments, 6 samples were sequentially heated from 100 to 765 ^{o}C with an increment of 10 °C/min to desorb ammonia and from 35 to 450 ^{o}C to desorb carbon dioxide. The rates of desorbing species were monitored by mass spectrometry (Balzers QME 200). For the quantification of acidity amount, a standard HZSM-5 zeolite (Si/Al=45) with known acid site concentration was used to calibrate the signal. The response of the CO_2 signal was calibrated based on the decomposition of $NaHCO_3$.

X-Ray powder diffraction (XRD)

The structures of the catalysts were analyzed by X-ray diffraction using a Philips X'Pert Pro System. The radiation source was Cu K_α operating at 40 kV/45 mA. The sample was measured with a scanning rate of 1 ^{o}/min from 5 to 70° (2θ). The metal particle size was calculated from diffraction by Scherrer equation.

Transmission electron microscopy (TEM)

Transmission electron microscopy was measured on a JEOL-2011 electron microscope operating at 200 kV. Prior to the measurements, the samples were suspended in ethanol and dried on a copper-carbon-grid.

3.2.4. Reaction procedure and analysis method

The catalytic experiments with palmitic acid and the reaction intermediates such as 1-hexadecanol and palmityl palmitate were carried out in a 300 ml autoclave (Parr Instrument) under semi-batch mode. The difference with batch operation was that the carrier gas (H_2, or N_2, or H_2-N_2 mixture) continuously flowed through (in and out of) the reactor during the whole process (see **Fig. 3-1**). The flow of carrier gas was controlled by mass flow controller and the reaction pressure was controlled by back pressure regulator. Typical reaction was conducted as follows: reactant (1.0 g), dodecane (100 ml), and catalyst (0.5 g) were loaded into the autoclave. Then it was purged thoroughly with carrier gas (20 ml/min) at ambient temperature and the pressure was adjusted to 12 bar prior to reaction. Finally, the reaction mixture was heated to the required temperature at 260 $^{\circ}$C, and the reaction time began to count by stirring. The stirring speed was maintained properly high, e.g., 600 rpm, to exclude external mass transfer limitation.
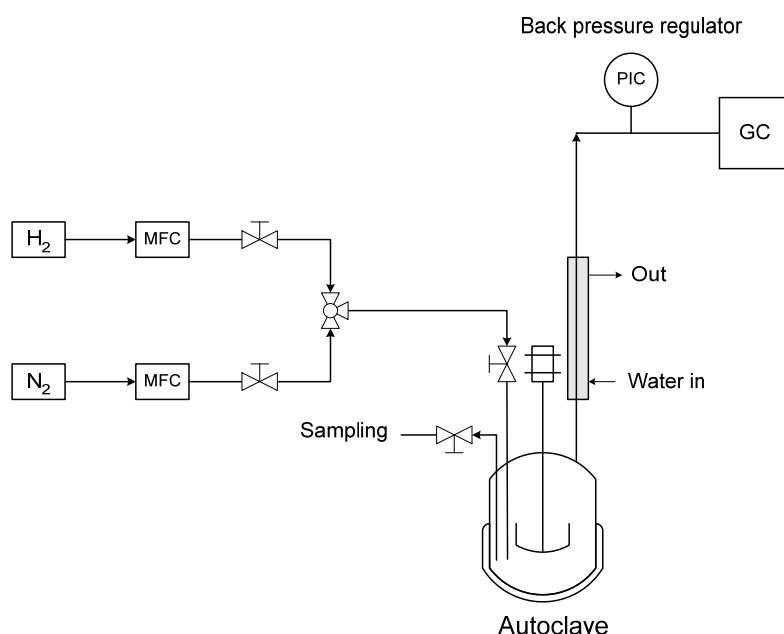
Figure 3-1. Scheme of semi-batch reactor for palmitic acid conversion

The products in the vapor phase were analyzed by an online gas chromatograph (GC) with TCD detector and two capillary columns (MS-5A and HP-Plot Q), while the liquid samples were manually collected during the run and later analyzed by a Shimadzu 2010 GC-MS equipped with a HP-5 capillary column (30 m, 0.32 mm inner diameter, 0.25 μm film). Internal standard, i.e., eicosane, was used for quantification. Both injection and detection temperature are 320 $^{\circ}$C. The temperature program is set as: initial from 60 $^{\circ}$C to 80 $^{\circ}$C (rate: 2 $^{\circ}$C/min), subsequently increase to 300 $^{\circ}$C (rate: 10 $^{\circ}$C/min) holding for 15 min. Note that by using a high injection port temperature, e.g., 320 $^{\circ}$C, reliable and direct quantification for fatty acids can be achieved without chemical derivitization.[14]

Conversion = (weight of converted reactant/weight of the starting reactant) × 100%. Yield (C%) = (C atoms in each product/C atoms in the starting reactant) × 100%. Selectivity (C%) = (C atoms in each product/sum of C atoms in all the products) × 100%.

3.3. Results

3.3.1. Catalyst characterization

The physicochemical properties of the selected catalysts in the present work are summarized in **Table 3-1**. The specific surface areas of the screened catalysts gradually varied from the high surface areas of carbon support (>1000 m^2/g), to the medium surface areas of HZSM-5 and HBeta zeolites (300-500 m^2/g), and to the low surface areas of oxide supports such as ZrO$_2$, SiO$_2$, and Al$_2$O$_3$ (100 m^2/g). The specific surface areas of C, HBeta, HZSM-5, ZrO$_2$, Al$_2$O$_3$ and SiO$_2$ supported Ni (or Pt, or Pd) catalysts were approximately at 1050, 560, 310, 100, 85 and 180 m^2/g, respectively. The commercial pure metal catalysts such as Pt black, Pd black, and Raney$^{\circledR}$Ni [15] roughly had specific surface areas of 25, 50 and 100 m^2/g, respectively.

Table 3-1. Physicochemical properties of catalysts

Catalysts	Metal loading (wt%)	BET surface area (m^2/g)	Metal particle size (nm) [a]	Acidity (mmol·g^{-1}) [b]	Basicity (mmol·g^{-1}) [b]
ZrO$_2$	-	113	-	0.103	0.169
Ni/ZrO$_2$	3	103	5.2	0.094	0.159
Ni/ZrO$_2$	5	98	7.0	0.093	0.151
Ni/ZrO$_2$	10	97	11.6	0.077	0.139
Ni/ZrO$_2$	15	93	18.0	0.065	0.135
Ni/Al$_2$O$_3$	5	86	7.9	0.089	0.014
Ni/SiO$_2$	5	182	8.8	0	0
Ni/HBeta [c]	5	565	18	0.069	-
Ni/HZSM-5 [d]	5	310	17	0.053	-
Raney$^®$Ni	-	80-120 [15]	-	-	-
Pt black	-	25	-	-	-
Pd black	-	40-60	-	-	-
Pt/C	5	1015	3.5	0	0
Pd/C	5	1062	5.0	0	0
Pt/ZrO$_2$	5	105	6.7	0.095	0.155
Pd/ZrO$_2$	5	101	5.2	0.094	0.152

[a] Calculated from XRD by Scherrer equation

[b] Determined by TPD of ammonia or carbon dioxide

[c] Si/Al = 180

[d] Si/Al = 200

The XRD patterns of pure ZrO_2 and Ni based catalysts are complied at **Fig. 3-2**. The selected ZrO_2 support showed a much weaker diffraction of tetragonal crystallite ($2\theta=30.4^{\circ}$) than that of monoclinic crystallites ($2\theta=28.5^{\circ}$ and 31.7°). The calcined Ni/ZrO_2 sample exhibited distinct nickel oxide diffractions of NiO(111), NiO(200), and NiO(220) at $2\theta=37.4^{\circ}$, 43.4° and 63.0°, respectively, which completely disappeared after reduction in H_2 at 500 $^{\circ}$C and transformed to metallic Ni with Ni(111) at $2\theta=44.6^{\circ}$ and Ni(200) at $2\theta=52.1^{\circ}$. The Ni particle sizes of Ni/ZrO_2 increased from 5 to 18 nm (calculated from XRD by the Scherrer equation) when the Ni content increased from 3 to 15 wt%. The HBeta, HZSM-5, Al_2O_3, and SiO_2 supported Ni catalysts (5 wt% loading) had Ni particle sizes of 18, 17, 8 and 9 nm, respectively. By comparison, the particle sizes of noble metal catalysts (Pt and Pd, 5 wt% loading) on carbon material were much smaller, i.e., 3.5 for Pt/C and 5 nm for Pd/C, which is in accordance with the larger BET surface areas of carbon supports ((>1000 m^2/g).
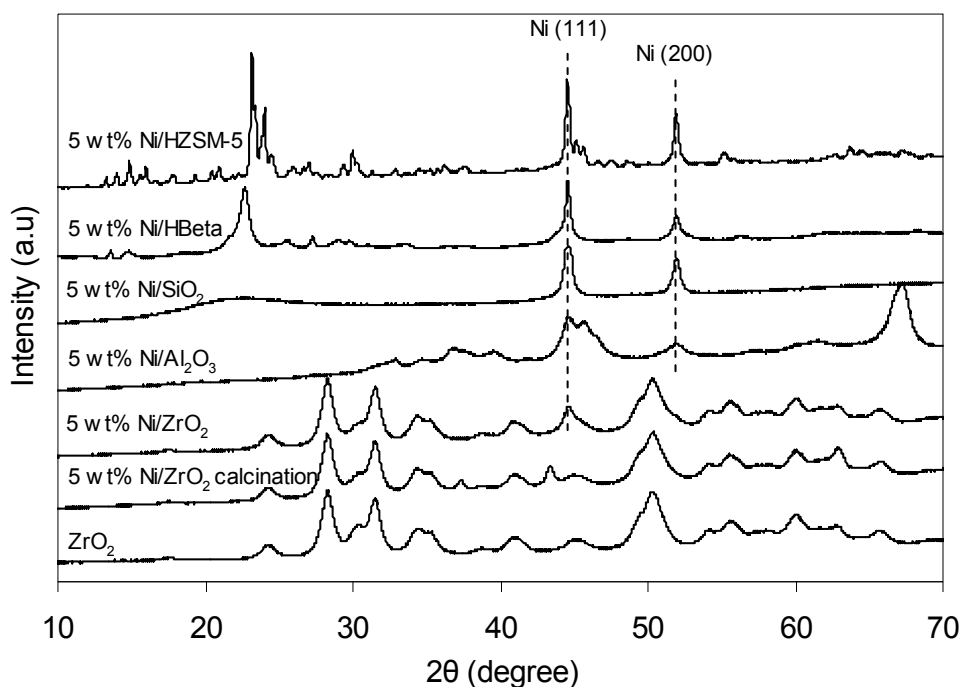
Figure 3-2. X-ray diffraction patterns of Ni based catalysts

The acid and base properties were measured by temperature programmed desorption of ammonia and carbon dioxide, respectively. The neutral material C supported catalysts did not show any acid or base characters, while the Ni/Al_2O_3 catalyst exhibited a weak Lewis acid concentration of 0.089 mmol·g^{-1}. Ni/SiO_2 would a have very weak Lewis acid site (0.009 mmol·g^{-1}) as reported in the literature,[16] but here the ammonia desorption signal was too weak to be detected. The bifunctional acid-base ZrO_2 supported Ni catalysts showed acid and base concentrations of 0.103 and 0.169 mmol·g^{-1}, respectively, both of which gradually decreased as the metal content increased. The HZSM-5 (Si/Al=200) and HBeta (Si/Al=180) supported Ni catalysts had relatively lower acid concentrations of 0.053 and 0.069 mmol·g^{-1}, but they possessed a larger fraction of Brønsted acid sites compared to other oxides supported catalysts.

3.3.2. Exploration of palmitic acid deoxygenation over Ni/ZrO$_2$

3.3.2.1 Kinetics of palmitic acid conversion over Ni/ZrO$_2$ with H$_2$

To explore the fundamental chemistry and the involved reaction mechanism of palmitic acid deoxygenation, the kinetics was investigated with the representative catalyst Ni/ZrO_2 (5 wt%) at 260 ^{o}C in the dodecane solvent under semi-batch mode in the presence of H_2. The results (see **Fig. 3-3**) showed that C_{16} 1-hexadecanol was the primary product at initial conversion, indicating that hydrogenation is the first major step with a hydrogenation rate of 1.3 mmol·h^{-1}·g$_{Cat}^{-1}$ (see **Table 3-2**). The yield of intermediate C_{16} 1-hexadecanol firstly reached a maximum of 27% and then slowly decreased to zero because it was further converted over Ni/ZrO_2. Meanwhile, the yield of C_{15} *n*-pentadecane gradually increased to 90% as the reaction proceeded. Interestingly, the formation rate of *n*-pentadecane dramatically increased after 40% conversion. This is related to the fact that C_{15} *n*-pentadecane was mainly produced by a slow direct decarbonylation/decarboxylation pathway at initial conversion, while as the reaction time extended the deoxygenation of C_{16} 1-hexadecanol could also produce C_{15} *n*-pentadecane with a faster rate which would dramatically promote the reaction rates. The intermediate C_{32} palmityl palmitate, formed from the esterification of palmitic acid and 1-hexadecanol, was firstly increased to a maximum yield of 2.5% and then gradually decreased to zero

when the conversion completed, and its conversion showed quite similar trend to 1-hexadecanol. Whereas another expected intermediate hexadecanal was only observed in trace (concentration < 0.45%).
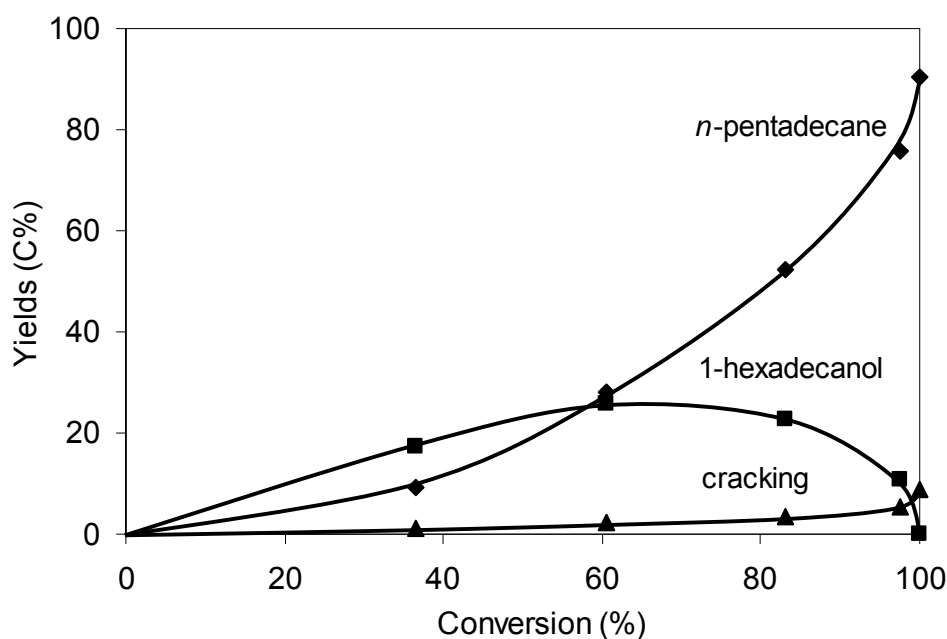
Figure 3-3. Yields of *n*-pentadecane (◆), 1-hexadecanol (■), and cracking products (▲) as a function of palmitic acid conversion over 5 wt% Ni/ZrO$_2$. (Experimental conditions: 1 g palmitic acid, 100 ml dodecane, 0.5 g catalyst, 260 $^{\circ}$C, 12 bar H$_2$ with a flowing rate of 20 ml/min)

It has been noted that cracking of the hydrocarbons also occurred on the dual functional sites (metallic and acidic) of Ni/ZrO$_2$. The yield of lighter hydrocarbons continuously increased, with a yield lower than 10% at complete conversion. In the vapor phase, CH$_4$ was the exclusive gas product derived from the methanation of CO or CO$_2$ with H$_2$. In order to better understand the catalytic chemistry in deoxygenation of the individual alcohol and ester intermediates, the kinetics with 1-hexadecanol and palmityl palmitate were explored at identical conditions, and the results are compiled at **Figs. 3-4 and 3-5**.
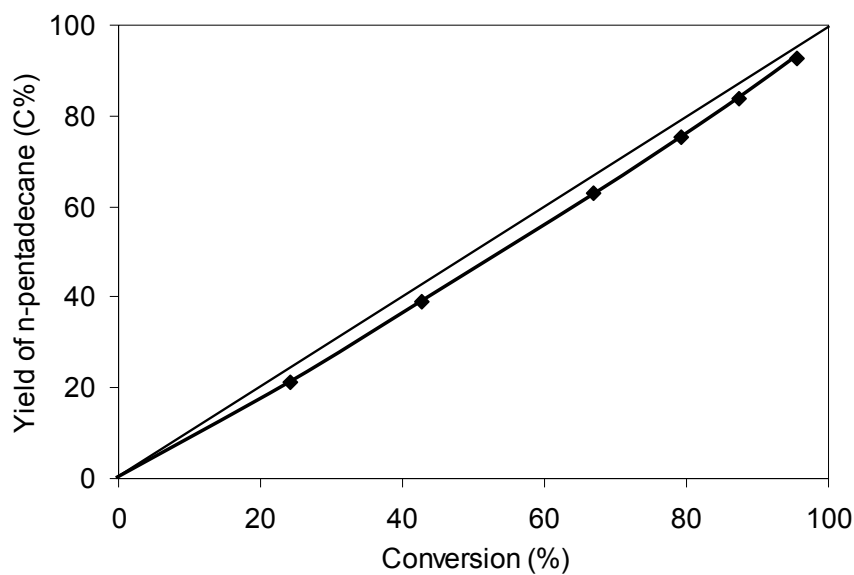
Figure 3-4. Yield of *n*-pentadecane on conversion of 1-hexadecanol over 5 wt% Ni/ZrO$_2$. (Experimental conditions: 1 g 1-hexadecanol, 100 ml dodecane, 0.05 g catalyst, 12 bar H$_2$ with a flowing rate of 20 ml/min)
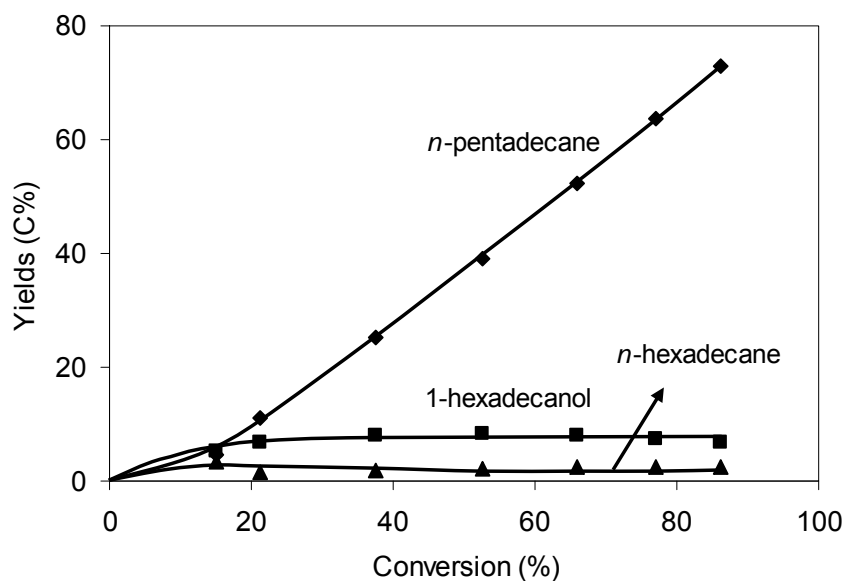
Figure 3-5. Yield of *n*-pentadecane (◆), 1-hexadecanol (■), and *n*-hexadecane (▲) on conversion of palmityl palmitate over 5 wt% Ni/ZrO$_2$. (Experimental conditions: 1 g palmityl palmitate, 100 ml dodecane, 0.25 g catalyst, 260 ^{o}C, 12 bar H$_2$ with a flowing rate of 20 ml/min)

3.3.2.2 Kinetics of 1-hexadecanol (intermediate) conversion over Ni/ZrO₂ with H₂

The kinetics on reaction of C_{16} 1-hexadecanol with Ni/ZrO$_2$ in presence of H$_2$ demonstrates that C_{15} *n*-pentadecane was the exclusive product (see **Fig. 3-4**). The yield of *n*-pentadecane was almost linearly increased with the conversion of C_{16} 1-hexadecanol, exhibiting a deoxygenation rate of 13.1 mmol·h^{-1}·g$_{Cat}$$^{-1}$. Finally, it led to 93% yield of *n*-pentadecane after 6 h reaction time.

Less than 0.6% yield of hexadecanal was detected during the whole conversion. It has been estimated that the expected equilibrated hexadecanal concentration in presence of 12 bar H$_2$ is only 0.9% calculated by HSC software, which is comparable to the experimental data (0.6%). As 1-hexadecanol and hexadecanal are supposed in quasi-equilibrium, C_{15} *n*-pentadecane is concluded to be formed from Ni catalyzed decarbonylation of hexadecanal by eliminating 1 mole of CO. Such mechanism on deoxygenation of 1-hexadecanol is quite similar to our previous reported conversion of C_3 alcohols over Pt/Al$_2$O$_3$ catalysts that C_3 alcohols with terminal hydroxyl groups were converted to ethane via decarbonylation route.[17, 18]

3.3.2.3 Kinetics of palmityl palmitate (intermediate) conversion over Ni/ZrO₂ with H₂

In the conversion of palmitic acid, palmityl palmitate was formed by esterification of palmitic acid and 1-hexadecanol, but it was further converted when the reaction proceeded. The separate experiment on kinetics of palmityl palmitate conversion was conducted at identical conditions (see **Fig. 3-5**). The results demonstrated that C_{16} 1-hexadecanol was the primary product at initial conversion, suggesting that the first step appeared to be Ni catalyzed hydrogenolysis of palmityl palmitate leading to 1-hexadecanol and hexadecanal formation with a rate of 2.4 mmol·h^{-1}·g$_{Cat}$$^{-1}$. Only trace amount of hexadecanal was detected, as it was further hydrogenated to 1-hexadecanol and limited by thermodynamic equilibrium in the presence of 12 bar H$_2$. Followed by similar steps as discussed above, the Ni catalyzed decarbonylation of 1-hexadecanol led to the formation of C_{15} *n*-pentadecane as final product with a 73% yield at 86% conversion. Meanwhile, a small amount of C_{16} 1-hexadecane was observed with a yield being lower than 5%, which was formed by sequential dehydration and hydrogenation of 1-hexadecanol. Through sequential hydrogenolysis and decarbonylation steps, the

palmityl palmitate is firstly cleaved by Ni metallic sites to form aldehyde and alcohol, and then these two intermediates are in turn converted to the hydrocarbons through decarbonylation by eliminating CO.

3.3.2.4 Proposed reaction pathways for palmitic acid conversion over Ni/ZrO_2 with H_2

Combining the kinetic performances of palmitic acid and two intermediates of 1-hexadecanol and palmityl palmitate allows us to formulate the overall reaction pathways for the conversion of palmitic acid with Ni/ZrO_2 catalysts in presence of H_2 (see **Scheme 3-1**). It proceeds with either an initial hydrogenation of the carboxylic group of the palmitic acid for producing hexadecanal (major route), or the direct decarboxylation of palmitic acid to produce *n*-pentadecane and carbon dioxide (minor route), and the former route benefits a hydrogenation/dehydrogenation equilibrium towards 1-hexadecanol formation, and subsequently, the hexadecanal is decarbonylated to the target *n*-pentadecane and carbon monoxide. Meanwhile, the equilibrated intermediate 1-hexadecanol also esterificates with palmitic acid to form palmityl palmitate, which is catalyzed by the ZrO_2 support. As the reaction proceeds, such ester is cleaved again by metal catalyzed hydrogenolysis leading to 1-hexadecanol and hexadecanal formation, which are decarbonylated to the target *n*-pentadecane by eliminating 1 mole of carbon monoxide. The weak acidic sites of ZrO_2 cause slight cracking and isomerization of the straight chain alkanes. The produced CO_2/CO may further react with H_2 to produce methane and water.

Table 3-2. Kinetic data of elementary steps in the overall deoxygenation of palmitic acid with 5 wt% Ni/ZrO_2 at 260 ^{o}C in presence of H_2.

	Reaction rate $(\text{mmol·h}^{-1}\text{·g}_{cat}^{-1})$
Hydrogenation of palmitic acid (rate determining step)	$r_1 = 1.3$ ($E_a = 156$ kJ/mol)
Decarbonylation of 1-hexdecanol	$r_2 = 13.1$
Hydrogenolysis and deoxygenation of palmityl palmitate	$r_3 = 2.4$
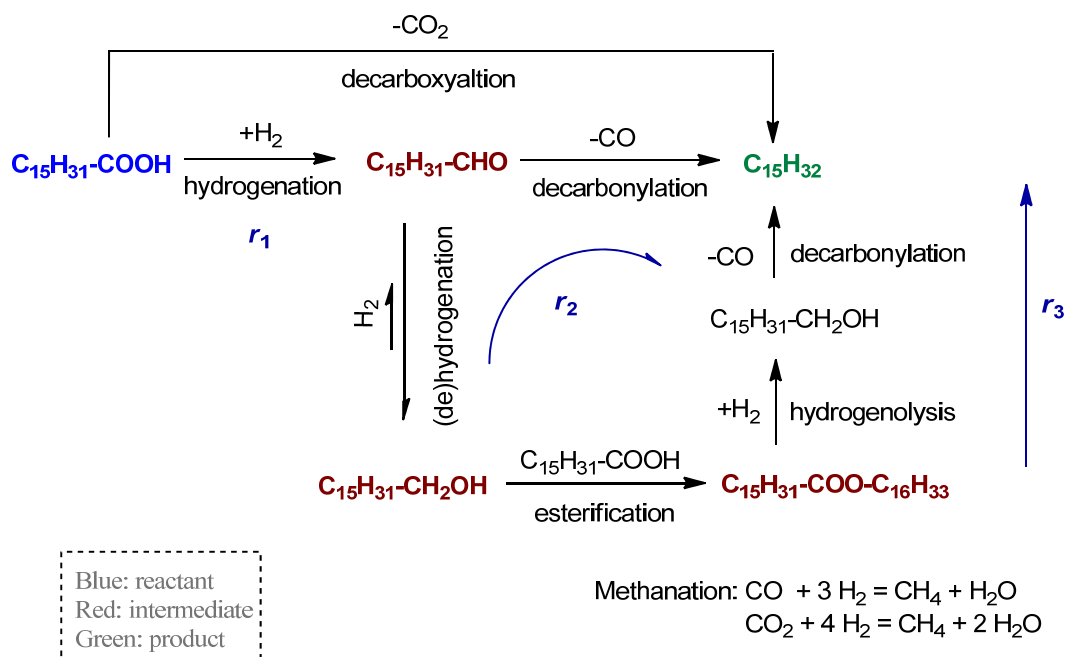
Scheme 3-1. Proposed main reaction pathways for palmitic acid conversion over Ni/ZrO$_2$ in the presence of H$_2$

To illuminate the rate determining step (the slowest reaction), the individual kinetics on conversion of palmitic acid, 1-hexadecanol, and palmityl palmitate are compared in **Table 3-2**. As the 1-hexadecanol and hexadecanal are supposed to be in equilibrium during 1-hexadecanol reaction, it is estimated that the decarbonylation of hexadecanal (13.1 mmol·h^{-1}·g$_{Cat}^{-1}$) is approximately an order of magnitude faster than the hydrogenation of palmitic acid (1.3 mmol·h^{-1}·g$_{Cat}^{-1}$) with 5 wt% Ni/ZrO$_2$ under the present reaction conditions. Additionally the hydrogenolysis-deoxygenation of palmityl palmitate (2.4 mmol·h^{-1}·g$_{Cat}^{-1}$) is around two times faster than the fatty acid hydrogenation step (1.3 mmol·h^{-1}·g$_{Cat}^{-1}$). Therefore, we conclude that the hydrogenation step of palmitic acid to hexadecanal is the rate determining step in the overall reaction of palmitic acid.

The impact of reaction temperature on the conversion of palmitic acid with 5 wt% Ni/ZrO$_2$ is shown in **Fig. 3-6**. With the increasing reaction temperature from 250 to 270 ^{o}C, the initial reaction rates enhanced remarkably from 0.6 to 2.8 mmol·h^{-1}·g$_{Cat}^{-1}$, and the yield of C$_{15}$ *n*-pentadecane increased from 58 to 85% after 6 h reaction time. This

indicates a high apparent activation energy (E_a = 156 kJ/mol) for palmitic acid conversion over Ni/ZrO$_2$ catalyst, which is in line with the slowest reaction rate for this step.
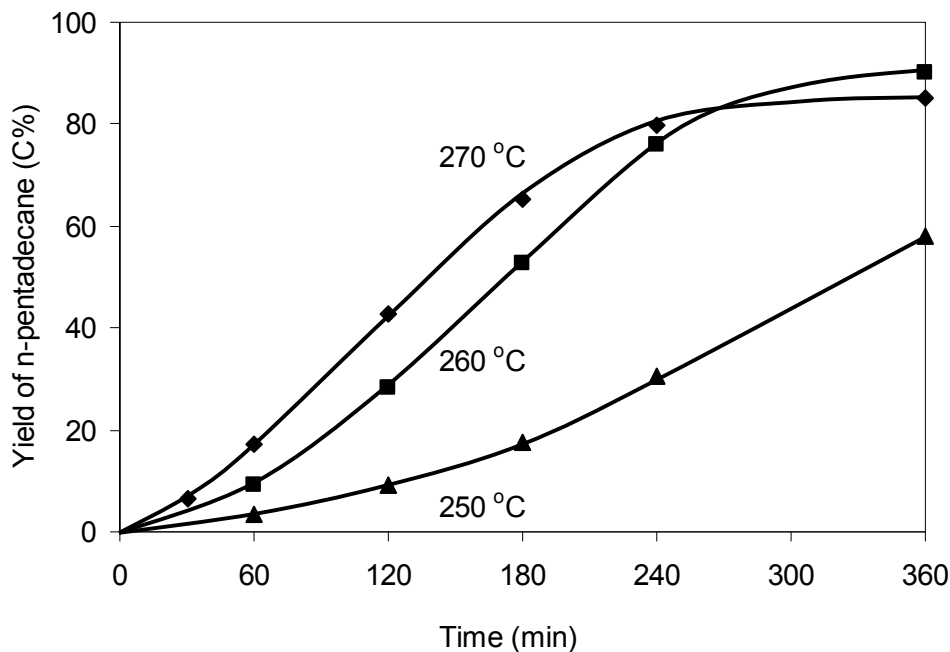
Figure 3-6. Impact of reaction temperature on the yield of *n*-pentadecane over 5 wt% Ni/ZrO$_2$. (Experimental conditions: 1 g palmitic acid, 100 ml dodecane, 0.5 g catalyst, 12 bar H$_2$ with a flowing rate of 20 ml/min)

3.3.2.5 Impact of gas carrier

With altering the carrier gas of pure H$_2$ to pure N$_2$ or H$_2$-N$_2$ mixture, the product distribution on conversion of palmitic acid was compared over Ni/ZrO$_2$ in **Fig. 3-7**. It shows that the conversion remarkably decreased from 100% to 80%, 20%, to 3.5% at 260 $^{\circ}$C after 6 h reaction time as the H$_2$ content in the carrier gas decreased from 100%, 25%, 10% to 0. This result agrees with our kinetic performances that the major initial step is the hydrogenation (rate determining step) but not the direct decarbonylation of fatty acid, so the H$_2$ pressure plays an important role on influencing the overall reaction rates. It is worthwhile mentioning that as the carrier gas varied from H$_2$ to N$_2$, the selectivity of C$_{15}$ *n*-pentadecane decreased from 90% to 16% while the selectivity of palmitone (formed from the ketonization of palmitic acid, see Eq. 7) increased from 0 to 60%.

Ketonization: 2 C$_{15}$-COOH $\longrightarrow$ C$_{15}$-CO-C$_{15}$ + CO$_2$ + H$_2$O   (3-7)
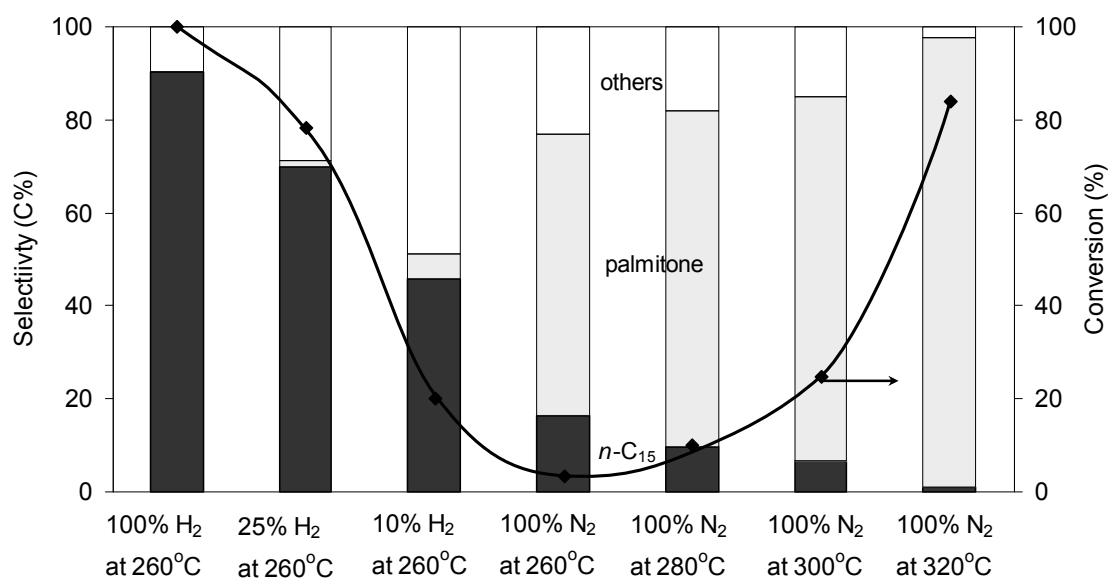
Figure 3-7. Impact of gas carrier on palmitic acid conversion wit 5 wt% Ni/ZrO$_2$ catalysts. (Experimental conditions: 1 g palmitic acid, 100 ml dodecane, 0.5 g catalyst, 12 bar flow gas with a flow speed of 20 ml/min, 6 h)
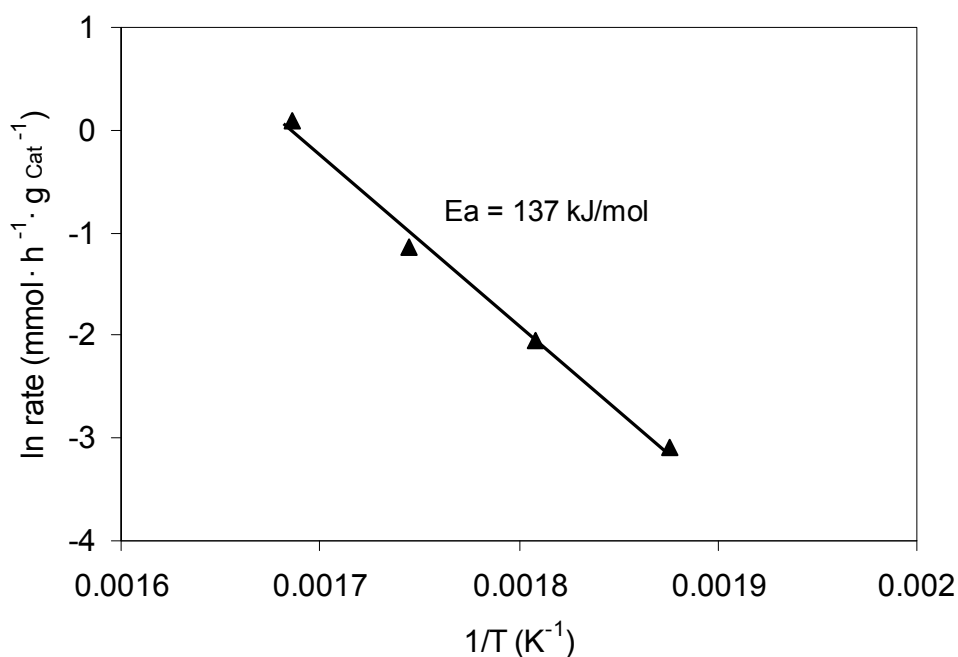
Figure 3-8. Arrhenius plot for the ketonization of palmitic acid to palmitone with 5 wt% Ni/ZrO$_2$.

With increasing the reaction temperature from 260, 280, 300, to 320 $^{\circ}$C in presence of N$_2$, the conversion of palmitic acid dramatically increased from 3.5, 10, 25, to 84% with 5 wt% Ni/ZrO$_2$ after 6 h (see **Fig. 3-7**). Palmitone became the dominating product with a selectivity of approximately 97% at 320 $^{\circ}$C. The rate of palmitic acid ketonization exhibits very strong temperature dependence, and the activation energy of palmitic acid ketonization was calculated to be 137 kJ/mol from the Arrhenius plot of the reaction rate (see **Fig. 3-8**). This value is very close to the reported activation energy of hexanoic acid ketonization (i.e., 134 kJ/mol) over Ce$_{0.5}$Zr$_{0.5}$O$_2$ catalyst.[19]

By comparison, the ketonization rate on ZrO$_2$ (1.6 mmol·h^{-1}·g$_{Cat}^{-1}$) was slightly faster than that on Ni/ZrO$_2$ (1.1 mmol·h^{-1}·g$_{Cat}^{-1}$) at 320 $^{\circ}$C (see **Fig. 3-9**). This is consistent with the reports that ZrO$_2$ is the active component for the ketonization of carboxylic acids.[20, 21] When Ni is incorporated onto ZrO$_2$ support, the rate of ketonization should decrease as part of acid and base active sites are both blocked (see **Table 3-1**). ZrO$_2$ led to nearly quantitative palmitone production from palmitic acid after 6 h. The linear increase of the palmitone yield with ZrO$_2$ (below 80% conversion) or Ni/ZrO$_2$ catalysts reveals a near zero reaction-order for the ketonization of palmitic acid to palmitone in presence of N$_2$.
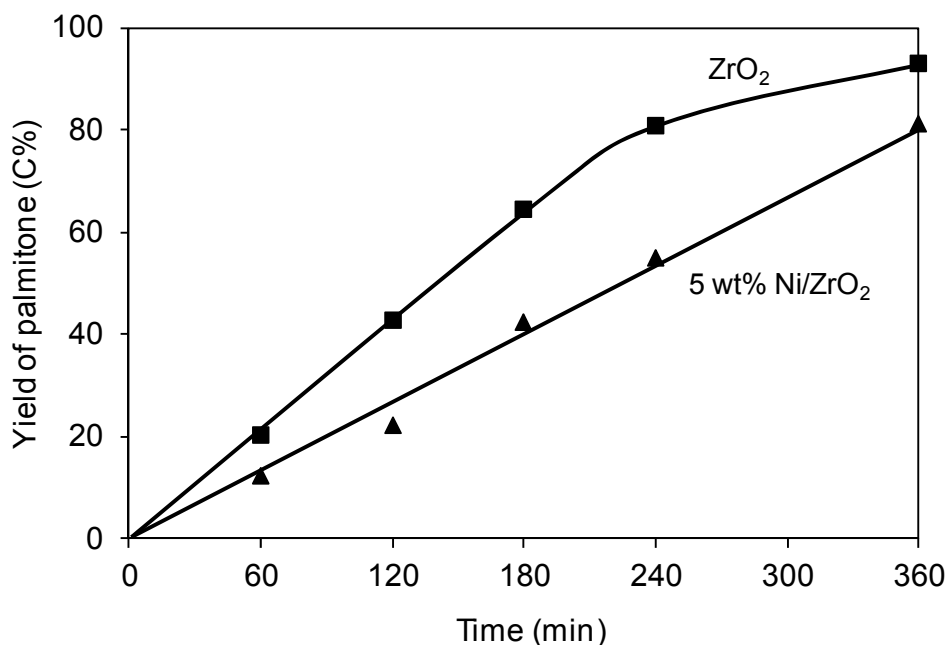
Figure 3-9. Comparison the yield of palmitone over ZrO$_2$ (■) and 5 wt% Ni/ZrO$_2$ (▲) in the presence of N$_2$. (Experimental conditions: 1 g palmitic acid, 100 ml dodecane, 0.5 g catalyst, 320 $^{\circ}$C, 12 bar N$_2$ with a flowing rate of 20 ml/min)

3.3.3. Impact of metal sites

As the metal sites can simultaneously catalyze the elementary steps such as hydrogenation of fatty acid, decarbonylation and decarboxylation of fatty acid, decarbonylation of intermediate aldehyde in the overall deoxygenation reaction, the metal sites should be very critical for determining the product distribution and reaction rates. Firstly, three metal catalysts including Pt/C, Pd/C, and Raney Ni were tested for palmitic acid conversion at 260 ^{o}C in presence of H_2 (see **Table 3-3**). High selectivity to C_{15} *n*-pentadecane was obtained on three metals (70% on Ni, 98% on Pt and Pd), but relatively low conversions were attained on Pt and Pd at 31% and 20%, respectively. A quite high selectivity of lighter hydrocarbons (16%) was obtained through hydrogenolysis at high concentrated skeletal Ni bulk catalysts, and additionally a low selectivity of palmityl palmitate (4.6%) was also observed over Raney Ni.

Table 3-3. Comparison of palmitic acid conversion on C or ZrO_2 supported catalysts [a]

Catalysts	Conv. (%)	Selectivity (C%)				
		n-C_{15}	*n*-C_{16}	Cracking	1-Hexadecanol	Palmityl palmitate
Raney Ni [b]	100	71	3.7	16	4.6	4.6
Pt/C	31	98	1.6	0.2	-	-
Pd/C	20	98	1.9	0.3	-	-
Ni/ZrO_2	100	90	0.8	9.0	-	-
Pt/ZrO_2	99	61	6.5	0.5	22	7.3
Pd/ZrO_2	98	98	0.7	1.0	-	0.1

[a] Reaction conditions: 1 g palmitic acid, 100 ml dodecane, 0.5 g catalyst (metal loading: 5 wt%), 260 ^{o}C, 12 bar H_2 with a flowing rate of 20 ml/min, 6 h.

[b] 0.25 g catalyst

By changing the support from C to ZrO_2, it is surprisingly found that the conversion nearly increased from 20-30% to 100% on Pt and Pd supported catalysts at identical conditions, which indicates the hydrogenation rate of fatty acid can be greatly promoted by the ZrO_2 support. The high selectivity of C_{15} *n*-pentadecane (98%) was obtained with Pd/ZrO_2, while Pt/ZrO_2 led to relatively low selectivity of 61% C_{15} alkanes due to the high concentration of reaction intermediate 1-hexadecanol (32%). Besides, the Ni/ZrO_2 also led to 90% selectivity of *n*-pentadecane at high activities of 100% conversion. These results imply that the hydrogenation step is highly enhanced on ZrO_2 supported metal catalysts compared to C based catalyst, and the decarbonylation step of 1-hexadecanol on Pt is much slower than that on Pd.

To differentiate the two routes of decarbonylation (-CO) and decarboxylation ($-CO_2$) with varying metal sites, the reactions of palmitic acid were conducted over pure metal catalysts of Raney Ni, Pt black and Pd black by comparing the produced ratio of CO_2 to CO. Because methanation and water gas shift reactions would interfere the ratio of CO_2/CO, these reactions were carried out at N_2 atmosphere and Raney nickel was pre-dried under inert atmosphere to remove water. The kinetics of palmitic acid over three metals at 300 $^{\circ}$C in presence of 12 bar N_2 are displayed in **Fig. 3-10a and 3-10b**. The activities of Pt black and Pd black (77 and 66 $mmol \cdot h^{-1} \cdot mol_{metal}^{-1}$, respectively) were at least 5 times higher than that of Raney nickel (9 $mmol \cdot h^{-1} \cdot mol_{metal}^{-1}$). Meanwhile, it should be noted that the decarboxylation ($-CO_2$) of palmitic acid was the dominating pathway for Pd black, as the ratio of CO_2/CO was higher than 1.8. However, the decarbonylation reaction (-CO) was more profound with Pt and Ni metals, with CO_2/CO ratios being stable at approximately 0.5. This is in accordance with a previous report that the decarboxylation reaction is more favored over Pd/C while Pt/C favors the decarbonylation route.[3]
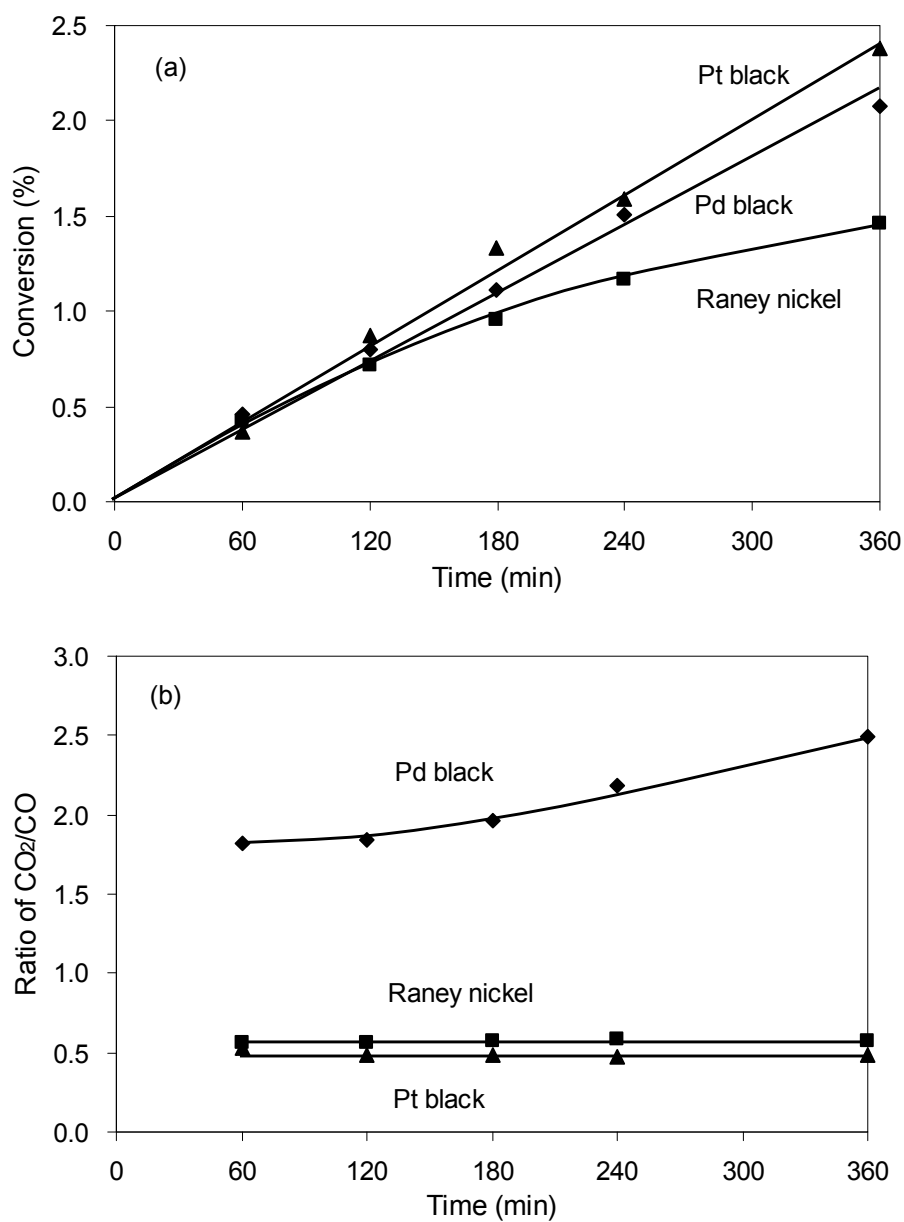
Figure 3-10. (a) Conversion and (b) the ratio of CO_2/CO for palmitic acid reaction with Pt black, Pd black, and Raney nickel in the presence of N_2. (Experimental conditions: 1 g palmitic acid, 100 ml dodecane, 0.2 mmol Pt black or Pd black, or 1 mmol Raney nickel, 300 $^{\circ}$C, 12 bar N_2 with a flowing rate of 20 ml/min)

3.3.4. Impact of supports

The effect of support is focused on ZrO_2, Al_2O_3, SiO_2, HBeta, and HZSM-5 supported Ni catalysts for conversion of palmitic acid at 260 ^{o}C in presence of 12 bar H_2 for 6 h (see **Table 3-4**). The catalyst screening on these five supported catalysts shows some interesting results. With the two forms of H-zetolite supported Ni catalysts (HBeta and HZSM-5 with Si/Al ratio of 180 and 200, respectively), the major product was C_{16} hexadecane (65-72% yield) at full conversion without carbon loss. This suggests that the tandem hydrogenation-dehydration-hydrogenation reaction is the dominating pathway on supports with Brønsted acid sites. By contrast, the Lewis oxides such as ZrO_2, Al_2O_3, or SiO_2 are not active for producing C_{16} hexadecane at selected conditions, which suggests that Lewis acid sites are much less active than Brønsted acid sites for dehydration in liquid phase. In addition, the abundance of Brønsted acid sites in HZSM-5 and HBeta catalyzed some extent of hydroisomerization with yields of *iso*-C_{15} and *iso*-C_{16} up to 20.8%, together with a small fraction of hydrocracking with 4.9-6.0% yields.

When the supports varied from H-zeolite to ZrO_2, the Ni/ZrO_2 catalysts with Ni loading of 5, 10, and 15wt% led to very high selectivity to C_{15} *n*-pentadecane (>80%) at full conversion. As the metal loading was lowered to 3 wt%, the conversion was decreased to 67% and the selectivity to C_{15} *n*-pentadecane was also lowered to 55% in accompanied with the increased 32% and 6% selectivities to C_{16} 1-hexadecanol and C_{32} palmityl palmitate, respectively. This result indicates that the Ni loading is crucial to influence both fatty acid hydrogenation and alcohol decarbonylation steps. It has also been found that the yield of lighter alkanes was enhanced from 2.5% to 14% with increasing Ni loading from 3 to 15 wt%, suggesting that the C-C bond cleavage can be realized either by the Brønsted acid sites catalyzed cracking or by Ni metal sites catalyzed hydrogenolysis. If the employed temperature was lowered to 250 ^{o}C, the cracking was suppressed from 9 to 4.2% over 5 wt% Ni/ZrO_2 indicating that the rate of cracking shows high temperature dependence. With pure ZrO_2 support, the main product was palmitone obtained from ketonization of palmitic acid with 62.8% selectivity at 6.2% conversion. The pure ZrO_2 also showed somewhat hydrogenation ability on fatty acid conversion leading to selectivities of 18% 1-hexadecanol, 7.6% palmityl palmitate, and

4% C_{15} and C_{16} hydrocarbons (see **Table 3-4**).

Table 3-4. Comparison of palmitic acid conversion on different Ni based catalysts [a]

Catalysts	Metal loading (wt%)	Conv. (%)	Selectivity (C%)						
			n- C_{15}	*iso-* C_{15}	*n-* C_{16}	*iso-* C_{16}	Cracking	1-Hexadecanol	Palmityl palmitate
ZrO_2 [b]	-	6.2	3.1	-	0.9	-	-	18	7.6
Ni/ZrO_2	3	67	55	-	2.0	-	2.5	32	5.8
Ni/ZrO_2	5	100	90	-	0.8	-	9.0	-	-
Ni/ZrO_2 [c]	5	100	95	-	0.6	-	4.2	-	-
Ni/ZrO_2	10	100	85	-	0.7	-	14	-	-
Ni/ZrO_2	15	100	83	-	0.7	-	17	-	-
Ni/Al_2O_3	5	51	74	-	1.5	-	6.8	15	3.2
Ni/SiO_2	5	41	59	-	0.7	-	5.3	33	2.3
Ni/HBeta [d]	5	100	24	4.8	49	16	6.0	-	-
Ni/HZSM-5 [e]	5	100	21	2.1	59	13	4.9	-	-

[a] Reaction conditions: 1 g palmitic acid, 100 ml dodecane, 0.5 g catalyst, 260 °C, 12 bar H_2 with a flowing rate of 20 ml/min, 6 h

[b] 62.8% selectivity: palmitone obtained from ketonization of palmitic acid

[c] Reaction at 250 °C, 8 h

[d] Si/Al = 180

[e] Si/Al = 200

The Ni supported on Al_2O_3 and SiO_2 showed similar product distribution as Ni/ZrO_2. However, the activities were much lower at 40-50% conversion, and the selectivities of C_{15} *n*-pentadecane were also decreased to 60-70% in accompanied with an increased 1-hexadecanol selectivity of 15-33%. This could be attributed either to the larger Ni particle sizes compared to Ni/ZrO_2 (8-8.8 nm *vs* 7.0 nm), or to the fact that the hydrogenation activity is promoted by ZrO_2 support.

3.4. Discussion

3.4.1. The role of metals on influencing the deoxygenation pathway

In N_2 atmosphere, the deoxygenation activity ($mmol \cdot h^{-1} \cdot mol_{metal}^{-1}$) of palmitic acid conversion follows the sequence as r (Pt black) $\approx r$ (Pd black) $> r$ (Raney nickel) (see **Fig. 3-10**). Note that Pd favors producing CO_2 from direct decarboxylation pathway, and Pt and Ni prefer forming CO via decarbonylation route (see **Scheme 3-2**). This could be attributed to the different absorption species derived from fatty acid precursor. As reported, CH_3COO^* is the main formed species for acetic acid adsorption on the surface of Pd (111), whereas both CH_3COO^* and CH_3CO^* transition state species are observed at Pt (111) surface.[22,23] This distinct adsorption behavior of the transition state species may reveal the different CO or CO_2 removal pathway, where the former absorption mode favors dropping out CO_2 via the decarboxylation route on Pd sites and the latter tends to remove CO by the decarbonylation route with Pt sites.

In N_2 atmosphere:

Route 1: Ketonization reaction

$$2\ C_{15}H_{31}\text{-COOH} \xrightarrow[\text{-CO}_2,\ \text{-H}_2\text{O}]{\text{ZrO}_2,\ \text{N}_2} C_{15}H_{31}\overset{\overset{\displaystyle O}{\|}}{\text{-C-}}C_{15}H_{31}$$

Route 2: Decarboxylation reaction

$$C_{15}H_{31}\text{-COOH} \xrightarrow[\text{-CO}_2]{\text{Pd/C},\ \text{N}_2} C_{15}H_{32}$$
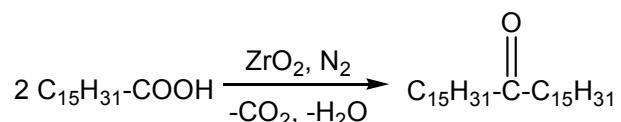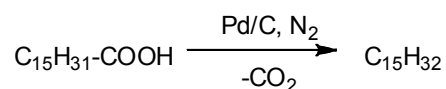
Route 3: Decarbonylation reaction

$$C_{15}H_{31}\text{-COOH} \xrightarrow[\text{-CO}]{\text{Pt/C or Raney Ni},\ \text{N}_2} C_{15}H_{32}$$
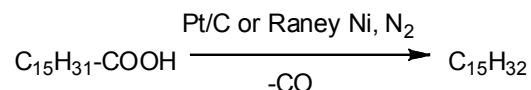
The reaction rates (unit: $mmol \cdot h^{-1} \cdot mol_{metal}^{-1}$) on deoxygenation of palmitic acid in N_2 decrease as: r Pt (Route 3) $\approx r$ Pd (Route 2) $> r$ Ni (Route 3)

In H_2 atmosphere:

Route 1: Decarbonylation route

$$C_{15}H_{31}\text{-COOH} \xrightarrow[\text{-CO}]{\text{Pt/C or Pd/C, } H_2} C_{15}H_{32}$$
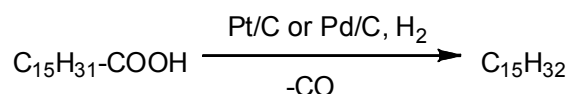
Route 2: Hydrogenation/decarbonylation reactions

$$C_{15}H_{31}\text{-COOH} \xrightarrow[H_2]{\text{Ni/ZrO}_2} C_{15}H_{31}CHO \xrightarrow[\text{-CO}]{\text{Ni/ZrO}_2} C_{15}H_{32}$$
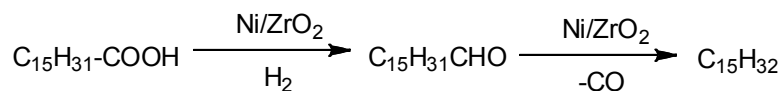
Route 3: Hydrogenation/dehydration/hydrogenation reactions

$$C_{15}H_{31}\text{-COOH} \xrightarrow[H_2]{\text{Ni/HBeta}} C_{15}H_{31}CHO \xrightarrow[H_2]{\text{Ni/HBeta}} C_{16}H_{34}O \xrightarrow[\text{-H}_2\text{O/H}_2]{\text{Ni/HBeta}} C_{16}H_{34}$$
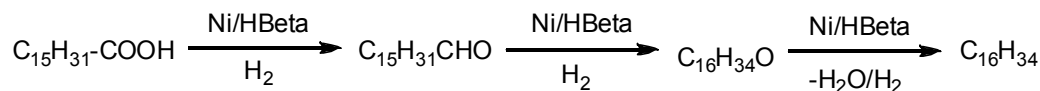
The rates (unit: mmol·g_{cat}^{-1}·h^{-1}) on deoxygenation of palmitic acid in H_2 decrease as: r Ni/HBeta (Route **3**) $> r$ Ni/ZrO2 (Route **2**) $> r$ Pd/C or Pt/C (Route **1**)

Scheme 3-2. Reaction network on deoxygenation of palmitic acid on oxide supported metal catalysts in presence of H_2 or N_2.

In H_2 atmosphere, in principle the direct decarboxylation or decarbonylation routes and the hydrogenation-decarbonylation pathway would occur in parallel. 1-Hexadecanol intermediate was not detected with Pt/C or Pd/C catalysts, but relatively large amount of 1-hexadecanol was observed with Raney nickel catalysts on conversion of palmitic acid (see **Table 3-3**). These results suggest that the direct decarboxylation or decarbonylation of fatty acid is the major pathway with the neutral carbon supported Pt or Pd catalysts, in another word, with Pt/C or Pd/C such direct route occurs much faster than the hydrogenation-decarbonylation of fatty acid. However, the latter route may take precedence over decarbonylation on the pure Ni metal sites, as the decarbonylation rate on Ni is much slower than that on Pt or Pd sites (see **Fig. 3-10**).

By employing ZrO_2 as support, the three metals (Pt, Pd, and Ni) supported catalysts varied the primary route from direct decarboxylation/decarbonylation to hydrogenation-decarbonylation, as large amount of alcohol intermediate was observed during the reaction. Meanwhile, the overall reaction rates of Pd/ZrO_2 and Pt/ZrO_2 had been greatly enhanced to full conversion through promoting the hydrogenation rates, in comparison, Pd/C and Pt/C only led to 20-30% conversions at identical conditions. Thus it can be concluded that the hydrogenation becomes the primary dominating route on these ZrO_2

based catalysts in the H_2 carrier gas. In addition, the three metal sites would also lead to different hydrogenolysis activities, e.g., Pt/ZrO_2 or Pd/ZrO_2 only attained less than 1% lighter alkanes, while in a comparative test Ni/ZrO_2 led to 9% yield due to the strong hydrogenolysis abilities of Ni sites on hydrocarbons.[24]

3.4.2. The role of supports on influencing the deoxygenation pathway

The supports possess acid and/or base sites, thus the different acid-base properties of the support would dramatically influence the dehydration of 1-hexadecanol intermediate, which finally alters the major overall reaction route. On the other side, the diverse support carriers with various BET surface areas lead to different particle sizes of supported Ni nanoclusters, and additionally some support itself such as ZrO_2 can co-catalyze the hydrogenation of fatty acids.[25] Thus, from this point the support would play an important role on influencing the metal catalyzed hydrogenation, decarbonylation, and decarboxylation steps which are also critical for determining the overall deoxygenation pathway.

The exposed six supports can be classified into four types, i) the neutral type as C, ii) the Brønsted solid acids including HBeta and HZSM-5 zeolites, iii) the Lewis acid oxides such as Al_2O_3 and SiO_2, and iv) the bifunctional acid-base oxides like ZrO_2 (see **Table 3-4**). Each type of support favors a different primary reaction route on fatty acid conversion (see **Scheme 3-2**). The C support basically would not affect the performance of metal sites, so the carbon supported metal catalysts perform similarly as the pure metal based catalysts such as Pd black or Pt black or Raney Ni which favors the direct decarbonylation route on fatty acid. When the Brønsted solid acids (HBeta and HZSM-5) are involved in, the primary route is changed into tandem hydrogenation-dehydration reactions for producing C_{16} hexadecane (yield up to 72%) because the elementary step of alcohol dehydration is highly promoted. The isomerization of hydrocarbons is also enhanced (yield: 16%) with H-zeolites due to the presence of Brønsted acid sites. If the Lewis acid oxides such as Al_2O_3 and SiO_2 are relied on, the tandem reactions hydrogenation-decarbonylation are the dominating route for producing C_{15} *n*-pentadecane with selectivity up to 74%. But the activities on these two catalysts were quite low as 40-

50% due to the low hydrogenation abilities on these two supported Ni nanoclusters. Finally, almost quantitative C_{15} *n*-pentadecane was attained over bifunctional acid-base ZrO_2 supported Ni catalysts. This promising result demonstrates that the hydrogenation rate of fatty acid (rate determining step) is significantly increased over Ni/ZrO_2 which shows remarkable support effect compared with Ni/Al_2O_3 and Ni/SiO_2. In the presence of H_2, the deoxygenation rates on palmitic acid follow the sequence (unit: mmol·h^{-1}·g$_{Cat}$$^{-1}$) of

r (Ni/HBeta or Ni/HZSM-5) $> r$ (Ni/ZrO2) $> r$ (Ni/Al2O3 or Ni/SiO2).

It has been reported that ZrO_2 with bifunctional acid and base properties are demonstrated to be a selective and active catalyst for the hydrogenation of carboxylic acid to aldehyde,[25-28] which proceeds through absorbing the carboxylic acid molecules on the oxygen vacancies of ZrO_2 to form carboxylate species. On the other hand, the dissociative activation of hydrogen molecules to hydrogen atoms occurs on the oxide surface.[27, 28] In our experiment with pure ZrO_2 (see **Table 3-4**), it indeed showed somewhat activity for the hydrogenation of palmitic acid with a conversion of 6.2 %. Therefore, ZrO_2 supported metal catalysts actually possess two active hydrogenation components (metallic Ni and ZrO_2), which would in principle promote the higher hydrogenation activity on fatty acid conversion than Al_2O_3, SiO_2 and C supported metal catalysts. Combining this knowledge allows us to generalize the plausible reaction mechanism for the hydrogenation of palmitic acid to hexadecanal with Ni/ZrO_2 in **Scheme 3-3a**. The carboxylic group of palmitic acid adsorbs at the oxygen vacancies of the ZrO_2 support to form adsorbed species, and the hydrogen molecule is dissociated to hydrogen atoms by either metallic Ni or ZrO_2, which subsequently migrates to the adsorbed species by spillover mechanism. The spillover hydrogen hydrogenates the absorbed species to hexadecanal by eliminating 1 molecular H_2O, and the oxygen vacancies on the ZrO_2 surface are recreated.

C$_{15}$H$_{31}$-COOH   C$_{15}$H$_{31}$-CHO   H$_2$O

(a)

CO$_2$ + C$_{15}$H$_{31}$—C—C$_{15}$H$_{31}$ + H$_2$O

C$_{15}$H$_{31}$-COOH   C$_{15}$H$_{31}$-COOH

(b)
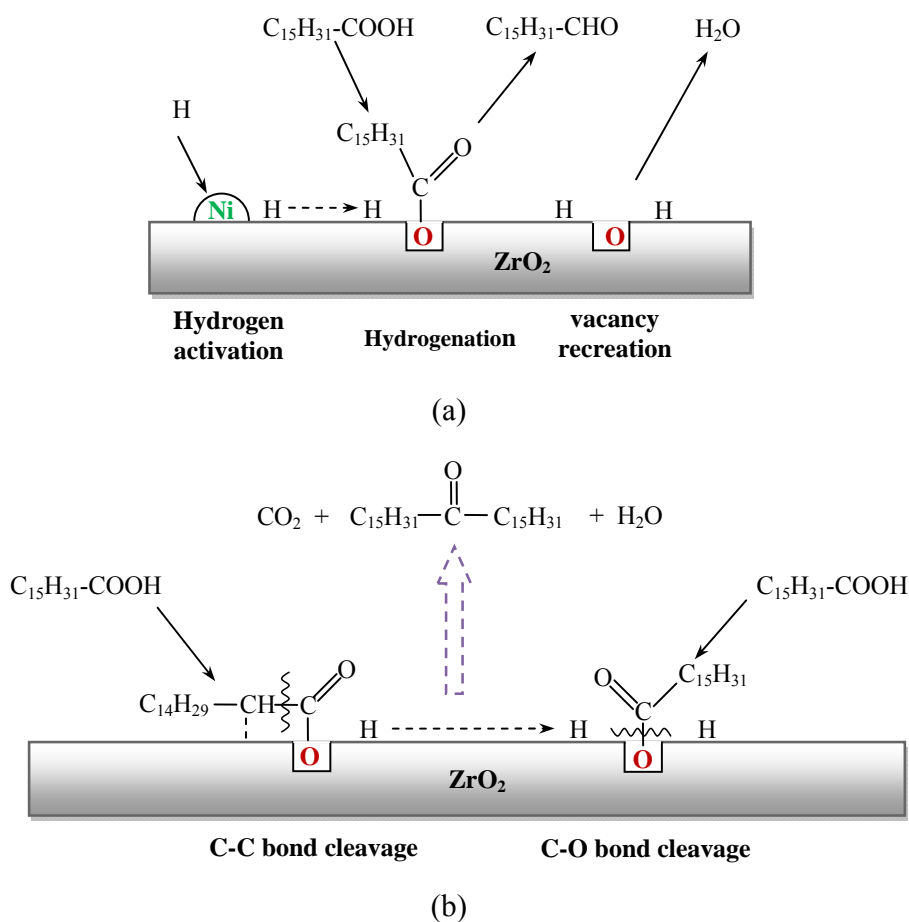
Scheme 3-3. Proposed reaction mechanism for (a) the hydrogenation of palmitic acid to hexadecanal via synergetic catalysis over Ni/ZrO$_2$ in presence of H$_2$, and (b) for the ketonization of palmitic acid to palmitone over ZrO$_2$ in presence of N$_2$.

3.4.3. The role of gas carriers on influencing the deoxygenation pathway

Employing the gas carrier from H$_2$ to inert gas such as N$_2$ would completely change the reaction pathway, because in N$_2$ atmosphere either the hydrogenation step is ruled away or the decarboxylation and decarbonylation are highly suppressed. The experimental results in **Fig. 3-7** show that with altering the gas carrier from H$_2$ to N$_2$, the conversion of palmitic acid substantially decreased from 100% to 3.5% with Ni/ZrO$_2$ as the hydrogenation step (rate determining step) is suppressed, and the product distribution shifted from C$_{15}$ *n*-pentadecane to palmitone obtained from ketonization of palmitic acid

during the variation of gas carrier. But note that the ketonization reaction of fatty acid in N_2 (rate: 0.03 mmol·h^{-1}·g$_{Cat}^{-1}$) exhibited to be much slower than the hydrogenation step in H_2 (rate: 1.3 mmol·h^{-1}·g$_{Cat}^{-1}$) at 260 ^{o}C with Ni/ZrO$_2$ (see **Scheme 3-2**).

The route of hydrogenation-decarbonylation over Ni/ZrO$_2$ has been illuminated as mentioned above (see **Scheme 3-1 and 3-3a**). While the ketonization reaction on carboxylic acid is catalyzed by metal oxides with bifunctional acid-base oxides such as ZrO$_2$, CeO$_2$, Cr$_2$O$_3$, Fe$_2$O$_3$, ZnO, and TiO$_2$.[20,21,28] The ketonization of carboxylic acid usually follows two-step reactions. As reported, for example, acetic acid is firstly adsorbed on the vacancies of metal oxides to form acetate species which has the parallel configuration with the oxide surface due to the strong interaction of α-hydrogen atoms with the surface, and then the formed acetate species react with the adjoining acetate species to form acetone by eliminating 1mole of H_2O and CO_2.[28]

Overall, the reaction mechanism on conversion of palmitic acid with ZrO$_2$ supported metal catalysts in presence of H_2 or N_2 can be generalized. The adsorption of palmitic acid on the oxygen vacancies of ZrO$_2$ to form palmitate species occurs as the first step. Subsequently, these absorbed species would be further converted through different routes according to the different gas carrier. In the H_2 gas carrier, the formed palmitate species are hydrogenated with the dissociated hydrogen atoms to produce hexadecanal and water. In the N_2 gas carrier, the palmitate species prefer to react with the neighboring palmitate species to form palmitone over the ZrO$_2$ support by eliminating carbon dioxide and water (see **Scheme 3-3b**). Therefore, the hydrogen coverage on the active sites determined by the gas carrier guides the formed palmitate species to follow either hydrogenation-decarbonylation or self-condensation (ketonization) pathway.

3.5. Conclusions

A route for quantitative conversion of palmitic acid to *n*-pentadecane has been developed with Ni/ZrO$_2$ in the presence of H_2. The deoxygenation mechanism undergoes via an initial hydrogenation of the carboxylic group of the palmitic acid to hexadecanal (rate determining step), which is in a hydrogenation/dehydrogenation equilibrium towards 1-hexadecanol formation at a relatively high hydrogen pressure, followed by

subsequent decarbonylation of hexadecanal to produce the target *n*-pentadecane and carbon monoxide (major route). By contrast, the direct decarboxylation/decarbonylation or hydrogenation-dehydration route occurs as minor route. Furthermore, palmityl palmitate is formed through esterification of palmitic acid with the hydrogenation intermediate 1-hexadecanol, and as the reaction proceeds, such ester is sequentially hydrogenolyzed and decarbonylated to *n*-pentadecane on the Ni sites.

Concerning on the support effect, the C support would not affect the performance of metal sites such as Pd, Pt and Ni which favor the direct decarbonylation/decarboxylation route of fatty acid. If the Brønsted solid acids (HBeta and HZSM-5) are employed, the primary route appears to be tandem hydrogenation-dehydration reactions for producing C_{16} hexadecane. The Lewis acid oxides such as Al_2O_3 and SiO_2 lead to the tandem reactions of hydrogenation-decarbonylation for producing C_{15} *n*-pentadecane. Whereas, almost quantitative C_{15} *n*-pentadecane is attained over bifunctional acid-base ZrO_2 supported Ni catalysts. Note that the hydrogenation of fatty acid to aldehyde (the rate determining step) is synergistically promoted by the ZrO_2 support through adsorbing the carboxylic group at the oxygen vacancies. In the presence of H_2, the deoxygenation rates on palmitic acid follow the orders (unit: $mmol·h^{-1}·g_{Cat}^{-1}$) as r (Ni/HBeta or Ni/HZSM-5) > r (Ni/ZrO2) > r (Ni/Al2O3 or Ni/SiO2).

In the N_2 gas carrier, three metals showed the deoxygenation activity on palmitic acid following the sequence (unit: $mmol·h^{-1}·mol_{metal}^{-1}$) of r (Pt black) ≈ r (Pd black) > r (Raney nickel). In addition, Pd favors producing CO_2 from direct decarboxylation reaction, and Pt and Ni prefer forming CO via decarbonylation route. On the ZrO_2 support, ketonization becomes to be the primary reaction.

Summarizing the reaction mechanism on conversion of palmitic acid with ZrO_2 supported metal catalysts, the palmitic acid firstly adsorbs on the oxygen vacancies of ZrO_2 to form palmitate species. This absorbed species would select different following routes according to the presented gas carrier. In the H_2 gas carrier, the formed palmitate species are hydrogenated with the dissociated hydrogen atoms on the metal sites to produce hexadecanal and water. In the N_2 gas carrier, the palmitate species prefer to react with the neighboring palmitate species to form palmitone over the ZrO_2 support through

eliminating carbon dioxide and water. Thus, in principle the gas carrier determines the reaction pathway via modifying the adsorbed transition species.

3.6. Acknowledgments

3.7. References

1. D. Kubicka, J. Horacek, Appl. Catal. A: Gen. 394 (2011) 9.

2. L. X. Li, E. Coppola, J. Rine, J. L. Miller, D. Walker, Energy Fuels 24 (2010) 1305.

3. M. Snåre, I. Kubičková, P. Mäki-Arvela, K. Eränen, D. Y. Murzin, Ind. Eng. Chem. Res. 45 (2006) 5708.

4. M. Snåre, I. Kubičková, P. Mäki-Arvela, D. Chichova, K. Eränen, D. Yu. Murzin, Fuel 87 (2008) 933.

5. J. G. Immer, M. J. Kelly, H. H. Lamb, Appl. Catal. A: Gen. 375 (2010) 134.

6. G. W. Huber, P. O'Connor, A. Corma, Appl. Catal. A: Gen. 329 (2007) 120.

7. Kumar, R.; Rana, B. S.; Wiwari, R.; Verma, E.; Kumar, R.; Joshi, R. K.; Garg, M. O.; Sinha, A. K. Green Chem. 12 (2010) 2232.

8. Sotelo-Boyás, R.; Liu, Y. Y.; Minowa, T. Ind. Eng. Chem. Res. 50 (2011) 2791.

9. E. Laurent, B. Delmon, J. Catal. 146 (1994) 281.

10. A. Centeno, E. Laurent, D. Delmon, J. Catal. 154 (1995) 288.

11. T. R. Viljava, R. S. Komulanien, A. O. I. Krause, Catal. Today 60 (2000) 83.

12. B. Peng, Y. Yao, C. Zhao, J. A. Lercher, Angew. Chem. Int. Ed. (2011), DOI: 10.1002/anie.201106243.

13. K. Murata, Y. Liu, M. Inaba, I. Takahara, Energy Fuels 24 (2010) 2404.

14. J. Fu, X. Y. Lu, P. E. Savage, Energy Environ. Sci. 3 (2010) 311.

15. U. Birkenstock, R. Holm, B. Reinfandt, S. Storp, J. Catal. 93 (1985) 55.

16. P. K. Doolin, S. Alerasool, D. J. Zalewski, J. F. Hoffman, Catal. Lett. 25 (1994) 209.

17. A. Wawrzetz, B. Peng, A. Hrabar, A. Jentys, A. A. Lemonidou, J. A. Lercher, J. Catal. 269 (2010) 411.

18. B. Peng, C. Zhao, I. Mejía-Centeno, G. A. Fuentes, A. Jentys, J. A. Lercher, Catal. Today (2011), DOI: 10.1016/j.cattod.2011.10.022.

19. C. A. Gaertner, J. C. Serrano-Ruiz, D. J. Braden, J. A. Dumesic, J. Catal. 266 (2009) 71.

20. R. Pestman, R.M. Koster, A.V. Duijine, J.A.Z. Pieters, V. Ponec, J. Catal. 168 (1997) 265.

21. T. S. Hendren, K. M. Dooley, Catal. Today 85 (2003) 333.

22. R. D. Haley, M. S. Tikhov, R. M. Lambert, Catal. Lett. 76 (2001) 125.

23. K. I. Gursahani, R. Alcala, R. D. Cortright, J. A. Dumesic, Appl. Catal. A: Gen 222 (2001) 369.

24. G. Maire, G. Plouidy, J. C. Prudhomme, F. G. Gault, J. Catal. 4 (1965) 556.

25. R. Pestman, R.M. Koster, J.A.Z. Pieters, V. Ponec, J. Catal. 168 (1997) 255.

26. T. Yokoyama, T. Setoyama, N. Fujita, M. Nakajima, T. Maki, Appl. Catal. A: Gen. 88 (1992) 149.

27. R. Pestman, R. M. Koster, E. Boellaad, A. M. van der Kraan, V. Ponec, J. Catal. 174 (1998) 142.

28. T. Yokoyama, N. Yamagata, Appl. Catal. A: Gen. 221 (2001) 227.

Chapter 4

Selective C-O and C-C bonds cleavage for converting microalgae oil to alkanes with transition metal oxide supported nickel

The route on selectively cleaving C-O and C-C bonds is developed for converting crude microalgae oil into diesel range alkanes with ZrO_2 supported Ni catalysts. The integrated hydrogenolysis of triglyceride, the hydrogenation of functional groups (i.e., -COOH, -CHO, C=C), and the decarbonylation of aldehyde reactions (-CO) are catalyzed by metallic Ni sites. The elementary reaction rates follows, k_1 (hydrogenation of C=C double bonds in the alkyl chain) >> k_2 (hydrogenolysis of saturated triglycerides) > k_4 (decarbonylation of alcohol) > k_3 (hydrogenation of fatty acids. It should be emphasized that, the hydrogenation of fatty acid to aldehyde (the rate determining step) is synergistically promoted by the ZrO_2 support through simultaneously adsorbing the carboxylic group at the oxygen vacancy and dissociating the hydrogen molecules.

4.1. Introduction

The diesel range alkanes rather than biodiesel (fatty acid alkyl esters) produced from triglyceride is considered to be one of the most promising energy carriers. [1] Two methods can be efficiently utilized to refine triglycerides via oxygen removal process. One option is to employ the conventional hydrotreating catalysts, e.g., sulfided NiMo and CoMo, for upgrading. [2] However, the sulfided catalysts contaminate the alkane products through sulfur incorporation, and suffer from serious deactivation due to sulfur leaching, especially in presence of small trace amount of water. [3] The second is relied on using zeolite supported metal catalysts, e.g., Ni/HBeta and Pt-Re/HZSM-5, for producing C$_{15}$-C$_{18}$ alkanes via hydrodeoxygenation routes. [4] Considering that the hydrogen consumption for deoxygenation of triglycerides decreases in the sequence of hydrodeoxygenation > decarbonylation > decarboxylation, [5] the decarbonylation or decarboxylation route is more economical and feasible in principle.

Compared to the raw feedstock (triglycerides) originating from the animal fats and vegetable oils, microalgae is shown to be more attractive not only because of its high oil content (up to 60 wt%) [6] and rapid growth rates, [7] but also because of its uncompetitive growth mode with edible food/oil production. So herein, in the first part of this work, we report that a novel and stable catalyst, i.e., Ni/ZrO$_2$, can selectively cleave C-C and C-O bonds for converting C$_{18}$ fatty acid to C$_{17}$ *n*-heptadecane via tandem hydrogenation-decarbonylation route. In the second part we demonstrate that crude microalgae oil can also be efficiently converted into sulfur-free alkanes over Ni/ZrO$_2$ with high activity and stability in both batch and continuous flow reactors at 270 $^{\circ}$C in the presence of 40 bar H$_2$.

4.2. Experimental

4.2.1. Chemicals

All chemicals were obtained from commercial suppliers: stearic acid (Fluka, analytical standard), 1-octadecanol (Fluka, ≥99.5% GC assay), dodecane (Sigma-Aldrich,

≥99% Reagent Plus), eicosane (Aldrich, ≥99% GC assay), *n*-octadecane (Fluka, ≥99% GC assay), *n*-heptadecane (Fluka, ≥99% GC assay), nickel (II) nitrate hexahydrate (Sigma-Aldrich, ≥98.5%), ZrO$_2$ (MEL Chemicals), TiO$_2$ (Degussa P25), CeO$_2$ (Rhodia HAS-10), ZnO (Sigma-Aldrich), SiO$_2$ (Aeroxide Alu C-Degussa), Al$_2$O$_3$ (Aeroxide Alu C-Degussa). Microalgae oil was provided by VERFAHRENSTECHNIK Schwedt GmbH.

4.2.2. Catalyst preparation and characterization

Ni supported on ZrO$_2$, TiO$_2$, CeO$_2$, ZnO, SiO$_2$ and Al$_2$O$_3$ were synthesized by the wetness impregnation method. The ZrO$_2$ support was prepared from zirconium hydroxide by calcination in air at 400 ^{o}C for 4 h. For example, the procedure for preparing 10 wt% Ni/ZrO$_2$ follows: Ni(NO$_3$)$_2$·6H$_2$O (5.83 g) was dissolved in water (10 g), and then such solution was slowly dropped onto ZrO$_2$ (10 g) with continuous stirring. After metal incorporation with support at ambient temperature for 4 h, the catalyst was firstly dried overnight at ambient temperature and then dried at 110 ^{o}C for 12 h. Afterwards, the catalyst was calcined in synthetic air at 400 ^{o}C for 4 h (flow rate: 100 ml/min) and reduced at 500 ^{o}C for 4 h (ramp: 2 ^{o}C/min) in hydrogen (flow rate: 100 ml/min).

Atomic absorption spectroscopy (AAS) was used for analyzing the metal loading. The nitrogen adsorption-desorption was adopted for measuring BET surface area and pore size distribution. The temperature programmed desorption (TPD) of ammonia and carbon dioxide were used for acid and basic sites measuring. The characterization methods have been described in detail in Chapter 3.

4.2.3. Reaction procedures

Experimental procedure for autoclave batch reaction

The typical experiments with microalgae oil, stearic acid, or 1-octadecanol were carried out as follows, reactant (1.0 g), dodecane (100 ml), and catalyst (0.5 g) were loaded into the batch autoclave (Parr Instrument, 300 ml). Then it was purged with N$_2$ at ambient temperature, and until the required temperature achieved it was pressurized by H$_2$. The reaction was carried out at 260 ^{o}C in presence of 40 bar H$_2$ (reaction temperature)

at a stirring speed of 600 rpm for 8 h. The products in the vapor phase were analyzed by online gas chromatograph (GC), while the liquid samples were manually collected during the run and later analyzed by GC-MS.

Experimental procedure for continuous flow reactor

The continuous flow reaction system with trickle bed reactor used for catalyst stability and deactivation test is schematically shown in **Figure 4-1**. The stainless steel tubular reactor (1/4 inch o.d.) was loaded with 0.5 g catalyst with a particle size between 150-280 μm. After the reduction of the catalysts in H_2 at 450 ^{o}C for 2 h, the system was kept at 270 ^{o}C and pressurized with H_2 to 40 bar. A liquid solution of microalgae oil in dodecane (1.33 wt%, 0.2 ml/min) was introduced into the system with a HPLC pump. The liquid samples were separated from the effluents by the 16-port sampling loop, collected in sixteen vials, and finally analyzed by GC-MS. The analysis methods have also been described in detail in Chapter 3.
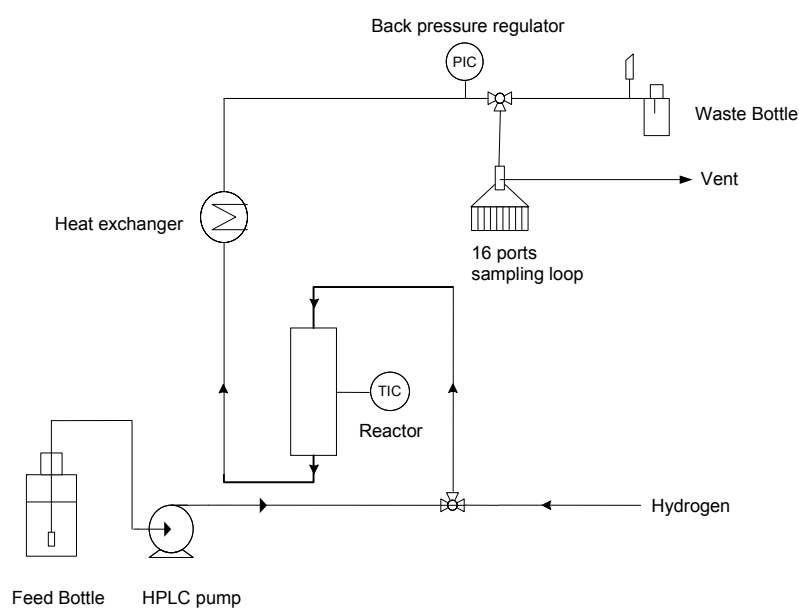

Figure 4-1. Scheme of trickle bed reactor for upgrading of microalgae oil in a continuous flow reactor.

4.3. Results and Discussion

4.3.1. Microalgae oil composition

Microalgae oil is a neutral lipid consisting of mono-, di-, and tri-glycerides. The microalgae oil (provided by Verfahrenstechnik Schwedt GmbH) used for this present work contains of fatty acids ranging from C_{14}-C_{24}, mainly of C_{18} fatty acids (88.4 wt% unsaturated and 4.4 wt% saturated, in total: 92.8 wt%) (see **Table 4-1**). Therefore, in the first step, the representative fatty acid component, C_{18} stearic acid, was selected as the model compound for developing the active catalysts and understanding the fundamental chemistry during the deoxygenation process.

Table 4-1. Fatty acid composition of microalgae oil [a]

Fatty acids composition [wt%]												
$C_{14:0}$[b]	$C_{16:0}$	$C_{18:2}$	$C_{18:1}$	$C_{18:0}$	$C_{20:4}$	$C_{20:0}$	$C_{22:6}$	$C_{22:4}$	$C_{22:1}$	$C_{22:0}$	$C_{24:0}$	Sterol
0.04	4.41	56.2	32.2	4.41	0.07	0.43	0.13	0.19	0.97	0.44	0.36	0.12

[a] Crude microalgae oil provided by VERFAHRENSTECHNIK Schwedt GmbH.

[b] The nomenclature shows the number of carbon atoms and the number of C=C double bonds: for example the alkyl chain of the present fatty acid contains14 C atoms and no double bonds.

4.3.2. Catalyst characterization and catalyst screening

Six supports including ZrO_2, TiO_2, CeO_2, ZnO, Al_2O_3, and SiO_2 were selected, and the Ni catalysts were incorporated on these supports by the incipient wetness impregnation method (metal loading: 3-15 wt%). They are characterized by AAS (metal loading), N_2 sorption (BET surface area), XRD for metal sites, TPD of NH_3 (acid sites), and TPD of CO_2 (base sites) (see **Table 4-2**). The specific surface areas of ZrO_2, TiO_2, CeO_2, ZnO, Al_2O_3 and SiO_2 supported Ni catalysts (10 wt.%) were approximately 100,

50, 95, 10, 80, and 170 m^2/g, respectively. The Ni particle sizes of Ni/ZrO$_2$ increased from 5 nm to 18 nm (determined from XRD patterns, see **Figure 4-2**) as the Ni content increased from 3 to 15 wt%. Whereas the average Ni particle sizes on the rest oxide support (loading: 10 wt%) were 10-21 nm. The acidic and basic site concentrations of the parent material of ZrO$_2$ were 0.103 and 0.169 mmol/g, both of which gradually decreased when the Ni content increased.

Table 4-2. Physicochemical properties of catalysts

Entry	Catalysts	Ni loading (wt%)	BET surface area (m^2/g)	$d_{Ni(111)}$ [a]	Acidity (mmol/g) [b]	Basicity (mmol/g) [c]
1	ZrO$_2$	-	113.3	-	0.103	0.169
2	Ni/ZrO$_2$	3.2	103.2	5.2	0.094	0.159
3	Ni/ZrO$_2$	5.1	97.8	7.0	0.093	0.151
4	Ni/ZrO$_2$	10.1	96.8	11.6	0.077	0.139
5	Ni/ZrO$_2$	14.8	93.0	18.0	0.065	0.135
6	Ni/TiO$_2$	10.0	48.2	15.5	0.104	0.007
7	Ni/CeO$_2$	9.8	95.3	10.3	0.039	0.031
8	Ni/Al$_2$O$_3$	9.9	81.6	13.3	0.063	0.012
9	Ni/SiO$_2$	10.0	173.2	20.2	0	0
10	Ni/ZnO	10.2	10.2	21.5	0	0.003

[a] Calculated from XRD by Scherrer equation.

[b] Determined by TPD of ammonia.

[c] Determined by TPD of carbon dioxide.
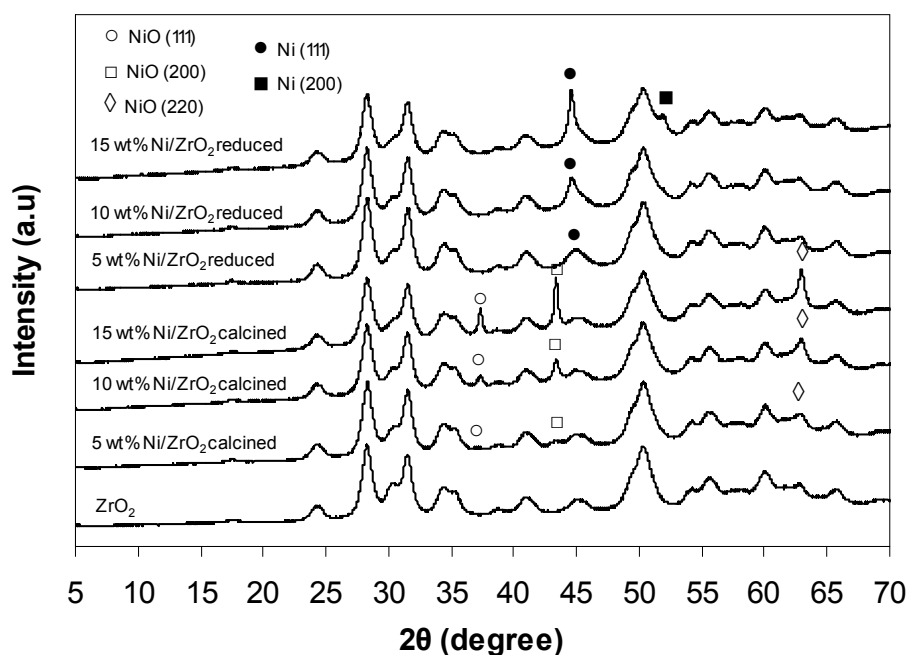
(a)

(b)

Figure 4-2. X-ray diffraction patterns of (a) ZrO$_2$ supported catalysts and (b) Ni supported on TiO$_2$, CeO$_2$, Al$_2$O$_3$, SiO$_2$ and ZnO catalysts

To screen a suitable catalyst, the catalytic conversion of stearic acid was carried out at a batch mode at 260 $^{\circ}$C in the presence of 40 bar H$_2$ (see **Table 4-3**). It showed that almost quantitative C$_{17}$ *n*-heptadecane was obtained over Ni/ZrO$_2$ with metal loading of 5-15 wt%. At the low Ni content of 3 wt%, 51% yield of C$_{17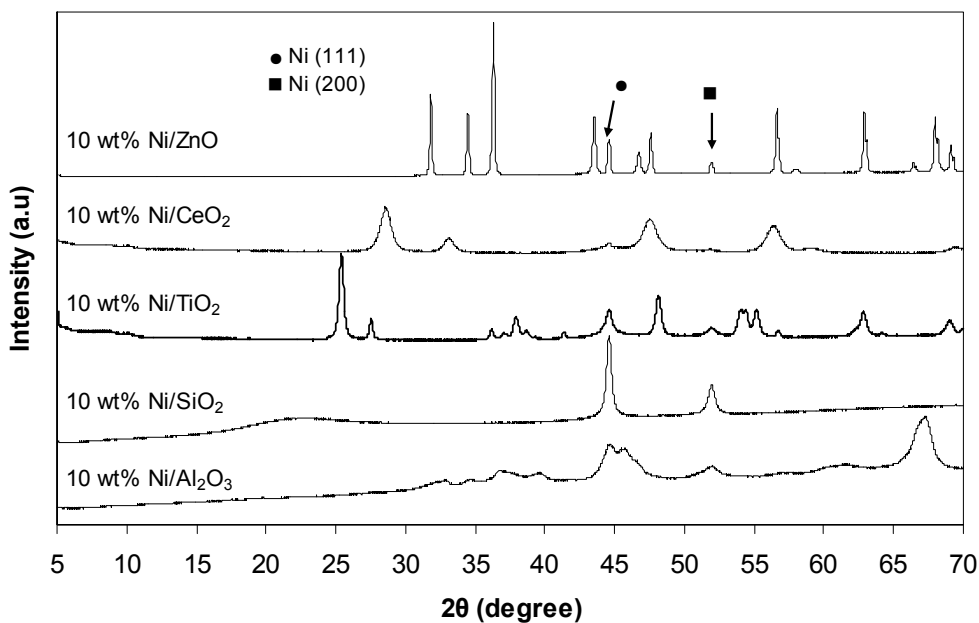}$ *n*-heptadecane was produced accompanied with 33% yield of C$_{18}$ 1-octadecanol and 7% yield of stearyl stearate. While on the pure ZrO$_2$ support, it led to 3.2% C$_{17}$ alkane, 29% C$_{18}$ 1-octadecanol, 56% C$_{31}$ stearone, and 12% C$_{32}$ stearyl stearate at 13% conversion. Stearone was produced by the ketonization of stearic acid, and stearyl stearate was formed through esterification of stearic acid with the intermediate 1-octadecanol on the acidic or basic sites. On the other side, Ni/TiO$_2$ and Ni/CeO$_2$ (10 wt%) also showed quantitative activity as Ni/ZrO$_2$ (10 wt%), but led to slightly lower selectivity to C$_{17}$ *n*-heptadecane at 87% and 93%, respectively. Ni/Al$_2$O$_3$, Ni/SiO$_2$ and Ni/ZnO, however, showed poor activity at 42-63% with C$_{17}$ *n*-heptadecane selectivity of 81%, 57% and 31%, respectively.

Table 4-3. Comparison of stearic acid conversion over different catalysts at 260 $^{\circ}$C [a]

Catalyst	Conv. (%)	Selectivity (C%)				
		n-C$_{17}$	*n*-C$_{18}$	1-Octadecanol	Cracking	Stearyl stearate
ZrO$_2$[b]	13	3.2	-	29	-	12
3 wt% Ni/ZrO$_2$	96	51	2.5	33	3.4	7.6
5 wt% Ni/ZrO$_2$	100	90	2.0	6.7	1.0	-
10 wt% Ni/ZrO$_2$	100	96	1.5	1.2	1.2	-
15 wt% Ni/ZrO$_2$	100	96	1.5	1.4	1.3	-
10 wt% Ni/TiO$_2$	98	87	5.0	6.7	0.9	0.7
10 wt% Ni/CeO$_2$	100	93	0.4	3.5	2.8	-
10 wt% Ni/Al$_2$O$_3$	63	81	0.7	14	0.9	3.5
10 wt% Ni/SiO$_2$	45	57	1.5	34	1.3	5.8
10 wt% Ni/ZnO	42	31	0.8	34	0.7	33

[a] Reaction conditions: stearic acid (1.0 g), dodecane (100 ml), catalyst (0.5 g), 40 bar H$_2$, 8 h.

[b] 56% selectivity: stearone obtained from ketonization of stearic acid.

4.3.3. Kinetics of stearic acid and intermediates reactions

To explore the reaction mechanism on deoxygenation of stearic acid, the kinetics was conducted on the best performed catalyst (10 wt% Ni/ZrO_2) at 260 ^{o}C (see **Figure 4-3**). It clearly showed that the yield to C_{17} *n*-heptadecane continuously increased to 96% with the increasing conversion of C_{18} stearic acid, while the yield of 1-octadecanol (main intermediate) firstly increased to 28% (maximum yield) and then decreased to zero when the reaction completed. However, the expected intermediate octadecanal was only observed in trace (concentration < 0.2%).
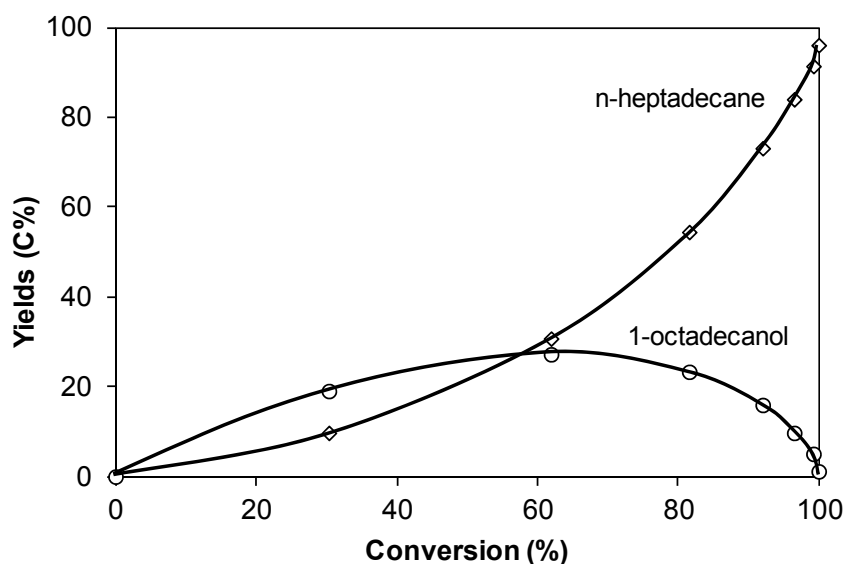
Figure 4-3. Yields of *n*-heptadecane and 1-octadecanaol as a function of stearic acid conversion over 10 wt% Ni/ZrO_2. Reaction conditions: stearic acid (1.0 g), 10 wt% Ni/ZrO_2 (0.5 g), dodecane (100 ml), 260 ^{o}C, 40 bar H_2 (reaction temperature), 8 h

The intermediate 1-octadecanol was further separately converted with 10 wt% Ni/ZrO_2 at identical conditions as a function of time in order to understand the chemistry in deoxygenation (-CO) of aliphatic alcohol (**Figure 4-4a**). The result showed that the yield of C_{17} *n*-heptadecane almost linearly increased with the conversion of C_{18} 1-octadecanol, attaining 92% yield at 96% conversion after 7 h, with only 3% yield of C_{18} alkane (produced by tandem dehydration-hydrogenation reactions) being formed. This suggests that an equilibrium between alcohol and aldehyde should exist, and the followed

decarbonylation of aldehyde (-CO) produces the target C$_{17}$ alkane at a relatively faster rate. This catalytic chemistry, i.e., C-C bond selective cleavage, is quite similar to our previous reported decarbonylation of C$_3$ alcohols over Pt/Al$_2$O$_3$ catalysts. [8]
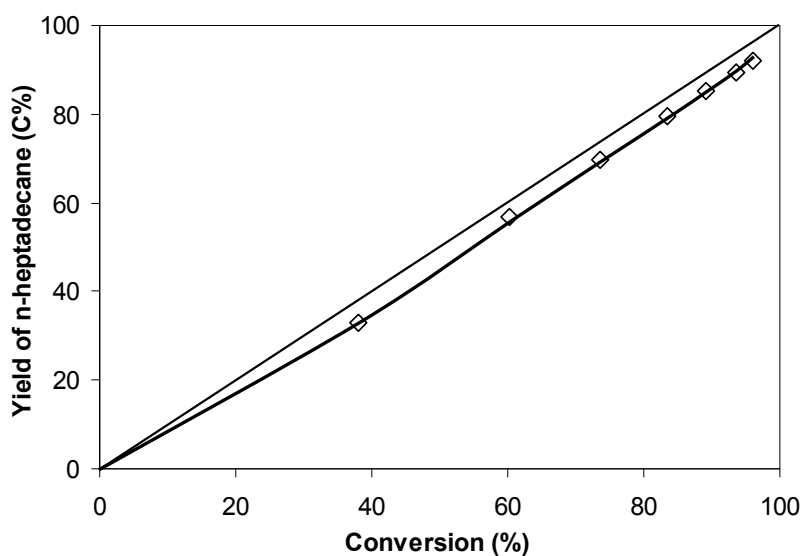
(a)
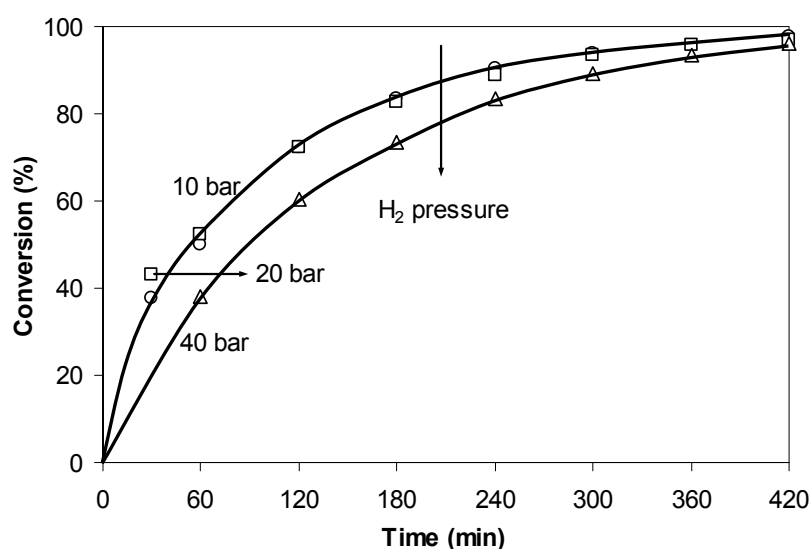
(b)

Figure 4-4. (a) Yield of C$_{17}$ *n*-heptadecane versus C$_{18}$ 1-octadecanol conversion. (b) Impact of H$_2$ pressure on C$_{18}$ 1-octadecanol conversion as a function of time. Reaction conditions: 1-octadecanol (1.0 g), 10 wt% Ni/ZrO$_2$ (0.15 g), dodecane (100 ml), 260 ^{o}C, for 7 h, stirred at 600 rpm; (a) 40 bar H$_2$; (b) 12, 20, 40 bar H$_2$.

The thermodynamic calculation on the hydrogenation-dehydrogenation equilibrium in gas phase (**Figure 4-5**) demonstrates that the higher pressure benefits the equilibrium shifts from octadecanal to 1-octadecanol at 260 °C. Furthermore, the equilibrium constant K (C$_{alcohol}$/C$_{aldehyde}$) is calculated to be ca. 57 in presence of 40 bar H$_2$ (present used), and this provides some insight for explaining of the detected trace concentration of C$_{18}$ aldehyde during the conversion of C$_{18}$ acid and C$_{18}$ alcohol at selected conditions. Meanwhile, we investigated the role of H$_2$ pressure (12, 20, 40 bar) on 1-octadecanol conversion with Ni/ZrO$_2$ at 260 °C (**Figure 4-4b**), and it revealed that the reaction rate dramatically speeded up at a lower pressure (12 bar). The initial decarbonylation rate of 1-octadecanol at 12 bar H$_2$ (6.0 mmol·g^{-1}·h^{-1}) is almost two times of that at 40 bar H$_2$ (3.0 mmol·g^{-1}·h^{-1}). This is consistent with the fact that the lower hydrogen pressure shifts the equilibrium to octadecanal, which would enhance the decarbonylation reaction due to the presence of a higher concentration of octadecanal.
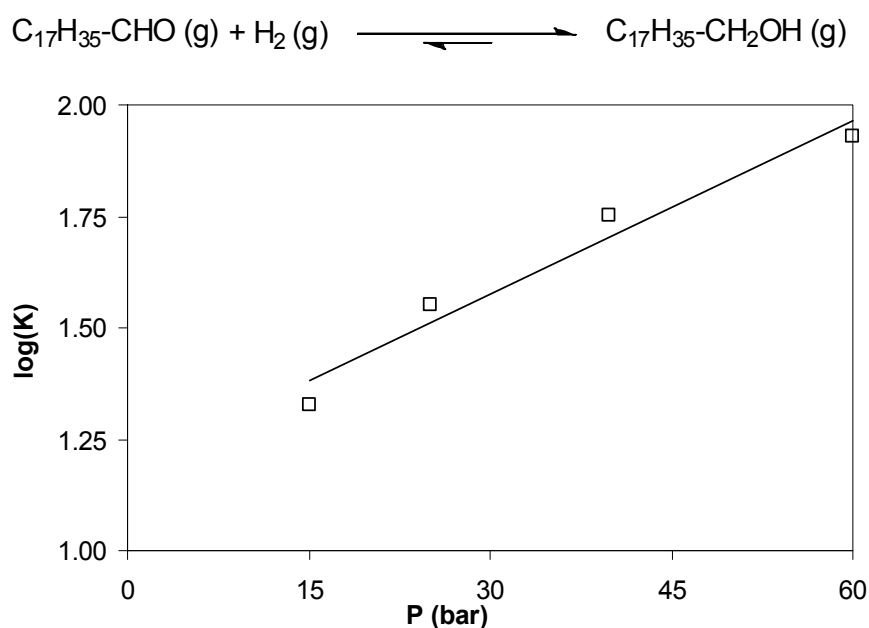
$$C_{17}H_{35}\text{-CHO (g)} + H_2 \text{(g)} \rightleftharpoons C_{17}H_{35}\text{-CH}_2\text{OH (g)}$$

Figure 4-5. Log K values for hydrogenation of octadecanal to 1-octadecanol as a function of varying hydrogen pressure at 260 °C.

4.3.4. Reaction pathways for stearic acid conversion

From the individual kinetics on conversion of stearic acid and 1-octadecanol, it can be estimated that the decarbonylation step (rate: 3.0 mmol·g^{-1}·h^{-1}) is around three times faster than the hydrogenation of stearic acid (rate: 0.9 mmol·g^{-1}·h^{-1}) on Ni/ZrO₂, thus the hydrogenation of fatty acid is concluded to be the slowest (rate determining) step in the overall reaction. The impact of temperatures (250 to 270 ^{o}C) reveals a high apparent activation energy of ca. 151 KJ/mol on stearic acid hydrogenation over Ni/ZrO₂ (see **Figure 4-6**). This high energy barrier of the hydrogenation step is in line with the slowest reaction rate.
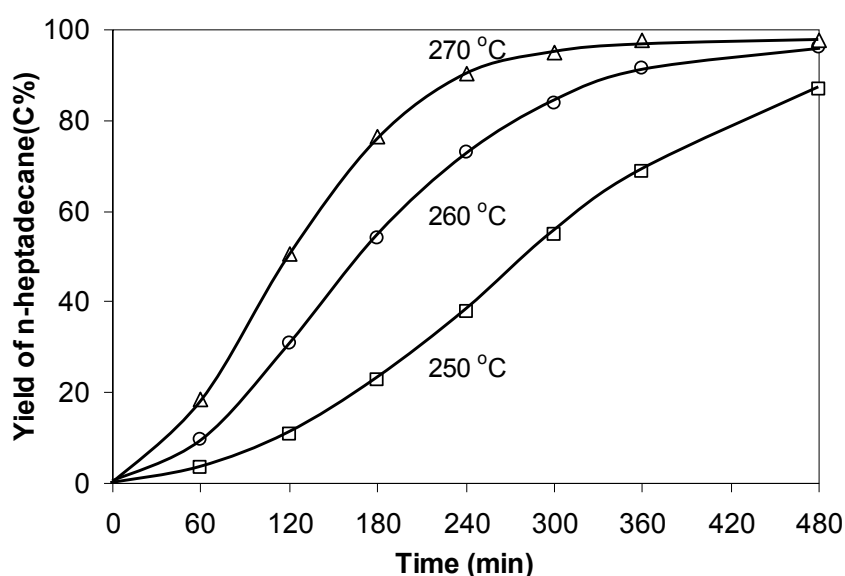
Figure 4-6. Impact of reaction temperature on stearic acid conversion with 10 wt% Ni/ZrO₂. Reaction conditions: stearic acid (1.0 g), dodecane (100 ml), 10 wt% Ni/ZrO₂ (0.5 g), 40 bar H₂ (reaction temperature), stirred at 600 rpm.

Based on the above experimental results and analysis, we generalize the main reaction route for stearic acid conversion on Ni/ZrO₂, it firstly proceeds with acid hydrogenation (rate determining step) to form aldehyde (in a hydrogenation/dehydrogenation equilibrium with alcohol), and such aldehyde is in turn rapidly decarbonylated to C$_{17}$ alkane on Ni particles by eliminating 1 mole of CO.
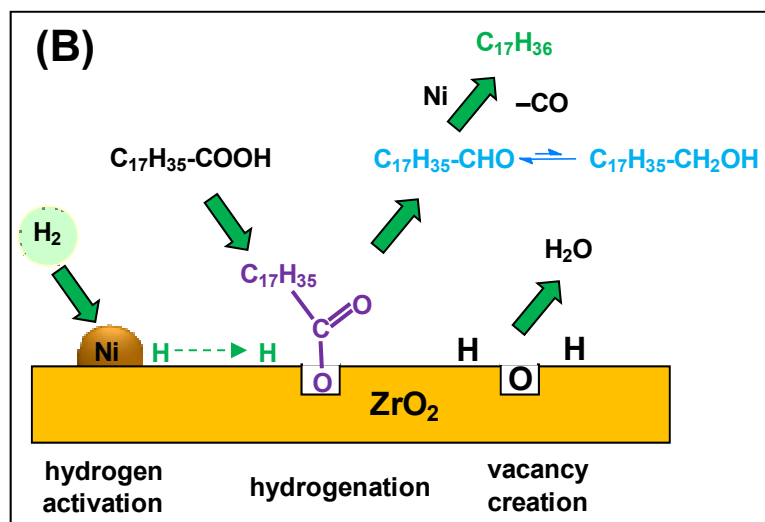
Figure 4-7. Proposed reaction mechanism for the deoxygenation of stearic acid to C_{17} *n*-heptadecane via synergetic catalysis over Ni/ZrO₂.

Note that the support plays a very important role in the stearic acid hydrogenation (the slowest step). Pure ZrO_2 as well as TiO_2, CeO_2, and ZnO have been reported to be able to selectively hydrogenate the aromatic carboxylic acid to aldehyde through both absorbing the acids on the oxygen vacancies of metal oxides to form carboxylate species and activating hydrogen molecule via dissociative adsorption on the catalyst surface.[9,10] For example, in the test with pure ZrO_2, it indeed showed somewhat hydrogenation capability for stearic acid (see **Table 4-3**). Thus, actually the ZrO_2, TiO_2, CeO_2, and ZnO supported Ni catalysts possess two hydrogenation active components (the metallic Ni and the oxide support), which in principle should led to higher hydrogenation activity on fatty acid than Ni/Al_2O_3 or Ni/SiO_2. Our results also supported this assumption, except for the less active Ni/ZnO catalyst which is probably due to the small specific surface area (10 m^2/g). We have proposed the plausible reaction mechanism on hydrogenation step of stearic acid to octadecanal on Ni/ZrO₂ at **Figure 4-7**, the carboxylic group of stearic acid adsorbs at the oxygen vacancy of the ZrO_2 support to form adsorbed specie. The hydrogen molecule can be dissociated by either metallic Ni or ZrO_2, which subsequently migrates to the adsorbed specie by spillover mechanism. The spillover hydrogen would hydrogenate the absorbed specie to octadecanal by eliminating 1 H_2O, and the oxygen

vacancies on the ZrO$_2$ surface were recreated. The produced octadecanal is in turn converted to C$_{17}$H$_{36}$ via decarbonylation of 1 mole of CO on Ni particles.

4.3.5. Microalgae oil transformation

After extensively investigating the stearic acid conversion, the crude microalgae oil was directly hydrotreated with Ni/ZrO$_2$ at 270 ^{o}C with 40 bar H$_2$. From the plotted yields versus reaction time (**Figure 4-8**), it demonstrates that 76 wt% yield of liquid alkanes including 68 wt% yield of C$_{17}$ *n*-heptadecane (main product) was attained after 8 h reaction time. This value is very close to the theoretical yield of liquid hydrocarbons (81 wt%).[11] Propane (3.6 wt%) and methane (4.6 wt%) were the main products in the vapor phase, which were formed by the hydrogenolysis of triglycerides and the methanation of CO/CO$_2$ with H$_2$, respectively. In addition, it was also observed that the yields of stearic acid (the primary intermediate) and 1-octadecanol (the secondary intermediate) both increased to a maximum value (18 wt% and 8 wt%, respectively) and then decreased to zero as reaction proceeded to 8 h. The final carbon distributes in the liquid phase as C$_{17}$ *n*-heptadecane (major) and other C$_{13}$-C$_{21}$ hydrocarbons (minor), and in the gas phase as propane and methane.

Combining the knowledge from deoxygenation of stearic acid and 1-octadecanol together with the kinetic of microalgae oil conversion, the overall reaction pathways for the transformation of microalgae oil with Ni/ZrO$_2$ has been proposed (**Scheme 4-1**). It proceeds via an initial hydrogenation of the C=C double bonds in the alkyl chain, followed by selectively cleaving C-O bond of the formed saturated triglyceride to fatty acid and propane through hydrogenolysis. The subsequent hydrogenation of the carboxylic group of fatty acid leads to the corresponding aldehyde such as octadecanal via synergetic catalysis by both metallic Ni and ZrO$_2$ support (rate determining step), followed by decarbonylation of octadecanal to the target C$_{17}$ *n*-heptadecane and carbon monoxide (C-C bond cleavage, major route). In addition, the hydrodeoxygenation and decarboxylation of stearic acid lead to C$_{18}$ *n*-octadecane and C$_{17}$ *n*-heptadecane formation (minor routes), respectively. The weak acid sites of ZrO$_2$ catalyzed slight cracking and

isomerization of the straight-chain alkanes. CO and CO$_2$ may react with H$_2$ to produce methane and water.

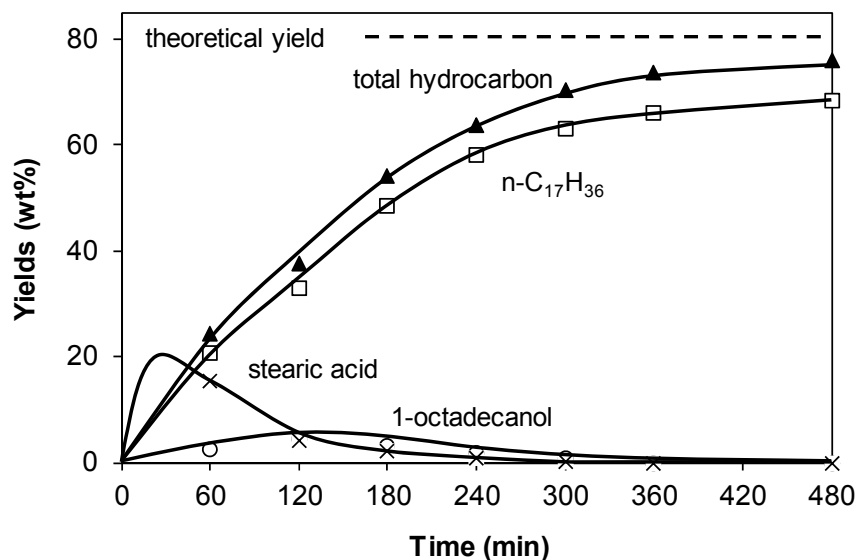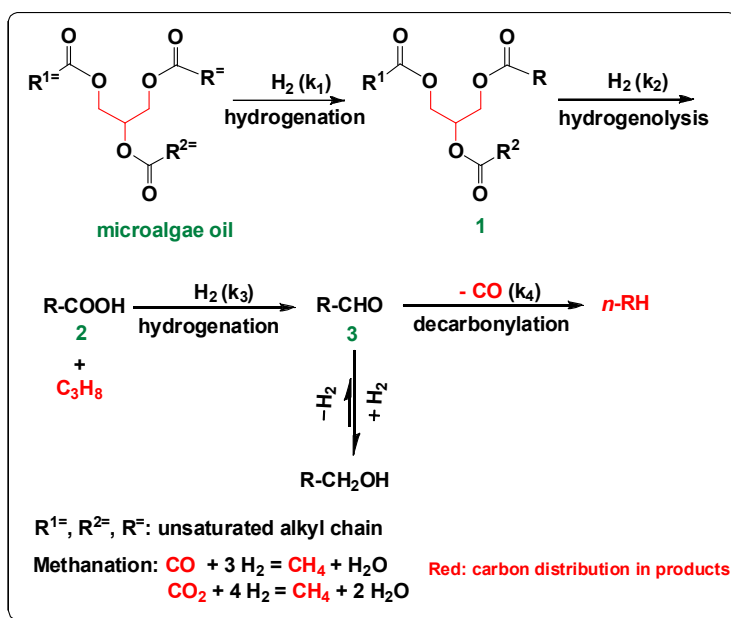**Figure 4-8.** Products distributions for the transformation of microalgae oil over 10 wt% Ni/ZrO$_2$ as a function of time. Reaction conditions: microalgae oil (1.0 g), 10 wt% Ni/ZrO$_2$ (0.5 g), dodecane (100 ml), 270 $^{\circ}$C, 40 bar H$_2$ (reaction temperature), stirred at 600 rpm.

Scheme 4-1. Proposed main reaction pathways for the transformation of microalgae oil to alkanes over Ni/ZrO$_2$ catalyst.

As the detected maximum concentration of intermediates follows the trend of hydrogenated triglyceride (**1**, trace) $\ll$ aldehyde $\leftrightarrow$ alcohol (**3**) $<$ fatty acid (**2**) in conversion of microalgae oil (see Figure 2), it can be deduced that the individual reaction rates of k_1 (hydrogenation of C=C double bonds in the alkyl chain) $\gg$ k_2 (hydrogenolysis of saturated triglycerides) $>$ k_4 (decarbonylation of alcohol) $>$ k_3 (hydrogenation of fatty acids, the rate determining step) with Ni/ZrO₂ catalyst in the overall reaction.
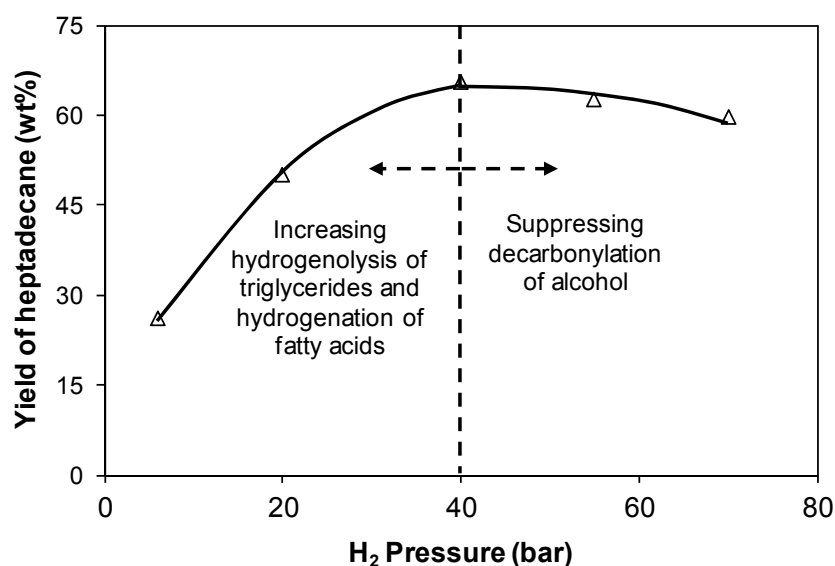
Figure 4-9. Impact of H₂ pressure on the yield *n*-heptadecane for microalgae oil conversion. Reaction conditions: microalgae oil (1.0 g), dodecane (100 ml), 10 wt% Ni/ZrO₂ (0.5 g), 260 °C, 8 h.

The role of hydrogen pressure on these cascade reactions was also explored on the yield of C_{17} *n*-heptadecane from microalgae oil conversion (see **Figure 4-9**). With the increasing H₂ pressure from 6 to 40 bar, the yield of C_{17} *n*-heptadecane remarkably increased from 26 to 66 wt% at 260 °C for 8 h, which is attributed to the greatly enhanced tandem hydrogenation reaction rates of k_1, k_2, and k_3. However, the further increase of the H₂ pressure from 40 to 70 bar led to a slight decrease of the C_{17} *n*-heptadecane yield

from 66 to 59 wt%, because the decarbonylation rate **k$_4$** is suppressed at high hydrogen pressure, as the equilibrium shifts from octadecanal to 1-octadecanol. But the slope of the curve at the increasing stage (6-40 bar) is much steeper than the latter one (40-70 bar) (see Figure 3), as the hydrogen impact on the rate determining steps would influence the overall reaction to a large extent.

This process was also transferred into the continuous flow operation to test the catalyst's activity and stability, in which the crude microalgae oil was hydrotreated in a trickle bed reactor using Ni/ZrO$_2$ catalysts at identical conditions (260 ^{o}C, 40 bar H$_2$) (see Supporting Information for detailed procedures). The catalyst led to 70 wt% yield of C$_{17}$ *n*-heptadecane and 75 wt% yield of total liquid alkanes in the continuous flow reactor, which was almost identical to the performance in the former slurry batch reactor. Note that the catalysts did not deactivate at all after 72 h running, demonstrating the high stability of the catalyst against sintering (**Figure 4-10**).
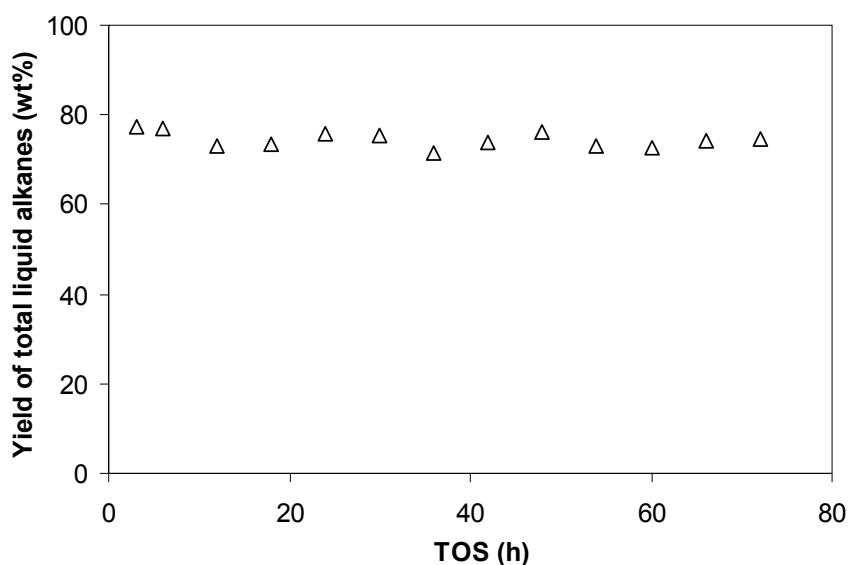
Figure 4-10. Time-on-stream performance of 10 wt% Ni/ZrO$_2$ for microalgae oil upgrading. Reaction conditions: microalgae oil in dodecane (1.33 wt%, liquid flow speed: 0.2 ml/min), 10 wt% Ni/ZrO$_2$ (0.5 g), H$_2$ (40 bar, gas flow rate: 50 ml/min), 260 ^{o}C.

4.4. Conclusions

In summary, a new efficient process for quantitative deoxygenation of microalgae oil to alkanes has been developed by selectively cleaving C-C and C-O bonds over ZrO_2 supported Ni catalyst. The hydrogenolysis of triglyceride, the hydrogenation of functional groups (i.e., -COOH, -CHO, C=C), and the decarbonylation of aldehyde are catalyzed by metallic Ni sites. It is worth mentioning that, the rate determining step (hydrogenation of fatty acid to aldehyde) is synergistically promoted by the ZrO_2 support through simultaneously adsorbing the carboxylic group at the oxygen vacancy and activating the hydrogen molecule. The hydrogenolysis/decarbonylation route is more advantageous over the hydrodeoxygenation pathway due to the less required hydrogen consumption. This approach shows great applicable potentials for producing sulfur-free green transportation fuels from microalgae oil at large scale.

4.5. References

1. (a) D. Kubicka, J. Horacek, Appl. Catal. A: Gen. 394 (2011) 9. (b) L.X. Li, E. Coppola, J. Rine, J. L. Miller, D. Walker, Energy Fuels 24 (2010) 1305.

2. (a) R. Sotelo-Boyás, Y. Y. Liu, T. Minowa, Ind. Eng. Chem. Res. 50 (2011) 2791. (b) R. Kumar, B. S. Rana, R. Wiwari, E. Verma, R. Kumar, R. K. Joshi, M. O. Garg, A. K. Sinha, Green Chem. 12 (2010) 2232. (c) G. W. Huber, P. O'Connor, A. Corma, Appl. Catal. A: Gen. 329 (2007) 120.

3. (a) T. R. Viljava, R. S. Komulanien, A. O. I. Krause, Catal. Today 60 (2000) 83. (b) A. Centeno, E. Laurent, B. Delmon, J. Catal. 154 (1995) 288. (c) E. Laurent, B. Delmon, J. Catal. 146 (1994) 281.

4. (a) B. Peng, Y. Yao, C. Zhao, J. A. Lercher, Angew. Chem. Int. Ed. 2011, DOI: 10.1002/anie.201106243. (b) K. Murata, Y. Liu, M. Inaba, I. Takahara, Energy Fuels 24 (2010) 2404.

The equations below display the hydrodeoxygenation, decarbonylation and decarboxylation pathways for alkane production using fatty acid as reactant. As fatty acid can be used as a representative reactant, similar equations can be written for triglycerides conversion.

$$\text{Hydrodeoxygenation: } R\text{-}COOH + 3H_2 \longrightarrow R\text{-}CH_3 + 2H_2O \tag{1}$$

$$\text{Decarbonylation: } \quad R\text{-}COOH + H_2 \longrightarrow R\text{-}H + CO + H_2O \tag{2}$$

$$\text{Decarboxylation: } \quad R\text{-}COOH \longrightarrow R\text{-}H + CO_2 \tag{3}$$
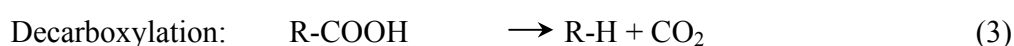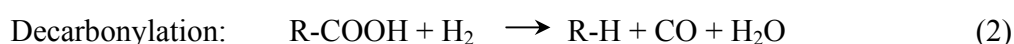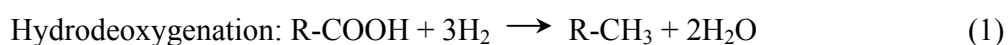
5. (a) T. M. Mata, A. A. Martins, N. S. Caetano, Renew. Sust. Energ. Rev. 14 (2010) 217. (b) P. M. Schenk, S. R. Thomas-Hall, E. Stephens, U. C. Marx, J. H. Mussgnug, C. Posten, O. Kruse, B. Hankamer, Bioenerg. Res. (1) 2008 20.

6. (a) Y. Chisti, Biotech. Adv. 25 (2007) 294. (b) G. W. Huber, S. Iborra, A. Corma, Chem. Rev. 106 (2006) 4044.

7. (a) A. Wawrzetz, B. Peng, A. Hrabar, A. Jentys, A. A. Lemonidou, J. A. Lercher, J. Catal. 269 (2010) 411. (b) B. Peng, C. Zhao, I. Mejía-Centeno, G. A. Fuentes, A. Jentys, J. A. Lercher, Catal. Today 2011, DOI: 10.1016/j.cattod.2011.10.022.

8. (a) T. Yokoyama, N. Yamagata, Appl. Catal. A: Gen. 221 (2001) 227. (b) T. Yokoyama, T. Setoyama, N. Fujita, M. Nakajima, T. Maki, Appl. Catal. A: Gen. 88 (1992) 149.

9. R. Pestman, R. M. Koster, E. Boellaad, A. M. van der Kraan, V. Ponec, J. Catal. 174 (1998) 142.

10. The theoretical yield of liquid alkanes from compositions of microalgae oil is 81 wt% based on decarbonylation pathway. The theoretical yields for propane and methane are 4.6 wt% and 5.3 wt%, respectively.

Chapter 5

Towards quantitative conversion of microalgae oil to diesel range alkanes with dual functional catalysts

A new and efficient catalytic approach allows selectively converting crude microalgae oil to diesel range alkanes using Ni nanoclusters supported on HBeta catalysts. The cascade of catalyzed reactions that convert microalgae oil needs two catalytic functions: a metallic function for the integrated hydrogenolysis, hydrogenation and decarbonylation, and acid function for dehydration and isomerization.

5.1. Introduction

Efficient conversion of biomass such as polysaccharides,[1] lignin,[2] and triglycerides[3] to biofuels has attracted considerable attention. Microalgae is being considered in that context as a promising renewable energy resource, having high triglyceride contents (up to 60 wt%)[4] and rapid growth rates that are 10-200 times faster than terrestrial oil crops such as soybean and rapeseed without directly competing with edible food/oil production.[5]

Currently, three approaches are used for microalgae oil refining. The first technique involves transesterification of triglycerides and alcohol into fatty acid alkyl esters (FAAEs) and glycerol, which is applied in the first generation biodiesel production. Such esters, however, have the problems of a relatively high oxygen content and poor flow property at low temperatures, limiting their application as high-grade fuels.[6] The second employs the conventional hydrotreating catalysts, e.g., sulfided NiMo and CoMo, for upgrading.[7] However, these sulfide catalysts contaminate products via sulfur leaching, and deactivate due to its removal from the surface by a reverse Mars van Krevelen mechanism.[8] The third relies on supported noble and base metal catalysts for decarboxylation and decarbonylation of carboxylic acids to alkanes at 300-330 ^{o}C,[9] but these catalysts showed low activities and selectivities to C_{15}-C_{18} alkanes when converting triglycerides, and the performance was only somewhat improved by a Pt-Re/ZSM-5 catalyst.[10] Contributions addressing microalgae oil upgrading using sulfur-free catalysts has not been reported. In this contribution, we report for the first time a novel and scalable catalyst, i.e., Ni supported on and in zeolite HBeta, to quantitatively convert crude microalgae oil under mild conditions (260 ^{o}C, 40 bar H_2) to diesel range alkanes as high-grade second generation transportation biofuels.

5.2. Experimental

All chemicals were obtained from commercial suppliers and used as received: stearic acid (Fluka, analytical standard), 1-octadecanol (Fluka, ≥99.5% GC assay), dodecane

(Sigma-Aldrich, ≥99% Reagent Plus), eicosane (Aldrich, ≥99% GC assay), *n*-octadecane (Fluka, ≥99% GC assay), *n*-heptadecane (Fluka, ≥99% GC assay), nickel (II) nitrate hexahydrate (Sigma-Aldrich, ≥98.5%). Microalgae oil was provided by Verfahrenstechnik Schwedt GmbH, HZSM-5 (Si/Al=45, 120, 200) and HBeta (Si/Al=75) were provided by Süd-Chemie AG, HBeta (Si/Al=180) was provided by Zeolyst.

Ni/zeolite catalysts were synthesized by wetness impregnation method. The procedures for catalyst synthesis, catalyst characterization, autoclave batch reaction, and continuous flow reaction as well as analysis method have been described in detail in Chapter 4.

5.3. Results and discussion

Microalgae oil mainly consists of neutral lipids such as mono-, di-, and tri-glyceride. The microalgae oil (provided by Verfahrens-technik Schwedt GmbH) used for this work consists of unsaturated C_{18} fatty acids (88.4 wt%), saturated C_{18} fatty acids (4.4 wt%), as well as some other C_{14}, C_{16}, C_{20}, C_{22}, and C_{24} fatty acids (7.1 wt% in total) (*see* **Table 4-1** in Chapter 4).

5.3.1. Microalgae oil conversion with Ni/HBeta catalyst

Without any purification, the crude microalgae oil was directly hydrotreated in a batch mode with 10 wt% Ni/HBeta (Si/Al=180) at 260 $^{\circ}$C in presence of 40 bar H_2 (*see* **Figure 5-1**). After 8 h reaction time, it led to 78 wt% yield of liquid alkanes (containing 60 wt% yield of C_{18} octadecane), which was very close to the theoretical maximum liquid hydrocarbon yield (84 wt%). Propane (3.6 wt%) and methane (0.6 wt%) were the main products in the vapor phase. The metal leaching after reaction was detected below the atomic absorption spectroscopy (AAS) detection limit (1 ppm). **Figure 5-1** shows that saturated fatty acids are the primary products for microalgae oil conversion, i.e., the yield of stearic acid exceeded 70 wt% within 1 h. Then, the yield of saturated fatty acids gradually decreased in accompanied with an increase of alkanes yield (mainly including

C_{18} and C_{17} alkanes) as a function of time. This shows that in the conversion of microalgae oil over Ni/HBeta catalyst, (i) the hydrogenation of double bonds in the alkyl chain occurs very fast, (ii) the slower hydrogenolysis of saturated triglycerides readily produces fatty acids and propane as initial primary products, and (iii) the following hydrodeoxygenation of fatty acids to alkanes is the slowest (rate determining) step in the overall reaction.
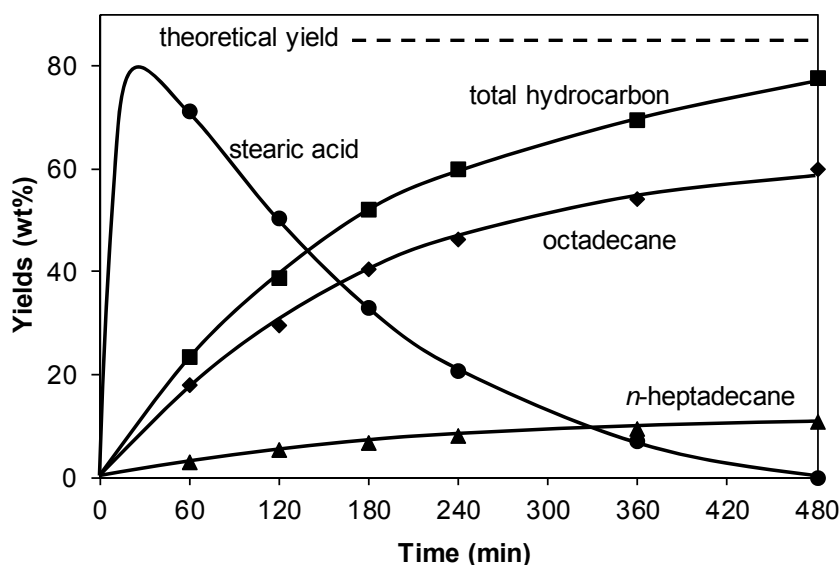
Figure 5-1. Products distribution for transformation of microalgae oil over 10 wt% Ni/HBeta as a function of time. Reaction conditions: microalgae oil (1.0 g), Ni/HBeta (Si/Al=180, 0.2 g), dodecane (100 ml), 40 bar H_2 (reaction temperature).

Variations of temperature and H_2 pressure showed that an increase of temperature from 250 to 270 $^{\circ}$C at 40 bar enhanced the liquid alkane yield from 68 to 78 wt%, and an increase of the hydrogen pressure from 15 to 60 bar at 260 $^{\circ}$C led to the decrease of n-C_{17} and iso-C_{18} yields from 28 to 11 wt%, while increasing the n-C_{18} yield from 23 to 61 wt% (*see* **Table 5-1**).

The upgrading of crude microalgae oil was also tested in a continuous flow system with a trickle bed reactor using 10 wt% Ni/HBeta catalysts at identical conditions (260 $^{\circ}$C, 40 bar H_2) (*see* Supporting Information). The results obtained from continuous flow reactor are almost identical to those from slurry batch reactor, in which the yield of C_{18}

octadecane attained was 60 wt% and the total liquid alkane yield reached 78 wt%. The catalyst showed high activity and good stability during 120 h testing (*see* **Figure 5-2**).

Table 5-1. Impacts of temperature and pressure on microalgae oil conversion[a]

Reaction conditions	Yields [wt%]			
	C_{17} hydrocarbon	*iso*-C_{18} hydrocarbon	*n*-C_{18} hydrocarbon	Total hydrocarbon
250 °C, 40 bar	5.1	3.8	54	68
260 °C, 40 bar	8.9	6.3	54	75
270 °C, 40 bar	13	11	48	78
260 °C, 15 bar	17	11	23	55
260 °C, 60 bar	7.1	3.9	61	78

[a] Reaction conditions: microalgae oil (1.0 g), dodecane (100 ml), 10 wt% Ni/HBeta (0.2 g, Si/Al=180), 8 h.
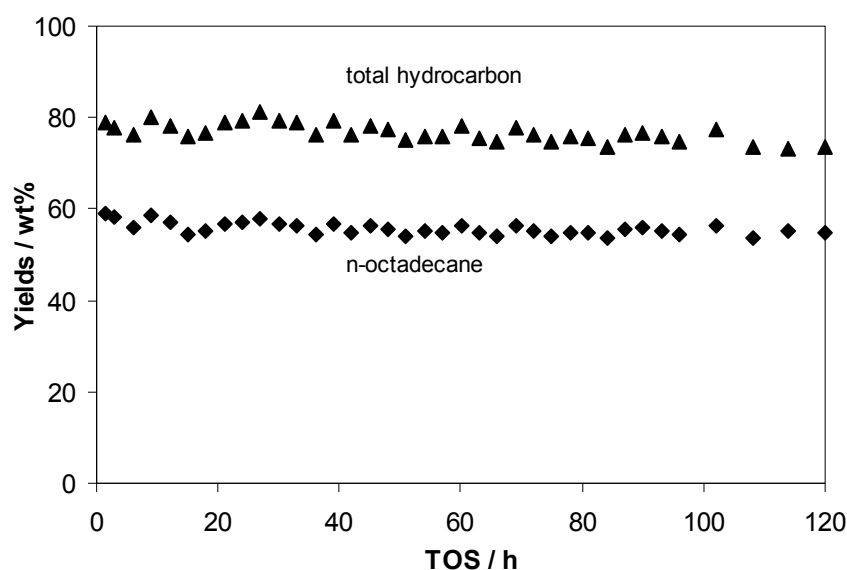

Figure 5-2. Time-on-stream performance of the 10 wt% Ni/HBeta (Si/Al=180) for microalgae oil upgrading. Reaction conditions: microalgae oil in dodecane (1.33 wt%, liquid flow speed: 0.2 ml/min), Ni/HBeta (0.2 g, 10 wt%), H_2 (40 bar, gas flow rate: 50 ml/min), 260 °C.

5.3.2. Catalyst screening for stearic acid conversion

To better understand the fundamental chemistry during the hydrodeoxygenation step of fatty acids to alkanes, the representative intermediate, stearic acid, was selected for further studies. Two types of acidic zeolite supports (HZSM-5 and HBeta) with Si/Al ratios of 45, 75, 120, 180, and 200 were explored. Ni supported on these zeolite catalysts were prepared by the incipient wetness impregnation method with metal loadings of 5 wt% or 10 wt%, and characterized by BET surface area, XRD for metal sites, and TPD of ammonia for acid sites (*see* **Table 5-1**, **Figures 5-3** and **5-4**). The apparent specific surface areas of HZSM-5 and HBeta supported Ni catalysts were approximately 300 and 550 m^2/g, respectively. The average Ni particle sizes were ca. 15-30 nm calculated from XRD patterns by the Scherrer equation. As expected a higher Si/Al ratio or higher Ni content led to a lower acid site concentration of HZSM-5 and HBeta based catalysts. The latter trend indicates that some Ni remained stabilized at the ion exchange sites also after reduction of the catalyst.

Table 5-2. Physicochemical properties of Ni/zeolite catalysts

Catalyst	Metal loading [wt%]	Si/Al [mol/mol]	BET surface area [m^2/g]	Acid density [mmol/g] [a]	$d_{Ni(111)}$ [nm] [b]	$d_{Ni(200)}$ [nm] [b]
Ni/HZSM-5	10	45	279	0.321	28	24
Ni/HZSM-5	10	120	286	0.089	29	23
Ni/HZSM-5	10	200	304	0.047	30	24
Ni/HBeta	5	75	603	0.188	20	15
Ni/HBeta	10	75	586	0.171	25	20
Ni/HBeta	5	180	565	0.069	21	18
Ni/HBeta	10	180	523	0.053	25	20

[a] Determined by TPD of ammonia

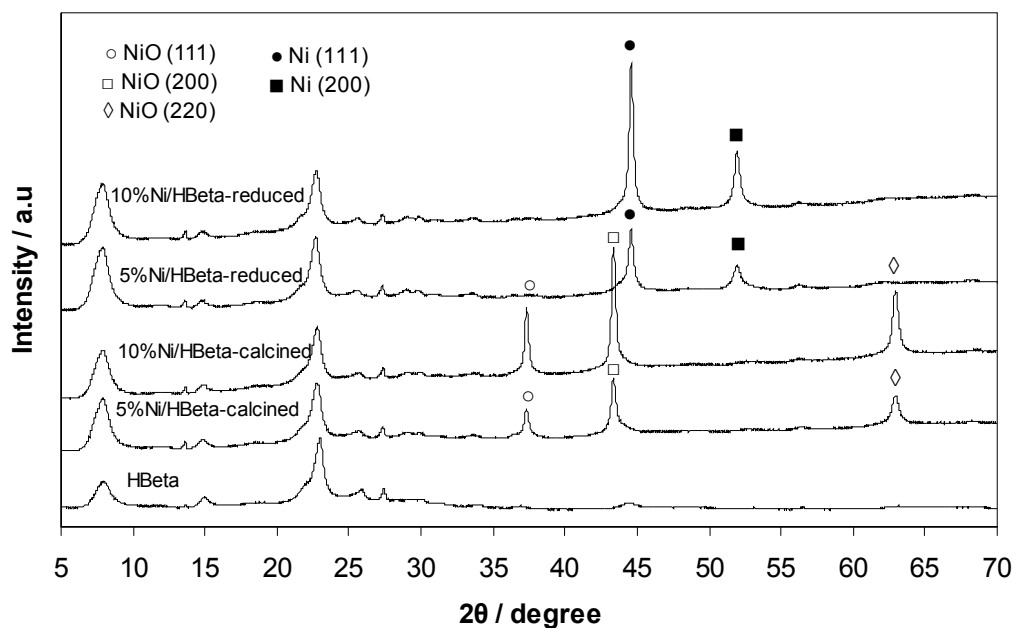[b] Calculated from XRD by Scherrer equation

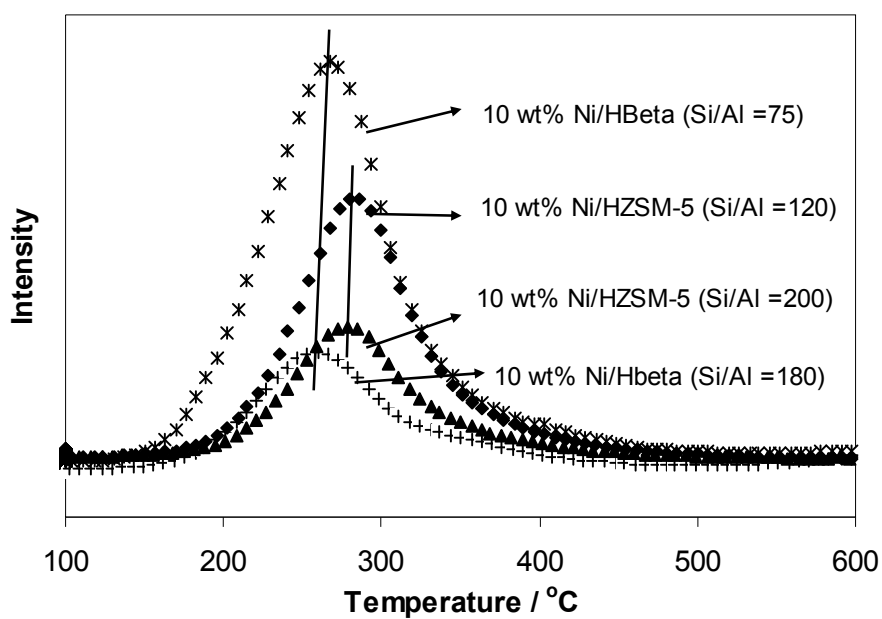**Figure 5-3.** X-ray diffraction patterns of Ni/HBeta (Si/Al=180)

Figure 5-4. Temperature programmed desorption of ammonia on Ni/zeolite catalysts

Full conversion of stearic acid was obtained with Ni/HZSM-5 (10 wt%, Si/Al=45, acid density=0.321 mmol/g) at 260 $^{\circ}$C in the presence of 40 bar H_2, but severe cracking of the produced alkanes (43% selectivity) was observed (*see* **Table 5-3**). By using HZSM-5 supported Ni catalysts with higher Si/Al ratios of 120 and 200 having lower acid site concentrations of 0.089 and 0.047 mmol/g, cracking was gradually suppressed, and the selectivity to C_{17} and C_{18} alkanes increased to 84% and 93%, respectively.

Table 5-3. Comparison of stearic acid conversion over Ni/zeolite catalysts at 260 $^{\circ}$C[a]

Catalyst	Conv. [%]	Selectivity [C%]				
		n-C_{18}	iso-C_{18}	*n*-C_{17}	iso-C_{17}	cracking
Ni/HZSM-5	10	41.1	6.3	9.2	0.4	42.7
Ni/HZSM-5	10	67.5	7.6	8.8	-	15.9
Ni/HZSM-5	10	80.1	6.3	6.1	-	7.2
Ni/HBeta	5	66.5	15.0	13.8	3.8	0.7
Ni/HBeta	10	72.6	10.1	14.8	1.6	0.6
Ni/HBeta	5	82.8	6.0	10.2	0.2	0.4
Ni/HBeta	10	84.6	5.2	9.5	-	0.4

[a] Reaction conditions: stearic acid (1.0 g), dodecane (100 ml), Ni/zeolite (0.2 g), H_2 (40 bar at 260 $^{\circ}$C), 8 h, stirred at 600 rpm.

The Ni/HBeta catalyst (5 wt%, Si/Al=75) led to a 96% conversion of stearic acid with selectivities of 82% to the C_{18} alkane and of 18% to the C_{17} alkane, almost eliminating cracking of the hydrocarbon chain. The HBeta catalyst with a higher Ni content (10 wt%, Si/Al=75) exhibited similar activity as the former catalyst, but showed a lower selectivity to isomerized alkane, indicating that its lower acid site concentration causes a lower isomerization rate. The Ni/HBeta catalyst with a higher Si/Al ratio of 180 led to quantitative conversion with ca. 90% C_{18} alkane selectivity, showing high atom economy. We speculate at present that the higher degree of cracking with Ni/HZSM-5 compared to Ni/HBeta is caused by a higher effective residence time caused by the higher Brønsted acid site concentration and the narrower pores in the HZSM-5 zeolite. The peaks in the

TPD of ammonia indicate very similar strength of acid sides in both materials (*see* **Figure 5-4**). In order to explore the potential to higher C_{18} alkane yields and lower cracking yields, Ni/HBeta (10 wt%, Si/Al=180) was chosen for a detailed kinetic study.

### 5.3.3. Kinetics of stearic acid reaction over 10 wt% Ni/HBeta

With Ni/HBeta (10 wt%, Si/Al=180), less than 10% C_{17} *n*-heptadecane and more than 90% C_{18} octadecane were formed at nearly complete conversion of stearic acid at 260 ^{o}C as seen in **Figure 5-5a**. The intermediates octadecanal (concentration < 0.02%) and 1-octadecanol (concentration < 0.1%) were only observed in traces. This suggests that stearic acid is hydrogenated with a slow rate to octadecanal in the first step, and then rapidly reduced to 1-octadecanol, and followed by rapid dehydration-hydrogenation reactions, producing the C_{18} alkane as the final product. The presence of the intermediates also shows that the hydrogenation-deoxygenation reactions are the main route for producing C_{18} alkanes without carbon loss (90% selectivity), while the decarbonylation of the intermediately formed C_{18} aldehyde is the minor route.

To verify this hypothesis, the kinetics of the intermediate product 1-octadecanol was also studied with Ni/HBeta (10 wt% Ni, Si/Al=180) under identical conditions (260 ^{o}C and 40 bar H_2) (*see* **Figure 5-5b**). *n*-Octadecane (85% yield) and C_{17} *n*-heptadecane (5% yield) were the main products at 94% conversion. Distearyl ether was observed as intermediates via intermolecular dehydration of the C_{18} alcohol, but as the reaction proceeded, the ether was cleaved again and deoxygenated via elimination of water and hydrogenation of alkene to *n*-octadecane. The dehydration product, *n*-octadecene, was not detected due to the fast hydrogenation of the double bond. This allows us to estimate that the dehydration rate of 1-octadecanol (8.6 mmol·g^{-1}·h^{-1}) is around four times faster than the hydrogenation rate of stearic acid (2.2 mmol·g^{-1}·h^{-1}), which explains that only the trace amounts of 1-octadecanol and octadecanal are observed during the conversion of stearic acid. We conclude therefore that the Ni catalyzed hydrogenation is the rate determining step in the overall reaction. In addition, based on our previous experiments with 1- and 2-propanol,[11] we infer that C_{17} *n*-heptadecane is produced by metal catalyzed decarbonylation of *n*-octadecanal, producing also 1 mol of CO. In addition, the

1-octadecanol and octadecanal are concluded to be equilibrated because their yields increased linearly with the increasing conversion (*see* **Figure 5-5a**).
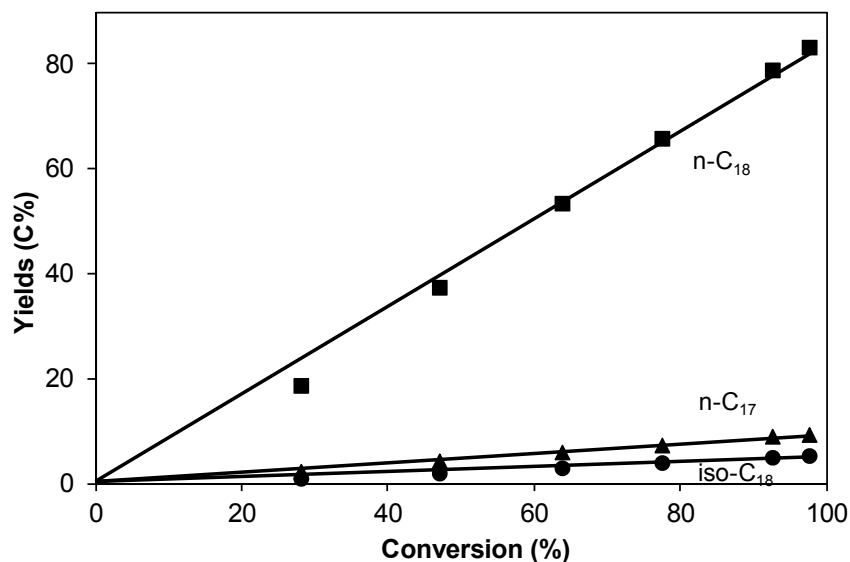
(a)
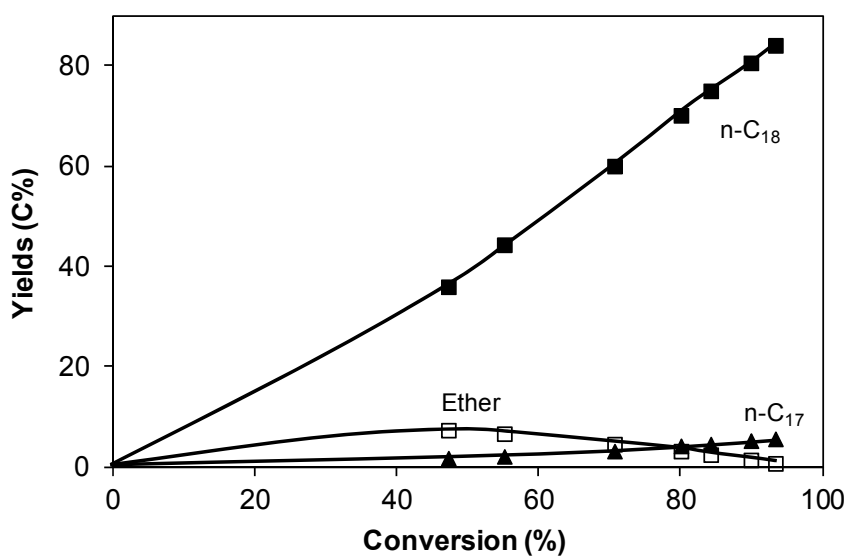
(b)

Figure 5-5. Yields of products as a function of (a) stearic acid and (b) 1-octadecanol conversion. Reaction conditions: (a) stearic acid (1.0 g), 10 wt% Ni/HBeta (Si/Al=180, 0.2 g); (b) 1-octadecanol (1.0 g), 10 wt% Ni/HBeta (Si/Al=180, 0.05 g); dodecane (100 ml), 260 $^{\circ}$C, 40 bar H_2 (reaction temperature), 8 h, stirred at 600 rpm.
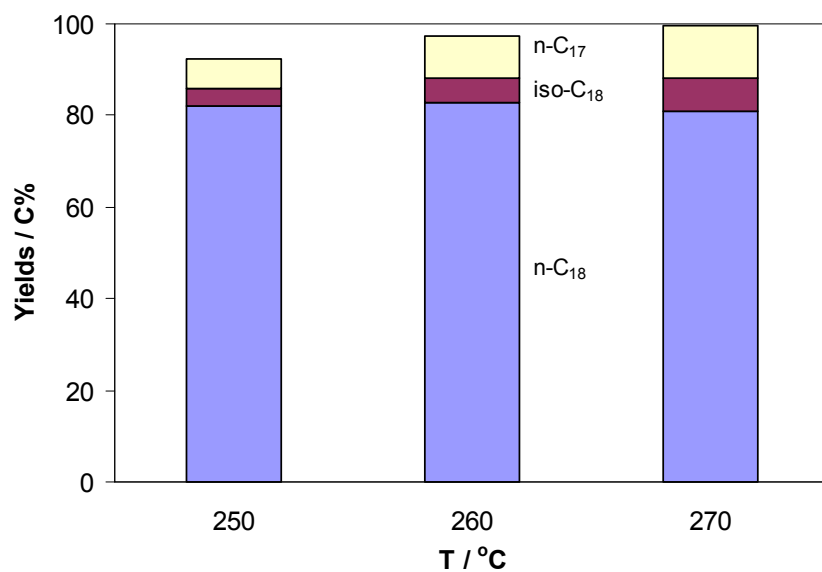
(a)
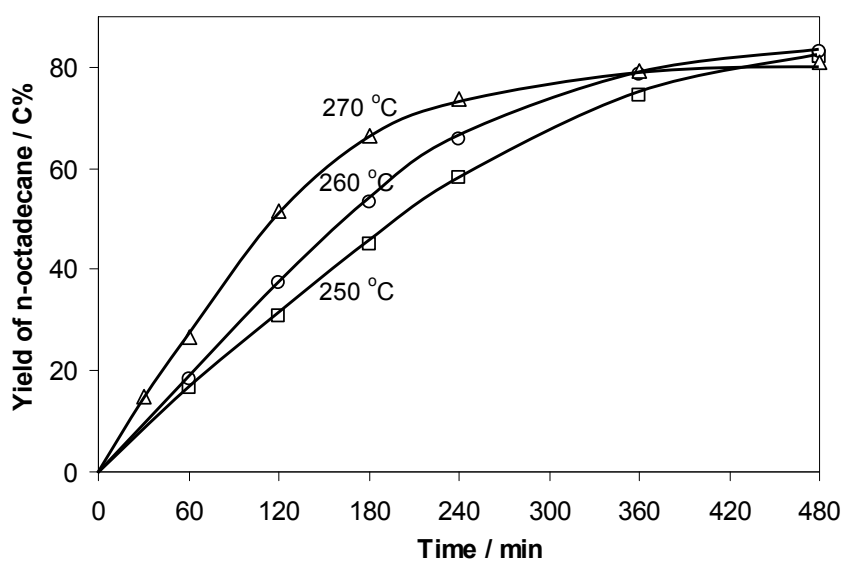
(b)

Figure 5-6. Product distributions on stearic acid conversion as a function of (a) temperature and (b) reaction time. Reaction conditions: stearic acid (1.0 g), 10 wt% Ni/HBeta (0.2 g, Si/Al=180), dodecane (100 ml), stirring at 600 rpm, 40 bar H_2 (reaction temperature), 8 h for (a), 40 bar H_2 (reaction temperature) for (b).
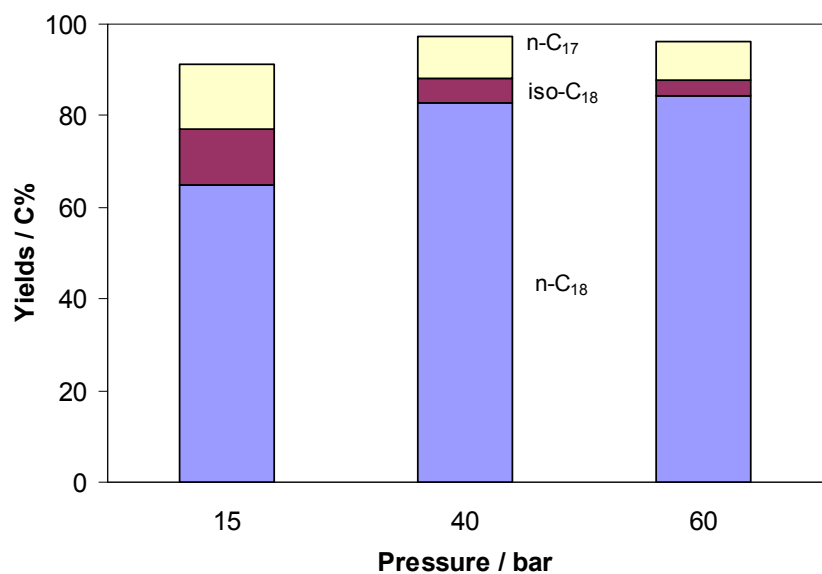
(a)
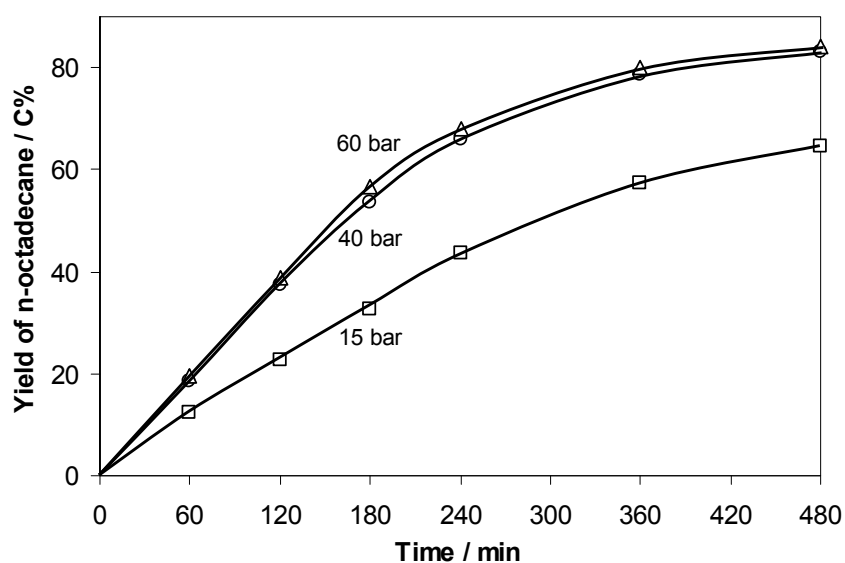
(b)

Figure 5-7. Product distributions on stearic acid conversion as a function of (a) hydrogen pressure and (b) reaction time. Reaction conditions: stearic acid (1.0 g), 10 wt% Ni/HBeta (0.2 g, Si/Al=180), dodecane (100 ml), stirring at 600 rpm, 260 $^{\circ}$C, 8 h for (a), and 260 $^{\circ}$C, 40 bar H_2 (reaction temperature) for (b).

The impacts of reaction temperature and pressure on the conversion of stearic acid with 10 wt% Ni/HBeta are documented in **Figures 5-6 and 5-7**. With increasing reaction temperature from 250 to 270 ^{o}C, the yields of C_{17} *n*-heptadecane and C_{18} *iso*-octadecane increased from 10 to 20%, but the yield of C_{18} *n*-octadecane was comparable (80%), indicating a higher increase of the rates of decarbonylation and isomerization. As the conversion was high in all three experiments, we infer that the effect is either related to a longer contact of the intermediates (produced in larger concentrations) or a higher apparent activation energy of the decarbonylation of the aldehyde and the isomerization of the alkane compared to the hydrogenation of stearic acid. **Figure 5-7** also shows that the increase of the H_2 pressure from 15 to 60 bar led to an increase of the C_{18} *n*-octadecane yield from 65 to 84% after 8 h, while the lower hydrogen pressure (15 bar) favored decarbonylation (C_{17} *n*-heptadecane (15%)), but also C_{18} *iso*-octadecane (15%) formation. This is related to the fact that the higher hydrogen pressure benefits the fatty acid hydrogenation step (rate determining step) and shifts the equilibrium from octadecanal to 1-octadecanol, and thus, the overall hydrodeoxygenation rate and the selectivity to C_{18} *n*-octadecane are enhanced, while the selectivities to C_{17} *n*-heptadecane and C_{18} *iso*-octadecane are suppressed.

5.3.4. Reaction pathways for microalgae oil transformation

Combining of these experiments allows formulating the overall reaction pathway for microalgae oil transformation (*see* **Scheme 5-1**). It proceeds via an initial metal catalyzed hydrogenation of the double bonds in the alkyl chain, followed by hydrogenolysis of the formed saturated triglyceride leading to fatty acid and propane. The subsequent hydrogenation of the carboxylic group of fatty acid leads to the corresponding aldehyde, e.g., octadecanal, (rate determining step), followed by either decarbonylation of octadecanal to *n*-heptadecane and carbon monoxide (minor route) or hydrogenation of octadecanal to 1-octadecanol (major route). Subsequently, the produced 1-octadecanol undergoes sequential acid catalyzed dehydration and metal catalyzed hydrogenation leading to the final *n*-octadecane. An abundance of acidic sites in the zeolite leads to

hydroisomerization and hydrocracking of the alkanes. CO may react with H_2 to produce methane and water.

Scheme 5-1. Proposed reaction pathway for transformation of microalgae oil to alkanes over bifunctional Ni/HBeta catalysts.

5.4. Conclusions

In summary, we have shown that microalgae oil can be nearly quantitatively hydrodeoxygenated to alkanes by cascade reactions on dual functional catalysts based on Ni and an acidic zeolite. Ni catalyzes efficiently the hydrogenolysis of the fatty acid ester, the decarbonylation of aldehyde intermediates, as well as the hydrogenation of –COOH, –CHO and C=C double bonds in reactants and intermediates. The acid function catalyzes the dehydration of alcohol intermediates and the hydroisomerization and hydrocracking of the alkane products. The knowledge of the individual reaction rates allows balancing

these rates by adjusting the concentration of catalytically active sites to design tailored and stable catalysts for selectively converting crude microalgae oil to diesel range alkanes. The approach opens new possibilities to produce sulfur-free high-grade green transportation fuels from microalgae in a large scale.

5.5. References

1. (a) G. W. Huber, J. N. Chheda, C. J. Barrett, J. A. Dumesic, Science 308 (2005) 1446. (b) J. Q. Bond, D. M. Alonso, D. Wang, R. M. West, J. A. Dumesic, Science 327 (2010) 1110. (c) J. P. Lange, R. Price, P. M. Ayoub, J. Louis, L. Petrus, L. Clarke, H. Gosselink, Angew. Chem. Int. Ed. 49 (2010) 4479.

2. (a) C. Zhao, Y. Kou, A. A. Lemonidou, X. Li, J. A. Lercher, Angew. Chem. Int. Ed. 48 (2009) 3987. (b) C. Zhao, Y. Kou, A. A. Lemonidou, X. Li, J. A. Lercher, Chem. Commun. 46 (2010) 412. (c) N. Yan, Y. Yuan, R. Dykeman, Y. Kou, P. J. Dyson, Angew. Chem. Int. Ed. 49 (2010) 5549. (d) C. Zhao, J. He, A. A. Lemonidou, X. Li, J. A. Lercher, J. Catal. 280 (2011) 8.

3. (a) F. R. Ma, M. A. Hanna, Bioresour. Technol. 70 (1999) 1. (b) B. X. Peng, Q. Shu, J. F. Wang, G. R. Wang, D. Z. Wang, M. H. Han, Process. Saf. Environ. Prot. 86 (2008) 441.

4. (a) P. M. Schenk, S. R. Thomas-Hall, E. Stephens, U. C. Marx, J. H. Mussgnug, C. Posten, O. Kruse, B. Hankamer, Bioenerg. Res. 1 (2008) 20. (b) T. M. Mata, A. A. Martins, N. S. Caetano, Renew. Sust. Energ. Rev. 14 (2010) 217.

5. (a) G. W. Huber, S. Iborra, A. Corma, Chem. Rev. 106 (2006) 4044. (b) Y. Chisti, Biotech. Adv. 25 (2007) 294.

6. P. Šimácek, D. Kubicka, G. Šebor, M. Pospíšil, Fuel 88 (2009) 456.

7. (a) G. W. Huber, P. O'Connor, A. Corma, Appl. Catal. A: Gen. 329 (2007) 120. (b) R. Kumar, B. S. Rana, R. Wiwari, E. Verma, R. Kumar, R. K. Joshi, M. O. Garg, A. K. Sinha, Green Chem. 12 (2010) 2232. (c) R. Sotelo-Boyás, Y. Y. Liu, T. Minowa, Ind. Eng. Chem. Res. 50 (2011) 2791.

8. (a) E. Laurent, B. Delmon, J. Catal. 146 (1994) 281. (b) T. R. Viljava, R. S. Komulanien, A. O. I. Krause, Catal. Today 60 (2000) 83.

9. (a) M. Snåre, I. Kubičková, P. Mäki-Arvela, K. Eränen, D. Y. Murzin, Ind. Eng. Chem. Res. 45 (2006) 5708. (b) M. Snåre, I. Kubičková, P. Mäki-Arvela, D. Chichova, K. Eränen, D. Yu. Murzin, Fuel 87 (2008) 933. (c) J. G. Immer, M. J. Kelly, H. H. Lamb, Appl. Catal. A: Gen. 375 (2010) 134. (d) W. F. Maier, W. Roth, I. Thies, P. Ragué Schleyer, Chem. Ber. 115 (1982) 808.

10. (a) I. Kubičková, M. Snåre, K. Eränen, P. Mäki-Arvela, D. Yu. Murzin, Catal. Today 106 (2005) 197. (b) K. Murata, Y. Liu, M. Inaba, I. Takahara, Energy Fuels 24 (2010) 2404..

11. (a) A. Wawrzetz, B. Peng, A. Hrabar, A. Jentys, A. A. Lemonidou, J. A. Lercher, J. Catal. 2010, 269, 411–420. (b) B. Peng, C. Zhao, I. Mejía-Centeno, G. A. Fuentes, A. Jentys, J. A. Lercher, Catal. Today 2011, DOI: 10.1016/j.cattod.2011.10.022.

Chapter 6

Summary and conclusions

The aim of this dissertation is the transformation of triglycerides (microalgae oil as a representative feedstock) into diesel range alkanes with sulfur-free catalysts, and the hydrodeoxygenation and aqueous phase reforming of glycerol, which provides a bio-hydrogen source for the triglyceride hydrotreating. The focus of glycerol conversion is the understanding of mechanistic details, i.e., the way and the extent of C-O and C-C bonds cleavage as well as the reaction pathways. The conversion of triglycerides focuses on four aspects, i) catalyst screening and reaction condition optimization; ii) process selection, e.g., batch, semi-batch and continuous flow operation; iii) the understanding of metal site, support, and carrier gas influences; iv) reaction network development.

The fundamental chemistry in the aqueous phase alcohol transformation is studied by comparing the kinetics in the catalytic conversion of C_3 alcohol molecules with different position of the hydroxyl group and number of hydroxyl groups (mono-alcohols, i.e., 1-propanol and 2-propanol; diols, i.e., 1,2-propanediol and 1,3-propanediol; and triol, i.e., glycerol). The C-O bonds of C_3 alcohols are cleaved by dehydration, while the C-C bonds of C_3 alcohols with terminal hydroxyl groups are cleaved by sequential dehydrogenation to aldehyde, followed by either disproportionation (Tishchenko or Cannizzaro type reactions) with a subsequent decarboxylation reaction, or decarbonylation with a subsequent water gas shift reaction. The presence of terminal hydroxyl group of alcohols is proved to be critical for C-C bond cleavage in this reaction sequence, as it allows forming the essential aldehyde intermediate, which opens the reaction pathway to decarbonylation and decarboxylation. The overall reaction rates decrease in the sequence of 1,3-propanediol ≈ glycerol > 1,2-propanediol ≈ 1-propanol, which depends on the number of hydroxyl groups in the molecule, as well as the number of primary hydroxyl groups. The higher concentration of the hydroxyl groups in one molecule weakens the C-O bond strengths, leading to higher dehydration rates.

Prior to the investigation of triglyceride transformation, the deoxygenation of fatty acids (palmitic acid as model compound) is explored, as this is the rate determining step during the whole conversion. Palmitic acid can be efficiently converted to *n*-pentadecane with Ni/ZrO_2 in the presence of H_2. The reaction mainly proceeds with hydrogenation of the carboxylic group of palmitic acid leading to hexadecanal (rate determining step),

which is subsequently decarbonylated on the metallic Ni sites to the target *n*-pentadecane and carbon monoxide. Note that the hydrogenation of fatty acid to aldehyde is synergistically promoted by the ZrO_2 support through simultaneously adsorbing the carboxylic group at the oxygen vacancies and dissociating the hydrogen molecules. However, ketonization is the dominating reaction on conversion of palmitic acid catalyzed by ZrO_2 in the presence of N_2.

Pd black favors direct decarboxylation route (-CO_2), while Pt black together with Raney Ni lead to the direct decarbonylation pathway (-CO). The individual rates (unit: $mmol \cdot h^{-1} \cdot mol_{metal}^{-1}$) decrease in the sequence of r (Pt black) $\approx r$ (Pd black) $> r$ (Raney Ni) in N_2 carrier gas. The C support would not affect the performance of metal sites such as Pd, Pt and Ni which favor the direct decarbonylation/decarboxylation route of fatty acid. If HBeta and HZSM-5 zeolites with Brønsted acidity are employed, the primary route appears to be tandem hydrogenation-dehydration reactions for producing C_{16} hexadecane. The oxides with Lewis acidity such as Al_2O_3, SiO_2 and ZrO_2 lead to the tandem reactions of hydrogenation-decarbonylation for producing C_{15} *n*-pentadecane. The deoxygenation rates (unit: $mmol \cdot g_{Cat}^{-1} \cdot h^{-1}$) of palmitic acid follow the orders as r (Ni/HBeta or Ni/HZSM-5) $> r$ (Ni/ZrO$_2$) $> r$ (Ni/Al$_2$O$_3$ or Ni/SiO$_2$).

After detailed study of fatty acid conversion, the deoxygenation of microalgae oil to alkanes has been achieved by selectively cleaving C-C and C-O bonds over ZrO_2 supported Ni catalyst. The hydrogenolysis of triglyceride, the hydrogenation of functional groups (i.e., -COOH, -CHO, C=C), and the decarbonylation of aldehyde are catalyzed by metallic Ni sites. As mentioned above, the rate determining step (hydrogenation of fatty acid to aldehyde) is synergistically promoted by the ZrO_2 support. The hydrogenolysis-decarbonylation route is more advantageous over the hydrodeoxygenation pathway due to the less required hydrogen consumption.

We have also demonstrated that microalgae oil can be nearly quantitatively hydrodeoxygenated to alkanes by cascade reactions on dual functional catalysts based on Ni and an acidic zeolite. The metallic Ni sites are responsible for the integrated hydrogenolysis, hydrogenation and decarbonylation. The acid function catalyzes the

dehydration of alcohol intermediates and the hydroisomerization and hydrocracking of the alkane products. The knowledge of the individual reaction kinetics allows balancing these rates by adjusting the concentration of catalytically active sites to design tailored and stable catalysts for selectively converting crude microalgae oil to diesel range alkanes. The approach opens new possibilities to produce sulfur-free high-grade green transportation fuels from microalgae in a large scale.

Chapter 7

Zusammenfassung und Folgerungen

Das Ziel dieser Dissertation ist die Umsetzung von Triglyceriden (Mikroalgenöl als repräsentatives Ausgangsmaterial) zu Alkanen im Diesel-Bereich mit schwefelfreien Katalysatoren, sowie die Hydrodeoxygenierung und das Reformieren von Glycerin in wässriger Phase, welches als Bio-Wasserstoffquelle für das Hydrotreating der Triglyceride dient. Das Hauptaugenmerk bei der Umsetzung von Glycerin liegt darauf, die mechanistischen Details zu verstehen, d.h. Art und Ausmaß der C-O und C-C Bindungsspaltung sowie die Reaktionswege. Die Umsetzung von Triglyceriden richtet sich nach vier Gesichtspunkte: i) Auswählen von Katalysatoren und Optimierung von Reaktionsbedingungen; ii) Prozessauswahl z.B. batch, semi-batch und kontinuierliche Durchführung; iii) das Verständnis des Einflusses von Metallzentrum, Träger und Trägergas; iv) Entwicklung des Reaktionsnetzwerkes.

Die grundlegende Chemie der Umsetzung von Alkoholen in wässriger Phase wird durch Vergleich der Kinetik der katalytischen Umsetzung von C_3-Alkohol-Molekülen mit unterschiedlicher Position und Anzahl der Hydroxylgruppen untersucht (Monoalkohol, d.h. Propan-1-ol, und Propan-2-ol; Diole d.h. Propan-1,2-diol und Propan-1,3-diol und Triol, d.h. Glycerin). Die C-O Bindungen werden durch Dehydratisierung gespalten, während die C-C Bindungen von C_3-Alkoholen mit terminalen Hydroxylgruppen durch fortlaufende Dehydrierung zum Aldehyd, entweder gefolgt von (einer) Disproportionierung (Tishchenko- oder Cannizzaro-artigen Reaktion) mit anschließender Decarboxylierung-Reaktion oder Decarbonylierung, mit einer anschließenden Wassergas-Shift-Reaktion, gespalten werden. Es wird gezeigt, dass das Vorhandensein von endständigen Hydroxylgrupppen der Alkohole für die Spaltung von C-C Bindungen in dieser Reaktions-Sequenz entscheidend ist, weil es die Bildung des essentiell wichtigen Aldehyd-Intermediates ermöglicht, welches den Reaktionsweg hin zu Decarbonylierung und Decarboxylierung eröffnet. Die Gesamtreaktionsgeschwindigkeit sinkt in der Reihenfolge Propan-1,3-diol $\approx$ Glycerin > Propan-1,2-diol $\approx$ Propan-1-ol, welche von der Anzahl der Hydroxylgruppen im Molekül sowie der Zahl an primären Hydroxylgruppen abhängt. Eine höhere Konzentration von Hydroxylgruppen in einem Molekül schwächt die C-O Bindungsstärke, was zu höheren Dehydratisierungsraten führt.

Vor der Untersuchung der Triglycerid-Umsetzung wird die Deoxygenierung von Fettsäuren (Palmitinsäure als Modelkomponente) untersucht, weil diese der geschwindigkeitsbestimmende Schritt während der gesamten Umsetzung ist. Mit Ni/ZrO$_2$ in Gegenwart von Wasserstoff kann Palmitinsäure effizient zu n-Pentadecan umgesetzt werden. Die Reaktion verläuft hauptsächlich durch Hydrierung der Carboxylgruppe der Palmitinsäure, was zu Hexadecanal führt (geschwindigkeitsbestimmender Schritt), welches darauffolgend an den metallischen Ni-Zentren zum gezielten n-Pentadecan und Kohlenstoffmonoxid decarbonyliert wird. Bemerkenswert ist, dass die Hydrierung der Fettsäure zum Aldehyd synergistisch durch den ZrO$_2$-Träger begünstigt ist, indem die Carboxylgruppe gleichzeitig an den Sauerstofffehlstellen adsorbiert und die Wasserstoff-Moleküle dissoziieren. Jedoch ist die Ketonisierung die vorherrschende/dominierende Reaktion bei der ZrO2-katalysierten Umsetzung von Palmitinsäure in N$_2$.

Pd schwarz begünstigt die direkte Decarboxylierungs-Route (-CO$_2$), während Pt schwarz mit Raney Ni zu direkter Decarbonylierung (-CO) führt. Die individuellen Reaktionsgeschwindigkeiten (Einheit: $mmol \cdot h^{-1} \cdot mol_{metal}^{-1}$) in N$_2$-Trägergas sinken in der Reihenfolge r (Pt black) $\approx$ r (Pd black) > r (Raney Ni). Der C-Träger würde die Eigenschaften der Metallzentren wie Pd, Pt und Ni nicht beeinflussen, welche die direkte Decarbonylierungs-/Decarboxylierungs-Route der Fettsäuren bevorzugen. Wenn die Brønsted-Säure enthaltenden Zeolithe wie HBeta und HZSM-5 eingesetzt werden, scheint die Hauptroute um C$_{16}$ Hexadecan zu produzieren eine hintereinander ablaufende Hydrierungs-Dehydrierungs-Reaktion zu sein. Die Lewis-Säuren enthaltenden Oxide wie Al$_2$O$_3$, SiO$_2$ und ZrO$_2$ führten zu Hydrierungs-Decarbonylierungs-Reaktionen hintereinander mit dem Produkt C$_{15}$ n-Pentadecan. Die Deoxygenierungs-Raten/-Reaktionsgeschwindigkeiten (Einheit: $mmol \cdot g_{Cat}^{-1} \cdot h^{-1}$) von Palmitinsäure folgten der Reihenfolge r (Ni/HBeta oder Ni/HZSM-5) > r (Ni/ZrO$_2$) > r (Ni/Al$_2$O$_3$ oder Ni/SiO$_2$).

Nach detaillierter Untersuchung der Umsetzung von Fettsäuren wurde die Deoxygenierung von Mikroalgenöl zu Alkanen durch selektive Spaltung von C-C und C-O Bindungen über ZrO$_2$ geträgerte Ni-Katalysatoren erreicht. Die Hydrogenolyse von Triglyceriden, die Hydrierung von funktionellen Gruppen (d.h. -COOH, -CHO, C=C) und die Decarbonylierung von Aldehyden werden durch metallische Ni-Zentren

katalysiert. Wie oben erwähnt ist der geschwindigkeitsbestimmende Schritt (Hydrierung der Fettsäuren zum Aldehyd) synergistisch durch den ZrO_2-Träger begünstigt. Die Hydrogenolyse-Decarbonylierungs-Route ist gegenüber der Hydrodeoxygenierungs-Route aufgrund des geringeren Wasserstoffbedarfs bevorzugt.

Wir haben auch gezeigt, dass Mikroalgenöl fast vollständig zu Alkanen durch Kaskaden-Reaktionen auf bifunktionellen Katalysatoren, basierend auf Ni und saurem Zeolith, hydrodeoxygeniert werden kann. Die metallischen Ni-Zentren sind für die gleichzeitige Hydrogenolyse, Hydrierung und Decarbonylierung verantwortlich. Die Säurezentren katalysieren die Dehydratisierung der Alkohol-Intermediate sowie die Hydroisomerisierung und das Hydrocracken der Alkan-Produkte. Die Kenntnis der individuellen Kinetik erlaubt es, die Reaktionsgeschwindigkeit durch Anpassung der Konzentration von katalytisch aktiven Zentren auszugleichen, um maßgeschneiderte und stabile Katalysatoren zur selektiven Umsetzung von Mikroalgenrohöl in Alkane des Diesel-Bereichs herzustellen. Dieser Ansatz eröffnet neue Möglichkeiten schwefelfreie, qualitativ hochwertige Bio-Kraftstoffe aus Mikroalgen im großen Maßstab zu produzieren.

Curriculum vitae

Baoxiang Peng was born on February 28th 1984 in Shandong, P. R. China. After accomplishing his high school education at hometown in 2001, he started his study in Department of Chemical Engineering at Tsinghua University, Beijing, China and received his bachelor degree in July 2005. In September 2005, he went on to study chemical reaction engineering and technology at Tsinghua University, Beijing, China, under the supervision of Prof. Jinfu Wang. In July 2008, he graduated as chemical engineer with a master degree, and his thesis was entitled "*Biodiesel production from waste oil feedstocks*". Based on this process, three biodiesel production pilot plants were built in China. He and Prof. Wang were awarded third-class prize "*progress in energy science and technology*" issued by the China Department of Energy in 2010. In September 2008, he joined the research group of Prof. Johannes A. Lercher and started his Ph.D. thesis at the Chair of Technical Chemistry II at the Technische Universität München, Germany. His research focuses on the transformation of microalgae oil into hydrocarbons with sulfur-free catalysts, as well as understanding the chemistry of hydrodeoxygenation and aqueous phase reforming of glycerol, which provides bio-hydrogen source for the hydrotreating of microalgae oil.

List of publications

Baoxiang Peng, Yuan Yao, Chen Zhao, and Johannes A. Lercher "*Towards quantitative conversion of microalgae oil to diesel range alkanes with dual functional catalysts*", *Angew. Chem. Int. Ed.* **2012**, *51*, 2072-2075. (Inside back cover paper, hot paper)

Baoxiang Peng, Xiaoguo Yuan, Chen Zhao, and Johannes A. Lercher "*Stabilizing catalytic pathways via redundancy - selective reduction of microalgae oil to alkanes*", *J. Am. Chem. Soc.* **2012**, submitted.

Baoxiang Peng, Xiaoguo Yuan, Chen Zhao, and Johannes A. Lercher "*Catalytic deoxygenation of palmitic acid on the influence of metal site, support, and carrier gas*", *J. Catal.* **2011**, in preparation.

Baoxiang Peng, Chen Zhao, Isidro Mejía-Centeno, Gustavo A. Fuentes, Andreas Jentys, and Johannes A. Lercher "*Comparison of kinetics and reaction pathways for hydrodeoxygenation of C_3 alcohols on Pt/Al_2O_3*", *Catal. Today* **2012**, *183*, 3-9.

Aysegul Ciftci, Baoxiang Peng, Andreas Jentys, Johannes A. Lercher, Emiel J. M. Hensen, "*Support effects in the aqueous phase reforming of glycerol over supported platinum catalysts*", *Appl. Catal. A* **2012**, submitted.

A. Wawrzetz, B. Peng, A. Hrabar, A. Jentys, A. A. Lemonidou, J. A. Lercher "*Towards understanding the bifunctional hydrodeoxygenation and aqueous phase reforming of glycerol*", *J. Catal.* **2010**, *269*, 411-420.

Baoxiang Peng, Qing Shu, Jinfu Wang, Guangrun Wang, Dezheng Wang, and Minghan Han "*Biodiesel production from waste oil feedstocks by solid acid catalysis*", *Process. Saf. Environ. Prot.* **2008**, *86*, 441-447.

Qing Shu, Jinfu Wang, Baoxiang Peng, Dezheng Wang, and Guangrun Wang "*Predicting the surface tension of biodiesel fuels by a mixture topological index method, at 313 K*", *Fuel* **2008**, *87*, 3586-3590.